UNIVERSITY OF OKLAHOMA

GRADUATE COLLEGE

NON-CONTACT SENSOR FOR THE REAL-TIME MEASUREMENT OF QUALITY OF ASPHALT PAVEMENTS DURING COMPACTION

A DISSERTATION

SUBMITTED TO THE GRADUATE FACULTY

in partial fulfillment of the requirements for the

Degree of

DOCTOR OF PHILOSOPHY

By

FARES NIZAM BEAINY
Norman, Oklahoma
2011

NON-CONTACT SENSOR FOR THE REAL-TIME MEASUREMENT OF STIFFNESS OF ASPHALT PAVEMENTS DURING COMPACTION

A DISSERTATION APPROVED FOR THE
SCHOOL OF ELECTRICAL AND COMPUTER ENGINEERING

BY

Dr. Sesh Commuri, Chair

Dr. Musharraf Zaman

Dr. James Sluss

Dr. Gerald Crain

Dr. Monte Tull

This Dissertation is dedicated to my parents, ***Nizam*** *and* ***Hanane Beainy****, who taught me the value of education, and to my brother* ***Captain Khalil****, my beloved sister* ***May,*** *and my little baby* ***Chloe****, with love!!!*

Fares Beainy

ACKNOWLEDGMENTS

I would like to start by thanking my advisor, Dr. Sesh Commuri, and express to him my appreciation and gratitude for providing all the support, encouragement and guidance in my quest to complete this dissertation. His technical background, his passion for research and his vision for the future have all been an inspiration.

I am indebted to Dr. James Sluss for all the support he provided me, especially sponsoring me to come back for my graduate studies at the University of Oklahoma. I would like to express my appreciation to Dr. Musharraf Zaman for his valuable role that allowed me to approach this interdisciplinary problem. I am also thankful to Dr. Monte Tull for all the support he provided in completing this dissertation. Dr. Gerald Crain's constructive criticism has had a significant impact on the quality of my dissertation. I am very thankful to him.

I would like to acknowledge all my colleagues and friends who helped me during this endeavor; there are too many to name. However, I would like to thank Mr. Mohammad Saim from Volvo Construction Equipment (VCE) for providing vibratory roller specification for the numerical simulation, and Dr. Dharamveer Singh for conducting laboratory testing on asphalt specimens. Finally, I am grateful to Anh Mai, Harish Gadigota, and Imran Syed for their help with post processing the IACA data.

The exceptional support that Volvo Construction Equipment (VCE), especially Mr. Rich Van, provided during the course of this dissertation is notably appreciated.

The field demonstration reported in this dissertation would not have been possible without the unparalleled support of Haskell Lemon Construction Company (HLCC), Oklahoma City, Oklahoma. Access to HLCC's construction sites and equipment as well

as their technical staff has been vital to the success of this dissertation. I also wish to acknowledge the financial support of Federal Highway Administration (FHWA), Oklahoma Department of Transportation (ODOT), and Oklahoma Transportation Center (OkTC).

A special thank you for Dr. Naji Khoury, Mr. Marcel Hage, Dr. Younane Abousleiman, and Dr. Christian El Amm for their motivation and inspiration.

Finally, I would like to express my deepest gratitude to Erika Kohler for all the support that she provided me throughout my PhD studies.

TABLE OF CONTENTS

LIST OF TABLES

LIST OF FIGURES

ABSTRACT

The development of a non-contact sensor capable of determining the quality of asphalt pavements during their construction is addressed in this dissertation. Adequate compaction of asphalt pavement during its construction is necessary for the proper functioning of the pavement over its design life. Rutting, cracking, pot holes and other forms of distress in asphalt pavements can be attributed partly to improper compaction during the construction process. While the mechanism of pavement failure is well understood, there are no widely accepted tools that can determine the quality of the entire pavement during its construction. Furthermore, quality control and acceptance criteria require the extraction of roadway cores from the finished pavement. Such tests are destructive in nature and also contribute to the early deterioration of the pavements. The complexity of the compaction process and the limitations of the spot tests have led researchers to develop advanced compaction technologies, such as Intelligent Compaction (IC).

Intelligent Compaction is an emerging area of research that attempts to extend mechanistic-empirical design principles to the compaction of bound and unbound aggregate materials and soil subgrades. Intelligent Compaction is based on the hypothesis that the vibratory compactor and the underlying pavement layers form a coupled system whose response characteristics are influenced by the changing properties of the pavement material. IC techniques estimate the stiffness of the pavement layer by observing the vibratory response of the roller during compaction. One of the limitations of IC technologies is that the measurement values reported by these devices cannot be easily

verified through in-situ measurements of density or dynamic modulus. The lack of established theoretical foundations has also limited the widespread acceptance of these technologies.

In this dissertation, the problem of ensuring adequate compaction of asphalt pavement during construction is addressed through the development of a mathematical model that can replicate the compaction process in the field. The asphalt pavement is first modeled as a Visco-Elastic-Plastic (VEP) material and the equations governing the motion of the coupled system comprised of the vibratory compactor and the asphalt mat are developed. The parameters of the model are shown to depend on the properties of the asphalt mix, as well as the type of vibratory compactor. Numerical simulations show that this model can not only capture the effects of static rolling, but can also accurately predict the effects of vibratory compaction. The VEP model can also account for the effect of asphalt mat thickness and temperature on the quality of compaction. The simulation results along with the data recorded during the construction of asphalt pavements are used to validate the hypothesis of Intelligent Compaction.

The theoretical results of this dissertation are central to the development of verifiable Intelligent Compaction technology. The Intelligent Asphalt Compaction Analyzer (IACA) prototype that was developed during the course of this dissertation is the first step in this direction. This prototype was successfully tested on several types of dual drum vibratory compactors such as IR DD110, IR DD118, IR DD132, and IR DD138HF, manufactured by Volvo Construction Equipment Company, Shippensburg, Pennsylvania (formerly Ingersoll Rand). The field evaluation of the IACA was carried out at six different construction sites between June 2009 and April 2010. These results conclusively

show that the IACA can not only be used for effective quality control during the construction of asphalt pavements but can also serve as a non-destructive quality assurance tool.

It is anticipated that the research carried out in this dissertation will pave the way towards closed-loop control of vibratory compactors for intelligent compaction of aggregate materials and soil subgrades. Improving the quality and consistency of pavements during their construction will increase the life span of the roads, reduce the cost of their maintenance, and reduce the impact of road construction and traffic on the environment.

Chapter 1 INTRODUCTION

Improper compaction of an asphalt mat during construction is a leading cause for the early degradation of asphalt pavements. Excessive rutting, cracking, potholes, etc. that are signs of failure of asphalt pavements can be avoided by using good Quality Control tools during the compaction process and through the adoption of better construction practices. The most reliable method of measuring pavement density in the Quality Assurance process is the extraction of field cores at several locations and evaluating their air voids in the laboratory as specified in AASHTO T-166: "Bulk Specific Gravity of Compacted Bituminous Mixtures Using Saturated Surface-Dry Specimens" (AASHTO, 2007a). This test method, however, is time consuming, costly, destructive, and not indicative of the overall pavement quality. Alternative methods for in-place measurement of density of hot mix asphalt (HMA) layers include both nuclear density gauges and non-nuclear density gauges (Herbert and Jennette, 2011). The nuclear-based devices tend to have problems associated with licensing, equipment handling, and storage. Only recently, non-nuclear gauges have started to become an alternate tool for Quality Control (QC) and Quality Assurance (QA) measures. All of these technologies allow only point-wise measurements of density during the construction of an asphalt pavement. This manual process of measurement is time consuming and results in avoidable delays in the construction while not reflecting the overall quality of the pavement. *Thus, there is a need for integrating sensors into vibratory rollers and to develop automated processes that can provide real-time QA/QC data and serve as an indicator of the level of compaction achieved during construction.*

1.1 Importance of the Problem

The United States has over 6.4 million kilometers (4 million miles) of roads, paved and unpaved. About 4.3 million kilometers (2.7 million miles), 67 percent, of these roads are paved with asphalt (FHWA, 2008). The United States relies heavily on ground transportation for both commercial and personal travel. Paved roads are used for the delivery of 70 percent of all domestic freight in the country and 80 percent of the American communities receive their goods exclusively via trucks (ATA, 2008). Each year, these roads are used by truckers to transport 81 percent of total trade between the United States and Mexico and 64 percent between the United States and Canada (ATA, 2008). In addition, personal car ownership in the United States is one of the highest in the world. As a result, well maintained asphalt paved roads and highways are vital to the economic health of the nation. However, lack of proper tools for effective Quality Control and the burgeoning truck and commuter traffic has led to a rapid deterioration of road infrastructure in the nation. The statistics in Table 1 indicate that at a conservative estimate, about 53 percent of the roads and highways in the United States have a serviceability rating less than 3.5, which implies that these roads are in fair to very poor conditions (FHWA, 2005; 2006; 2007; 2008).

Table 1.1 US Roads with serviceability rating less than 3.5

	Percentage*			
	2005	**2006**	**2007**	**2008**
Rural Major Collector	54.9%	50.9%	52.8%	53.7%
Urban Minor Arterial	53.7%	52.2%	52.5%	53.9%
Urban Collector	55.9%	55.2%	56.1%	57.9%
All Highways and Roads	54.9%	52.3%	53.6%	54.9%

*The “Present Serviceability Rating” (PSR) values range from 0.1 to 5.0; higher PSR values represent smoother riding roadways.

In 2006, the US government was required to spend $139 billion for the maintenance of highways and bridges nationwide (USDOT, 2006). This number is expected to increase to $150 billion by 2015 due to inflation alone (USDOT, 2006). This spending does not take into consideration the expansion of roads and highways. The total expenditure for construction and maintenance of asphalt pavements is in excess of $25 billion annually and over 300,000 men and women are employed in the asphalt industry (NAPA, 2007). Therefore, the asphalt industry is central to the economic wellbeing of the nation.

Inadequate transportation infrastructure impacts the economy in many direct and indirect ways. According to the Minnesota Transportation Alliance in their report entitled 'A Roadmap to 2040.' poor roads lead to increased traffic congestion and cost of vehicle ownership (MTA, 2011). In 2009, Americans on an average spent 4.8 billion hours waiting in traffic at a cost of $115 billion. The cost to the average commuter due to traffic congestion was $916. The deficient transportation infrastructure also resulted in a loss of Gross Domestic Product (GDP) to the tune of $125 billion. It is anticipated that failing infrastructure will add cost of more than $2 trillion cost to the economy by the year 2040. In addition to this the cost of added business expenses is also expected to be over $1 trillion (MTA, 2011).

Poor quality of the paved roads also has an adverse impact on vehicular safety and the environment. A study to investigate the relationship between the frequency of accidents in highway segments and pavement distress variables suggested a direct relationship between the Present Serviceability Index (PSI) and the rate of accidents (Chan et al., 2008). Since over 550 million tons of hot mix asphalt (HMA) are produced and placed

each year, the construction and maintenance of these roads also have a costly impact on the environment. The construction of one mile of Hot Mix Asphalt (HMA) pavement emits an estimated 900,000 kilograms (2 million pounds) of carbon dioxide or CO_2 (Stripple, 2001).

In summary, high quality and long lasting asphalt paved roads are essential to ensure a strong economy, good riding quality, safer roads, less traffic congestion, reduced maintenance costs, and reduced air pollution.

1.2 Scope of the Problem

Asphalt pavements are designed to carry traffic loads with minimum physical deterioration, maximum safety, and maximum ride comfort. Based on the design, an asphalt pavement is expected to bear traffic loading up to 30 million ESALs (Equivalent Single Axle Load) over a 20 years life span (TxDOT, 2011). A finished asphalt pavement is the result of a multistage process: from pavement design to construction, Quality Assurance, and specifications. However, the compaction of asphalt mix is the last procedure that asphalt materials go through during this multistage process. Therefore, proper compaction of an asphalt pavement is necessary to achieve its designed properties and to ensure its performance and longevity.

Compaction in the field is commonly performed using a vibratory compactor. The vibratory compactor applies both static and dynamic forces (weight and vibration) in order to increase the interlocking between the aggregates and thereby reduce the air voids in the compacted mix. Compaction reduces the permeability of the mix, and increases the load bearing capacity, resistance to deformation (or rutting), and the durability of the

pavement (VLR, 1992). The compaction that is achieved depends to a large extent on the underlying base, the type of mix used, the thickness of the asphalt layers, and the environmental conditions at the time of placement. In addition, the final density and stiffness of the compacted pavement are affected by the number of rollers, the type of rollers, and the rolling pattern used during the compaction process (Scherocman and Dwight, 2008).

A well-designed and controlled compaction process is essential in order to achieve good quality and long-lasting asphalt pavements. Under-compaction generally leads to a high percentage of air voids in the pavement, making it susceptible to moisture infiltration, oxidation, and cracking (Arambula et al., 2007). On the other hand, over-compaction results in low air voids that could result in asphalt bleeding during hot weather (USACE, 2000). Over-compaction could also result in the crushing of aggregates, thus altering the mechanical properties of the pavement. Therefore, poorly compacted pavements do not perform up to designed specifications and are subject to early degradation and deterioration. *A good QC method during the construction process can identify and correct many of the issues mentioned above, thus leading to improved pavement quality.*

1.3 Motivation

The complexity of the compaction process and the limitations of the spot tests have led to the development of advanced compaction technologies (Zambrano et al., 2006). Intelligent Compaction (IC) is one such technology that can improve the quality of the road being constructed while reducing the associated cost and adverse environmental

impacts. This technology functions on the premise that the vibratory compactor and the material being compacted form a coupled system whose dynamic properties change as the material is compacted. The alterations in the vibratory response of the compactor can therefore be used to estimate the density and the stiffness of the material during the compaction process. Adequate Quality Control of asphalt pavements involves the ability to measure compaction quality in real-time, and then accordingly modify the compactive effort of the vibratory roller by changing its operational parameters, namely amplitude and frequency of eccentric forces.

Existing compaction monitoring devices from equipment manufacturers (Andregg, 2008; Connolly, 2008; Rawls and Potts, 2008; Åkesson, 2008; Rakowski, 2008) are based on a principle of vibration analysis that was developed in the early seventies (Thurner and Sandström, 2000). Many of these devices are based on the assumption that the first harmonic of the vertical acceleration of the drum is proportional to the magnitude of the impact caused by the rotating eccentrics in the drum (Thurner and Sandström, 2000). The measurement values that these devices provide cannot be compared to any in-situ measurements such as density or dynamic modulus. In addition, changing machine properties and the variability of individual machines make it harder to obtain accurate measurements using these devices. Since there is very little theoretical or mechanics background in the development of these techniques, very little insight can be gained into the compaction of asphalt pavements. While there have been a few studies on the compaction using these techniques, such studies have focused on soil compaction and very little research addressed the compaction of asphalt pavements (Mooney et al., 2010).

1.4 Scope and Contributions of the Dissertation

1.4.1 Scope of the Dissertation

While it is generally understood that the quality of asphalt pavements during construction can be improved using Intelligent Compaction techniques, some fundamental modeling and control issues have to be addressed before such techniques can be proven successful. A closed-loop control strategy for the roller cannot be developed without a proper understanding of the underlying dynamics and the ability to feedback required information in real-time. The aim of the dissertation is to develop a theoretical framework for studying vibratory compaction and to apply this framework to the development of IC strategy. In order to accomplish this goal, the dynamics of the interaction between the roller and asphalt mat will be first examined. A sensing technology that can estimate the level of compaction (density or stiffness) of the asphalt mat in real-time during construction will then be developed. In the dynamic model, the vibratory compactor is represented as a second order system comprised of mass, spring, and damping elements. The asphalt pavement is modeled as a Visco-Elastic-Plastic Burger's material using a combination of a Maxwell model and a Kelvin-Voigt model. Laboratory test results are used to determine the parameters of the proposed Visco-Elastic-Plastic (VEP) model.

The dynamic equations representing the behavior of the VEP model is shown to be computationally tractable and in a form that is conductive to numerical simulation. It is also shown that the parameters in these equations are dependent on the roller and the properties of the asphalt mix. Furthermore, it is shown that these parameters can be

calculated from experimental results in a straightforward fashion. Numerical simulations are used to show that the model accurately predicts the compaction of hot mix asphalt (HMA) in the field.

The experimental verification of the intelligent sensing proposed in this dissertation is accomplished through the development of a rugged, real-time Intelligent Asphalt Compaction Analyzer (IACA). The IACA technology was first demonstrated in 2006 and was shown to provide real-time measurements of the density of the asphalt specimen during laboratory compaction (Nino, 2006). The performance of the IACA prototype is evaluated during the construction of both full-depth and overlays of asphalt pavements.

Comparison of the simulation results with data gathered during the experimental verification of the IACA during the construction of asphalt pavements is used to study the utility of the proposed model in developing continuous compaction control for the Intelligent Compaction of asphalt pavements.

1.4.2 Contributions

In this dissertation, the problem of ensuring the adequate compaction of asphalt pavement during construction has been addressed through the development of a mathematical model that can replicate the compaction process in the field. A Visco-Elastic-Plastic (VEP) model of an asphalt pavement is developed that can effectively represent the dynamic properties of the asphalt mat during compaction. This model is then integrated with a mathematical model of a vibratory compactor in order to study the response of the coupled system during compaction. The parameters of the model are first estimated from the dynamic modulus master curves of the asphalt mix. These parameters

are then continuously updated to accurately represent the properties of the asphalt mat during compaction. Detailed mathematical equations are developed that relate the changes in the asphalt mat to the vibratory response of the roller during compaction. Numerical simulation of the VEP model shows that the response of coupled system can be used to study the compaction of asphalt pavements.

A rugged prototype of the IACA system has been developed. The prototype IACA is easily installable on any vibratory compactor, and is able to estimate the compaction with accuracy suitable for its use in Quality Control and Quality Assurance. The IACA prototype has been successfully tested on several types of dual drum vibratory compactors such as IR DD110, IR DD118, IR DD132, and IR DD138HF manufactured by Volvo Construction Equipment Company, Shippensburg, Pennsylvania (formerly Ingersoll Rand). The evaluation of the IACA was carried out during the construction/remediation of the asphalt pavements at six different sites across the United States. Roadway cores were extracted at randomly selected locations on the finished pavement and the density of the cores was measured in the lab using the AASHTO T-166 standard method. The validation of the IACA performance was achieved by the comparison of the IACA estimated density with the density of the roadway cores at these random locations.

The measurements from 180 roadway cores over the duration of the project showed that the IACA was able to measure the density of the compacted pavement with a mean error of 0.1 percent (of the Theoretical Maximum Density) and a standard deviation of 0.8. Furthermore, the measurement error had a 95 percent confidence interval of [-1.2, 1.2], thereby indicating that the IACA is suitable for use as a Quality Control tool during

the construction of asphalt pavements. The utility of using IACA for Quality Assurance was also demonstrated at two different construction sites. The results showed that the IACA estimated density has a statistically significant correlation with the density measurements obtained from roadway cores. Furthermore, the estimated density had a mean error of 0.1 with a 95 percent confidence interval [-0.4, 0.6] in terms of air voids in the compacted pavement. Statistical analysis of the IACA data showed that the IACA estimated density has a range comparable to that measured from the roadway cores. The results of the field tests disclosed in this dissertation justify the use of IACA for QC during field compaction as well as for computing the PWL for determining the pay factors.

1.5 Dissertation Structure

In Chapter 2, a mathematical model of the compactor and asphalt pavement is introduced. The parameters in the dynamic model from experimental data were then determined. In Chapter 3, simulation results for different compaction scenarios and their comparison with field compaction data are presented and discussed. In Chapter 4, background and operational principle of the IACA system and its development are discussed. Results of the field demonstrations and detailed descriptions of the field evaluations are then presented. In Chapter 5, statistical Quality Assurance using PWL calculations based on roadway cores and IACA estimations has been presented. In addition, the use of IACA system as a Quality Assurance and Quality Control method are discussed. Finally, conclusions and scope of future work are presented in Chapter 6.

Chapter 2 VISCO-ELASTIC-PLASTIC MODEL OF ASPHALT-ROLLER INTERACTION

2.1 Introduction

The long-term performance of an asphalt pavement is directly related to its load bearing capacity and is determined by the stiffness achieved during the construction process. Inadequate compaction is known to cause early deterioration of a pavement and ultimately reduce its useful lifespan (Bohuslav, 2008; VLR, 1992). Over the past two decades, several researchers have studied long-term pavement distresses, like rutting, fatigue, and thermal cracking, over a wide range of traffic and climate conditions (Bonaquist and Christensen, 2005; Cominsky et al., 1998; Chen and Huang, 2000; Pellinen and Witczak, 2002; Shenoy and Romero, 2002; Witczak, 2002; Zapata and Houston, 2008; Loulizi et al., 2007; Desai, 2008; Zapata and Houston, 2008; Woo et al., 2008; Goh et al., 2011). While the effect of compaction on the long-term performance of the pavement is well understood, Quality Control during the construction of these pavements is still an under-researched area. In recent years, several researchers have looked at Intelligent Compaction as a means of improving the quality of asphalt pavement during its construction (Gallivan et al., 2011; Minchin et al., 2008; Cao et al., 2010; Beainy et al., 2011; Singh et al., 2010; Commuri, 2009a; Commuri, 2009b; Commuri and Beainy, 2011; Commuri and Zaman, 2008; Commuri et al., 2009; Commuri et al., 2010a, 2010b).

Intelligent Compaction techniques are based on the hypothesis that the vibrations of the roller during the compaction process are dependent on the stiffness of the material being compacted. Since the vibratory compactor and the underlying asphalt mat form a dynamically coupled system, the vibrations of the compactor would depend on the properties of the material being compacted, as well as the operational factors such as the frequency of the eccentrics in the roller drum and the ground speed of the roller (Thurner and Sandström, 2000; Commuri and Zaman, 2010; Beainy et al., 2011). Over the past decade, this hypothesis was used to implement several Intelligent Compaction techniques (Anderegg and Kaufmann, 2004; Åkesson, 2008; Connolly, 2008; Rakowski, 2008; Rawls and Potts, 2008). These IC techniques are being evaluated by several Departments of Transportation (DOTs) and the Federal Highway Administration (Quintus et al., 2010), but have yet to be ratified and accepted as a Quality Assurance method. This is mainly due to the lack of theoretical and/or mechanistic models that can provide insight into the quality and accuracy of the estimated stiffness. Furthermore, the estimated measurements provided by these commercial devices are difficult to verify through in-situ tests in the field (Quintus et al., 2010; Chang et al., 2011; Hossain et al., 2006).

In recent years, some researchers have started to investigate the relationship between the roller and the material being compacted. However, a majority of these works is geared toward the study of soil compaction (Mooney et al., 2010). The stiffness of the soil depends on the moisture content and the density of the soil. This dependence makes it difficult to verify the results during field compaction. Furthermore, these results cannot be extended to the compaction of asphalt pavements in a straightforward manner.

Researchers have attempted to develop numerical techniques as well as analytical models to examine the behavior of asphalt pavement during its compaction. Pei-Hui Shen and Shu-Wen Lin (2008) used asymmetric hysteresis modeling to investigate the dynamic characteristics of a vibratory compaction system. Using the Bouc-Wen differential equation (Ismail et al., 2009), the authors derived an asymmetrical model and used it to describe the nonlinear characteristic of the roller vibrations. While this model addresses the nature of the observed vibrations, the properties of the asphalt mat were not taken into account in the analysis. Recently, Eyed Masad et al. (2010) used Finite Element Method (FEM) to describe laboratory as well as field compaction of an asphalt mix. Using a thermo-mechanical framework, these researchers developed a constituent model that was capable of capturing the mechanics of the compaction processes. In addition, the micromechanical model that was developed was able to predict the influence of material properties such as binder viscosity, aggregate shape characteristics, and aggregate gradation during the static compaction of asphalt specimen. Micaelo et al. (2009) used micromechanical Discrete Element Methods (DEM) to simulate field compaction of asphalt material. An inverse modeling scheme was used to specify the displacements as the input to the model. Similarly, Lodewikus (2004) developed a discrete element model to study their ability to simulate the compaction of HMA. While these results are encouraging, significant research remains to be done in order to be able to accurately model the compaction of asphalt mixes.

Analytical models such as the Maxwell, generalized Maxwell, Kelvin–Voigt, generalized Kelvin, Huet–Sayegh, and Burger models all represent the asphalt pavement as a combination of springs and dampers (Nillson et al., 2002; Pronk, 2005; Dave et al.,

2006). Unfortunately, barring Burger's model, these models are either complex or do not accurately predict the behavior of the asphalt mix (Xu and Solaimanian, 2009). Burger's model on the other hand is not only simple but can accurately describe the viscoelastic behavior of an asphalt pavement (Liu and You, 2009; Liu et al., 2009). However, these models were used by researchers to study the long-term behavior of the pavement under traffic loads and not the interaction of the roller and asphalt during field compaction.

In this chapter, a Visco-Elastic-Plastic (VEP) model of an asphalt pavement is developed that can effectively represent the dynamic properties of the asphalt mat during compaction. This model is then integrated with a mathematical model of a vibratory compactor in order to study the response of the coupled system during compaction. The proposed model captures the loading and unloading phenomenon that an asphalt mat experiences during compaction. The parameters of the VEP model are first estimated from the dynamic modulus master curves of the asphalt mix. During the numerical simulation of the compaction process, these parameters are continuously updated to represent the changing properties of the asphalt mat. In Chapter 3, numerical simulations of the proposed VEP model are used for validation.

The rest of Chapter 2 is organized as follows:

a) Representation of a vibratory roller using a second order lumped parameter model.
b) Determination of a mechanistic model that captures the visco-elastic-plastic behavior of the asphalt mat during field compaction.
c) Derivation of the interaction between the vibratory roller and the asphalt mat during field compaction.

d) Specification of the boundary conditions for the transition between the loading and unloading states of the asphalt pavement during compaction.
e) Method to estimate the parameters of the model as a function of the volumetric and rheological properties of the asphalt mix.

2.2 Development of the VEP Model

2.2.1 Modeling the Vibratory Compactor

Asphalt compaction is a densification process aimed at reducing the air voids in the mix and improving the interlocking between aggregates. Vibratory compaction using a smooth steel drum roller is typically used to compact the asphalt mix in order to achieve desired load bearing capacity in the pavement and to improve the smoothness of the ride. A combination of static forces (weight of the drum and the frame) and impact forces (caused by the rotation of eccentric mass in the drum) is applied by the roller to affect the compaction of the asphalt mixture. The impact force is directly related to the geometry of the eccentric weight and its rotational speed. The frequency and the amplitude of the centrifugal forces generated by the rotating mass are used to quantify the compactive effort of the roller (Lavin, 2003). On a particular compactor, these parameters can be adjusted either through mechanical or electronic settings.

The centrifugal force generated by the rotation of the eccentric weights in the drum of the compactor can be expressed as

$$F_{ec} = m_{ec} r_{ec} \omega_{ec}{}^2 \tag{2.1}$$

where $m_{ec}r_{ec}$ is the moment of the eccentric mass; and ω_{ec} is the angular frequency of rotation.

In the present study, the compaction achieved in response to vertical loading of an asphalt mat is considered. Lateral forces resulting from the motion of the compactor and lateral flows of the asphalt mix are ignored.

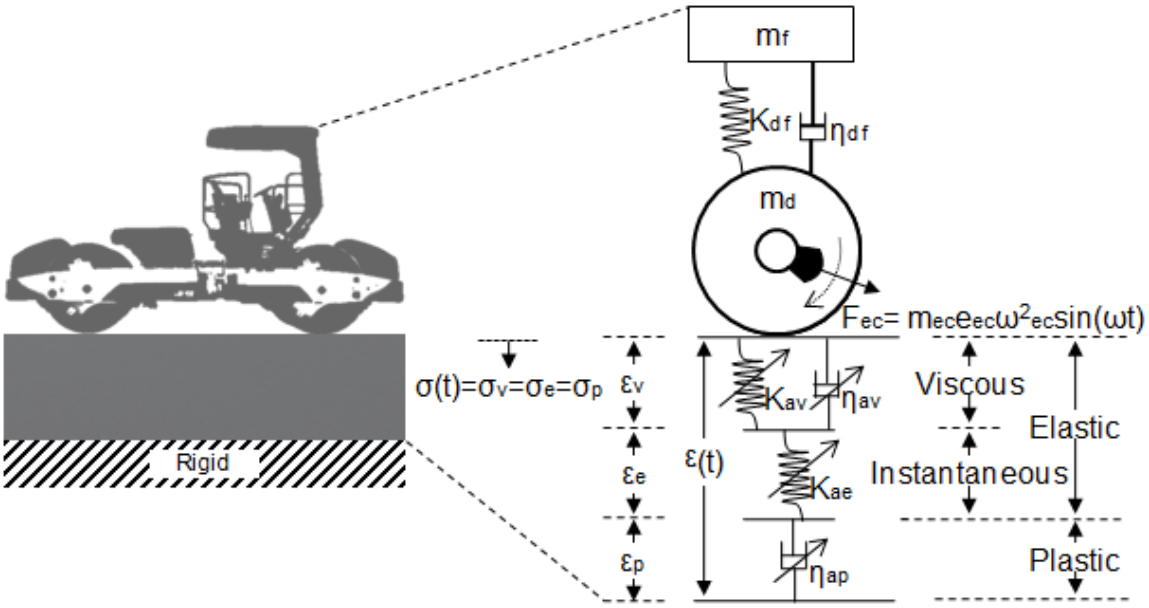

Figure 2.1 VEP model: a third order lumped element model of the interaction of vibratory roller and underlying asphalt pavement.

A compactor can be represented by a second order lumped element model with mass, spring, and dashpot components (see Figure 2.1). This model has been proven effective in modeling the dynamics of a vibratory compactor during soil compaction (Anderegg et al., 2006; Susante and Mooney, 2008; Dubravka and Davor, 2008). In this model, the spring and the dashpot represent the flexible coupling between the frame and the drum. The mass of the frame is denoted as m_f and the mass of the drum is denoted as m_d. The

centrifugal force caused by the rotation of the eccentrics is represented in the model as sinusoidal force acting in the vertical direction.

$$F_{ec} = m_{ec} r_{ec} \omega_{ec}{}^2 \sin(\omega_{ec} t) = m_{ec} r_{ec} \omega_{ec}{}^2 \sin(2\pi f_{ec} t) \quad (2.2)$$

where $t = k\left(\frac{T}{2}\right)$; $k = 0,1,2,3,$ and so on; and f_{ec} is the frequency of rotation of the eccentrics.

2.2.2 Modeling the Asphalt Pavement

Unlike soil, which can be effectively modeled using a parallel combination of a spring and a dashpot, asphalt material is a complex compound (Anderegg et al., 2006; Susante and Mooney, 2008; Dubravka and Davor, 2008). The viscoelastic behavior of asphalt mix depends on the volumetric and rheological properties, such as air voids content, binder viscosity, loading frequency, effective binder content, and the gradation, shape, and texture of the aggregates. In addition, the dependence of the viscosity of asphalt binder on the temperature makes the behavior of the material more complex. Several mechanical models have been proposed to describe the viscous, elastic, and plastic behaviors of an asphalt mixture. Maxwell, generalized Maxwell, Kelvin–Voigt, generalized Kelvin, Huet–Sayegh, and Burger are the most commonly used models (Xu and Solaimanian, 2009). Of these, Burger's model is the most effective in capturing the visco-elastic-plastic behavior of an asphalt mix. Furthermore, the process of determining the parameter values in the model is simple and straight forward.

In the study conducted in this dissertation, the underlying asphalt pavement is modeled as a Visco-Elastic-Plastic (VEP) material using a combination of a spring, a

damped spring (a spring and a dashpot in parallel), and a dashpot all in series (see Figure 2.1). In the discussion that follows, the applied stress is represented by σ and the resulting strain is represented by ε.

Using the nomenclature in Appendix A, the instantaneous elastic deformation, the delayed elastic deformation, and the permanent plastic deformation that asphalt pavement undergo during compaction are represented as follows:

1. The elastic delayed (viscous) deformation ε_v is represented using a spring and a dashpot in parallel, with corresponding stiffness K_{av} and damping η_{av}. The viscous deformation mimics the reversible but delayed deformation of the asphalt mat in response to a time varying stress.
2. The instantaneous elastic deformation ε_e is represented using an elastic spring with stiffness K_{ae}.
3. The plastic deformation ε_p is represented using a dashpot with viscosity η_{ap}.

The relationship between the stress and the strain occurring across each component of the model is first determined. These relationships are then used to develop the dynamic equations that represent the vibratory response of the coupled system shown in Figure 2.1.

2.2.2.1 Elastic Delayed (viscous) Deformation

The two components representing the delayed recoverable strain in the asphalt mat can be expressed as

$$\sigma_v = \varepsilon_v K_{av} + \dot{\varepsilon}_v \eta_{av}. \tag{2.3}$$

Denoting $\frac{d}{dt}\varepsilon_v = \dot{\varepsilon}_v$, Equation (2.3) can be written as a first order linear differential equation

$$\dot{\varepsilon}_v + \varepsilon_v \frac{K_{av}}{\eta_{av}} = \frac{\sigma_v}{\eta_{av}}, \tag{2.4}$$

which can be solved by taking an integrating factor. Defining

$$I(t) = e^{\int \frac{K_{av}}{\eta_{av}} dt}, \tag{2.5}$$

the general solution of the differential Equation (2.4) can be expressed as

$$\varepsilon_v = \left(\frac{\int \sigma_v e^{\frac{K_{av}}{\eta_{av}} t}\, dt}{\eta_{av}} + C \right) e^{-\frac{K_{av}}{\eta_{av}} t}, \tag{2.6}$$

where C is a constant of integration.

2.2.2.2 Instantaneous Elastic Deformation

Since $\sigma_e = \varepsilon_e K_{ae}$, the elastic strain ε_e can be expressed in terms of the applied stress as

$$\varepsilon_e = \frac{\sigma_e}{K_{ae}}, \tag{2.7}$$

where K_{ae} represents the elastic properties of the asphalt mat.

2.2.2.3 Plastic Deformation

Denoting $\frac{d}{dt}\varepsilon_p = \dot{\varepsilon}_p$,

$$\sigma_p = \dot{\varepsilon}_p \eta_{ap}, \tag{2.8}$$

where η_{ap} is the coefficient of viscous damping used to characterize the plastic deformation of the asphalt mat.

The plastic strain across the dashpot element can then be expressed in terms of σ_p as follows:

$$\varepsilon_p = \frac{\int \sigma_p dt + C}{\eta_{ap}}, \tag{2.9}$$

where C is a constant of integration.

2.2.2.4 Total Deformation

The stress experienced by the asphalt mat during vibratory compaction appears across all three components (viscous, elastic, and plastic) of the asphalt model as follows:

$$\sigma(t) = \sigma_v = \sigma_e = \sigma_p. \tag{2.10}$$

The resulting total instantaneous deformation of the asphalt mat is the sum of recoverable and non-recoverable strains, that is

$$\varepsilon(t) = \varepsilon_v + \varepsilon_e + \varepsilon_p, \tag{2.11}$$

where $\varepsilon(t)$ is the total instantaneous strain; ε_v is the viscous strain (delayed, recoverable); ε_e is the instantaneous elastic strain (recoverable); and ε_p is the plastic deformation (irrecoverable).

Finally, the constitutive equation of the VEP model can be obtained by substituting Equations (2.10), (2.6), (2.7), and (2.9) into Equation (2.11), as shown below:

$$\varepsilon(t) = \varepsilon_v + \varepsilon_e + \varepsilon_p$$
$$= \left(\frac{1}{\eta_{av}} \int \sigma e^{\frac{K_{av}}{\eta_{av}} t}\, dt + C_1\right) e^{-\frac{K_{av}}{\eta_{av}} t} + \frac{\sigma}{K_{ae}} + \frac{\int \sigma\, dt + C_2}{\eta_{ap}}, \tag{2.12}$$

where C_1, and C_2 are constants that represent the boundary conditions.

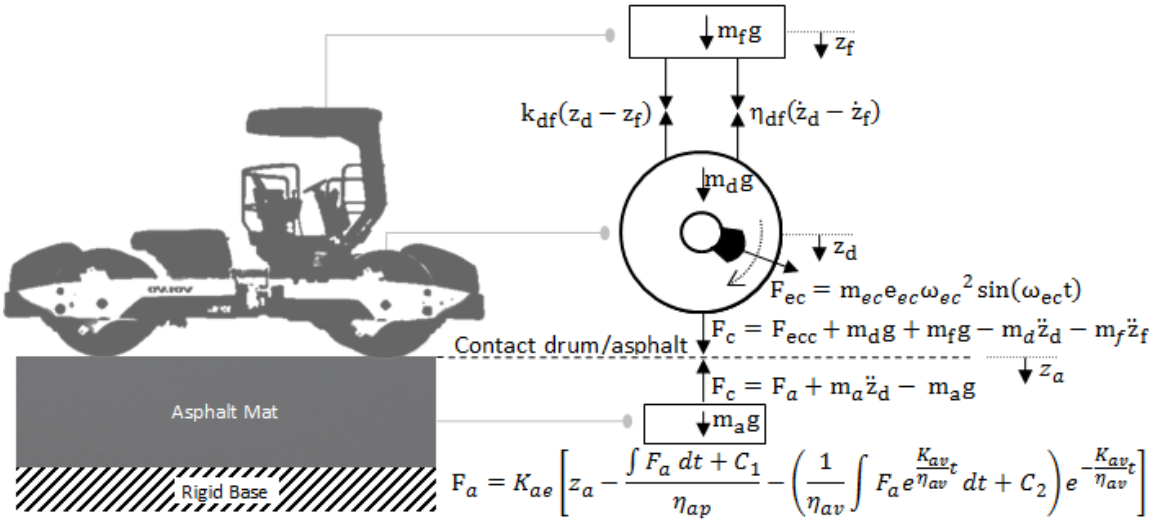

Figure 2.2 Free body diagram showing the interaction forces between the roller and the asphalt pavement.

2.3 Governing Equations of the VEP Model

The constitutive equation of the asphalt pavement model along with the equations of motion that express the dynamics of the vibratory roller are used to derive the interaction between the roller and the asphalt mat (see Figure 2.2). During field compaction, the roller would be moving at a given speed before vibratory compaction is applied to the asphalt mat. The roller drum is initially in contact with the asphalt mat. The asphalt mat becomes increasingly stiffer as the compaction proceeds and causes the drum to bounce. Therefore, the model has to accurately predict the dynamics of the coupled system during the 'contact' phase as well as during the non-contact, i.e. 'bounce' phase. The proposed VEP model takes this phenomenon into consideration.

2.3.1 Description of the Dynamics During 'contact' Phase

During the contact phase, the force required for acceleration of the drum and the frame in the vertical direction can be viewed as the sum of all reaction forces in the asphalt mat.

$$\begin{aligned}(m_d + m_a)\ddot{z}_d &= (m_d + m_a)\ddot{z}_a \\ &= m_{ec} r_{ec} {\omega_{ec}}^2 \sin(\omega_{ec} t) + m_d g + m_a g - k_{df}\left(z_d - z_f\right) \\ &\quad - \eta_{df}\left(\dot{z}_d - \dot{z}_f\right) \\ &\quad - K_{ae}\left[z_a - \left(\frac{1}{\eta_{av}}\int F_a e^{\frac{K_{av}}{\eta_{av}}t}\, dt + C_1\right) e^{-\frac{K_{av}}{\eta_{av}}t} - \frac{\int F_a\, dt + C_2}{\eta_{ap}}\right],\end{aligned} \tag{2.13}$$

$$m_f \ddot{z}_f = m_f g + k_{df}\left(z_d - z_f\right) + \eta_{df}\left(\dot{z}_d - \dot{z}_f\right), \tag{2.14}$$

$$F_c = m_{ec} r_{ec} {\omega_{ec}}^2 \sin(\omega_{ec} t) + m_d g + m_f g - m_d \ddot{z}_d - m_f \ddot{z}_f$$
$$= m_a \ddot{z}_d - m_a g + F_a, \tag{2.15}$$

where z_a is the displacement of the asphalt layer; F_a is the reaction force of the asphalt layer; F_c is the drum-asphalt contact force; z_d is the displacement of the drum; z_f is the displacement of the frame; k_{df} is the drum-frame stiffness coefficient; $\dot{z}_d$ is the velocity of the drum; $\dot{z}_f$ is the velocity of the frame; η_{df} is the drum-frame damping coefficient; m_a is the asphalt weight; $\ddot{z}_d$ is the vertical acceleration of the drum; $\ddot{z}_a$ is the vertical acceleration of the asphalt pavement; $\ddot{z}_f$ is the acceleration of the frame.

The reaction force of the asphalt mat F_a can be expressed in terms of the elastic strain,

$$F_a = K_{ae} \varepsilon_e, \tag{2.16}$$

where the elastic strain is expressed as,

$$\varepsilon_e = \varepsilon - \varepsilon_v - \varepsilon_p = z_a - \left(\frac{1}{\eta_{av}} \int F_a e^{\frac{K_{av}}{\eta_{av}} t} \, dt + C_2 \right) e^{-\frac{K_{av}}{\eta_{av}} t} - \frac{\int F_a \, dt + C_1}{\eta_{ap}}. \tag{2.17}$$

Then, F_a can be expressed as follows:

$$F_a = K_{ae} \left[z_a - \left(\frac{1}{\eta_{av}} \int F_a e^{\frac{K_{av}}{\eta_{av}} t} \, dt + C_1 \right) e^{-\frac{K_{av}}{\eta_{av}} t} - \frac{\int F_a \, dt + C_2}{\eta_{ap}} \right]. \tag{2.18}$$

2.3.2 Description of the Dynamics During 'bounce' Phase

Equations (2.13) - (2.18) are valid as long as the contact force is strictly greater than zero ($F_c > 0$). A negative value of contact force, i.e. $F_c \leq 0$, indicates that the drum has lost contact with the asphalt pavement. In this case, there is no coupling between the

roller and the asphalt mat (non-contact phase of the roller dynamics). Therefore, the governing equations during non-contact phase can be expressed as follows:

$$m_d\ddot{z}_d = m_d g + m_{ec} r_{ec} {\omega_{ec}}^2 \sin(\omega_{ec} t) - k_{df}\left(z_d - z_f\right) - \eta_{df}\left(\dot{z}_d - \dot{z}_f\right), \tag{2.19}$$

$$m_f\ddot{z}_f = m_f g + k_{df}\left(z_d - z_f\right) + \eta_{df}\left(\dot{z}_d - \dot{z}_f\right), \tag{2.20}$$

$$\begin{aligned}\ddot{z}_a = \frac{d}{dt}\dot{z}_a = \frac{d^2}{dt}z_a \\ = \frac{d^2}{dt}\left[\left(\frac{m_a g}{K_{av}} e^{\frac{K_{av}}{\eta_{av}}(t-t_{loc})} + C1\right) e^{-\frac{K_{av}}{\eta_{av}}(t-t_{loc})}\right. \\ \left. + \left(\frac{F_{a\_loc}}{K_{ae}}\right)\cos(w_n(t-t_{loc})) + \frac{m_a g}{K_{ae}} + \frac{m_a g(t-t_{loc})}{\eta_{ap}} + C2\right],\end{aligned} \tag{2.21}$$

where F_{a_loc} is the last value of F_a at loss of contact; w_n is the undamped natural frequency of the asphalt ($w_n = \sqrt{K_{ae}/m_a}$); t_{loc} is the time of loss of contact.

2.4 Boundary Conditions

Equations (2.13) - (2.21) represent the dynamics of the roller and the asphalt mat both during the 'loading' (contact) and 'unloading' (bounce) phases of the compaction process. For these equations to be useful, the boundary conditions that represent the transition between these two phases and the initial conditions have to be determined.

2.4.1 Initial Conditions

At the start of the simulation process both the compactor and the asphalt mat are assumed to be at rest. Therefore,

$$z_d = z_a = \varepsilon_v = \varepsilon_e = \varepsilon_p = 0. \tag{2.22}$$

Using these initial conditions, the constants C_1 and C_2 can be determined. Setting

$$\frac{1}{\eta_{av}} \int F_a e^{\frac{K_{av}}{\eta_{av}} t}\, dt + C_1 = 0, \tag{2.23}$$

$$C_1 = -\frac{\left(\int F_a e^{\frac{K_{av}}{\eta_{av}} t}\, dt \right)_{at\ t=0}}{\eta_{av}}. \tag{2.24}$$

Similarly, setting

$$\frac{\int F_a\, dt + C_2}{\eta_{ap}} = 0, \tag{2.25}$$

$$C_2 = -\left(\int F_a\, dt \right)_{at\ t=0}. \tag{2.26}$$

During compaction, the initial values of C_1 and C_2 would remain valid as long as the roller drum remains in contact with the asphalt mat. As the stiffness of the asphalt mat increases, the roller drum starts to bounce off the asphalt mat (loss of contact). During the loss of contact, the asphalt mat enters the 'bounce' state wherein the dynamics of the asphalt mat are independent of the dynamics of the roller. On the other hand, at ($t = t_{roc}$), the the roller would regain contact with the asphalt mat following the 'bounce' phase. Since the dynamics are different in the contact and the bounce phases, the initial conditions have to be determined at each of these transition points.

2.4.2 At $t \geq t_{loc}$ (during loss-of-contact)

Since the dynamics of the asphalt mat are independent of the roller during the 'bounce' phase, the viscous strain can be expressed as

$$\varepsilon_v K_{av} + \dot{\varepsilon}_v \eta_{av} = m_a g. \tag{2.27}$$

Equation (2.27) can be written as a first order linear differential equation in the form

$$\dot{\varepsilon}_v + \varepsilon_v \frac{K_{av}}{\eta_{av}} = \frac{m_a g}{\eta_{av}}, \tag{2.28}$$

that can be solved by defining an integrating factor $I(t)$. Setting

$$I(t) = e^{\int \frac{K_{av}}{\eta_{av}} dt}, \tag{2.29}$$

the strain can be expressed as

$$\varepsilon_v(t) = \left(\int_{t_{loc}}^{t} \frac{m_a g}{\eta_{av}} e^{\frac{K_{av}}{\eta_{av}} t} \, dt + C_1 \right) e^{-\frac{K_{av}}{\eta_{av}}(t - t_{loc})}. \tag{2.30}$$

Solving (30), one obtains

$$\varepsilon_v(t) = \left(\frac{m_a g}{K_{av}} e^{\frac{K_{av}}{\eta_{av}}(t - t_{loc})} + C_1 \right) e^{-\frac{K_{av}}{\eta_{av}}(t - t_{loc})}. \tag{2.31}$$

C_1 can now be determined by substituting $t = t_{loc}$ in Equation (2.31).

$$\varepsilon_v(t_{loc}) = \left(\frac{m_a g}{K_{av}} e^0 + C_1 \right) e^0, \tag{2.32}$$

which yields

$$C_1 = \varepsilon_{v\_loc} - \frac{m_a g}{K_{av}}, \tag{2.33}$$

where ε_{v_loc} is the value of the delayed strain at the moment the drum loses contact with the asphalt pavement.

As a result,

$$\varepsilon_v(t) = \left(\frac{m_a g}{K_{av}} e^{\frac{K_{av}}{\eta_{av}}(t-t_{loc})} + \varepsilon_{v\_loc} - \frac{m_a g}{K_{av}}\right) e^{-\frac{K_{av}}{\eta_{av}}(t-t_{loc})}. \tag{2.34}$$

During the 'bounce' state, the instantaneous elastic strain can be expressed as

$$m_a \ddot{\varepsilon}_e + K_{ae}\varepsilon_e = m_a g. \tag{2.35}$$

The solution to the Equation (2.35) can be expressed as

$$\varepsilon_e(t) = \left(\frac{F_{a\_loc}}{K_{ae}}\right)\cos(w_n(t - t_{loc})) + \frac{m_a g}{K_{ae}}, \tag{2.36}$$

where the instantaneous strain is oscillatory with an amplitude equal to F_{a_loc}/K_{ae} and with angular frequency $w_n = 2\pi f_n$; $'f_n'$ is the undamped natural frequency of the asphalt pavement, $f_n = (1/2\pi)\sqrt{K_{ma}/m_a}$.

The plastic deformation is not recovered, and it is expressed as follows:

$$\varepsilon_p(t) = \frac{\int_{t_{loc}}^{t} m_a g \, dt + C_2}{\eta_{ap}}, \tag{2.37}$$

where $C_2 = \eta_{ap}\varepsilon_{p\_loc}$. Then,

$$\varepsilon_p(t) = \frac{m_a g(t - t_{loc})}{\eta_{ap}} + \varepsilon_{p\_loc}. \tag{2.38}$$

2.4.3 At $t \geq t_{roc}$ (during regain-of-contact)

Since energy can neither be created nor destroyed, it follows from the Law of Conservation of Energy that

$$z_{d\_roc} = \frac{z_d + z_a}{2}, \tag{2.39}$$

and

$$\dot{z}_{d\_roc} = \frac{\dot{z}_d + \dot{z}_a}{2}. \tag{2.40}$$

On the other hand, at $t = t_{roc}$, strains ε_v and ε_p are greater than zero. Thus the two constant C_1 and C_2 are reinitialized as follows. If

$$\varepsilon_v(t_{roc}) = \frac{1}{\eta_{av}} \int F_a e^{\frac{K_{av}}{\eta_{av}} t}\, dt + C_1 = \varepsilon_{v\_roc} \tag{2.41}$$

resulting in

$$C_1 = \varepsilon_{v\_roc} - \frac{\int_{t_{roc}}^{t_{roc}} F_a e^{\frac{K_{av}}{\eta_{av}} t}\, dt}{\eta_{av}} = \varepsilon_{v\_roc}. \tag{2.42}$$

Similarly,

$$\varepsilon_p(t_{roc}) = \frac{\int F_a\, dt + C_2}{\eta_{ap}} = \varepsilon_{p\_roc}. \tag{2.43}$$

Then,

$$C_2 = \eta_{ma}\varepsilon_{p\_roc} - \int_{t_{roc}}^{t_{roc}} F_a \, dt = \eta_{ap}\varepsilon_{p\_roc}. \tag{2.44}$$

2.5 Determination of the Parameters of the VEP Model

The dynamics of the roller-asphalt pavement coupled system expressed in Equations (2.13) - (2.21) depend on the characteristics of both the vibratory roller and the asphalt pavement. Prior to using this model, the parameters in Equations (2.13) - (2.21) have to be determined. These parameters depend on the type of the roller, the design of the pavement layers, and the asphalt mix used. Furthermore, the utility of this model would depend to a large degree on the ease of determination of these parameters.

2.5.1 *Dynamic Model of The Roller*

During compaction, the roller exerts static and dynamic forces on the asphalt mat. In Equations (2.13) - (2.21), these forces are represented in term of the drum mass, frame mass, drum-asphalt contact area and contact length, drum width, drum-frame stiffness coefficient and damping coefficient, eccentric rotational frequency, and the eccentric moment. Most of these parameters can be obtained from the manufacturer's specifications for the selected compactor. The damping coefficient and stiffness coefficient are not usually published and were obtained from the manufacturer for the research presented in this dissertation. A list of these parameters is provided in Table 2.1.

The contact area or the indentation that the drum creates on the asphalt mat is proportional to the stiffness of the asphalt material, the contact force, and the drum

geometry (Kröber et al., 2001). However, the determination of the contact geometry is not trivial. In this study, the contact area is assumed to be a constant in order to simplify the computation, and is calculated as:

(2.45)

where is the drum-asphalt contact area; is the drum-asphalt contact length in the direction of the roller movement; and is the width of the drum (see Figure 2.3).

The mass of the asphalt mat in contact with the roller can then be determined using the contact area and the thickness of the pavement layer.

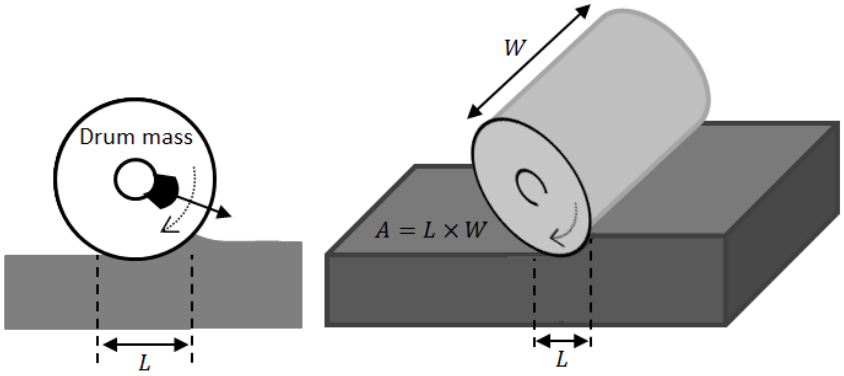

Figure 2.3 Contact area between the drum and the asphalt pavement.

Table 2.1 Dynamic parameters of an Ingersoll Rand DD118HF Roller

Symbol	Description	Unit	Source
	drum-frame damping coefficient	N/m	manufacturer
	drum-frame stiffness coefficient	N/m	manufacturer
	frame mass (@ a single drum)	kg	spec sheet
	drum mass	kg	spec sheet
	eccentric moment	kg.m	derived
	eccentric rotational frequency	rad/s	measured
	drum width	m	spec sheet
	drum/asphalt contact area	m^2	derived

2.5.2 Dynamic Model of the Asphalt Pavement

The model in Figure 2.1 represents the asphalt pavement in terms of the constants , , , and . Since the overall stiffness of the asphalt mix depends on these parameters, these parameters can be estimated indirectly through the measurement of the dynamic modulus of the compacted mix. In order to accomplish this, laboratory testing according to AASHTO TP-62 standard procedure (AASHTO, 2007) is first performed to determine the dynamic modulus and the phase angle of the mix at different temperatures, air void contents, and loading frequencies (see Figure 2.4).

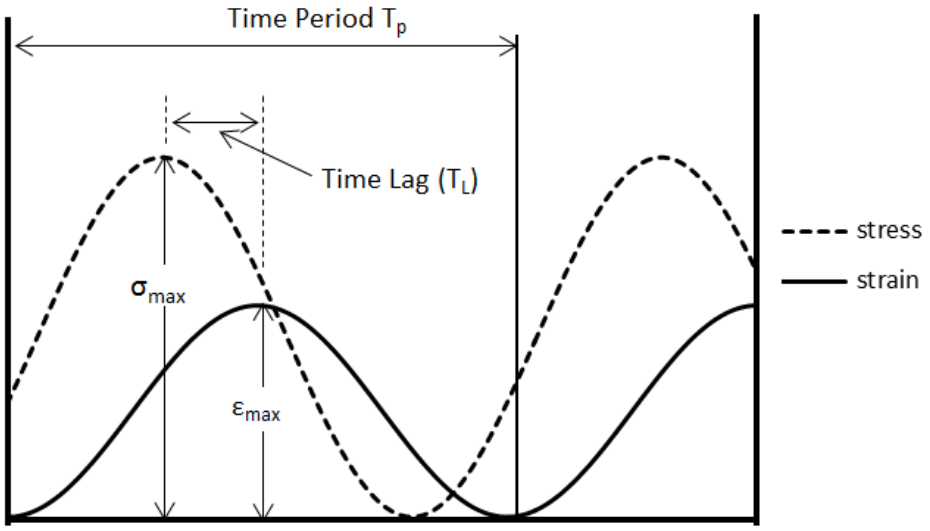

Figure 2.4 Stress and strain information to calculate and

.

The relationship between these parameters, , and can be represented by Equation (2.46) (Xu and Solaimanian, 2009; Liu et al., 2009).

$$E^*(i\omega) = \frac{1}{\left(\frac{1}{K_{ae}} + \frac{K_{av}}{{K_{av}}^2 + \omega^2{\eta_{av}}^2}\right) - \left(\frac{1}{\omega\eta_{ap}} + \frac{\omega\eta_{av}}{{K_{av}}^2 + \omega^2{\eta_{av}}^2}\right)i}, \quad (2.46)$$

where E^* is the complex modulus, $K_{ae}, \eta_{ap}, K_{av}$, and η_{av} are Burger's parameters; ω is the loading frequency and $i = \sqrt{-1}$.

The iterative procedure proposed by Liu et al. (2009) can be used to determine the parameters of Burger's model by fitting the test results into the following equations:

$$\tan\phi = K_{ae}[{K_{av}}^2 + \eta_{av}(\eta_{ap} + \eta_{av})\omega^2]/\omega\eta_{ap}({K_{av}}^2 + K_{ae}K_{av} + \omega^2{\eta_{av}}^2) \quad (2.47)$$

$$\frac{1}{|E^*|} = \frac{\Delta\varepsilon}{\Delta\sigma} = \frac{\varepsilon_{max} - \varepsilon_{min}}{\sigma_{max} - \sigma_{min}} = \sqrt{\frac{1}{{K_{ae}}^2} + \frac{1}{\omega^2{\eta_{ap}}^2} + \frac{1 + 2\left(K_{av}/K_{ae} + \eta_{av}/\eta_{ap}\right)}{{K_{av}}^2 + \omega^2{\eta_{av}}^2}} \quad (2.48)$$

$$K_{ae} = \lim_{\omega\to\infty} |E^*| \quad (2.49)$$

$$\eta_{ap} = \lim_{\omega\to 0} \frac{|E^*|}{\omega} \quad (2.50)$$

ε_{max} and ε_{min} are the maximum and the minimum compressive strain, respectively, as measured in a compacted specimen during the dynamic modulus tests. σ_{max} and σ_{min} are the corresponding maximum and minimum applied compressive stress.

Equations (2.46) - (2.50) help determine the parameters for a fixed temperature and air voids content and at different loading frequencies (Liu et al., 2009). However, the air voids content, mix temperature, and binder viscosity all vary during field compaction. In

order to account for these effects, the parameters $K_{ae}, \eta_{ap}, K_{av},$ and η_{av} are each expressed in the form stated in Equation (2.51):

$$f(V_a, T) = p_{00} + p_{10}V_a + p_{01}T + p_{20}{V_a}^2 + p_{11}V_aT + p_{02}T^2 + p_{30}{V_a}^3 + p_{21}{V_a}^2T + p_{12}V_aT^2 + p_{03}T^3 \quad (2.51)$$

where, V_a is the air voids content; T is the temperature; and p_{ij}'s are the coefficients of the polynomial to be determined.

2.6 Chapter Conclusions

In this chapter, a lumped element model was developed to capture the interaction of the vibratory roller and the asphalt pavement during field compaction. Viscoelastic properties of asphalt mixtures were used to describe three types of deformations (plastic, instantaneous elastic, and delayed viscoelastic) that an asphalt mat would undergo in response to the loading force of the vibratory roller. A mechanistic representation of the dynamics of the roller and the visco-elastic-plastic behavior of the asphalt pavement were first presented. The governing equations of the interaction between the vibratory roller and the asphalt mat during field compaction were then derived. The parameters of the model are shown to be easily determined from the roller specifications and from the material properties of the asphalt mix. The boundary conditions for the transition between the loading ('contact') and the unloading ('bounce') states of the asphalt pavement during compaction were specified.

Chapter 3 VALIDATION OF THE VISCO-ELASTIC-PLASTIC MODEL

3.1 Introduction

The Visco-Elastic-Plastic "VEP" model was introduced in Chapter 2. The derivation of the constitutive equations of the interaction between the roller and the asphalt mat were presented. A method to determine the parameters of the model elements and the specification of boundary conditions was also introduced in Chapter 2. The VEP model is capable of capturing the behaviors of both the asphalt mat and the vibratory roller during compaction. In this chapter, the validation of the VEP model is conducted using numerical simulations. In addition, the results of different simulation scenarios are presented and compared with field measured data.

3.2 Determination of the Model Parameters

3.2.1 Parameters of the Vibratory Roller

The VEP model and the method to estimate its parameters are evaluated in predicting the behavior of the roller-asphalt coupled system. An Ingersoll Rand DD118HF vibratory compactor is used to examine the validity of the proposed process. The drum mass, drum width, frame mass, drum-asphalt contact area and contact length, drum-frame stiffness coefficient and damping coefficient, eccentric rotational frequency, and the eccentric moment are determined from the manufacturer's specifications of the roller. The values for an Ingersoll Rand DD118HF compactor are shown in Table 3.1.

Table 3.1 Dynamic parameters of an Ingersoll Rand DD118HF vibratory compactor

Symbol	Description	Unit	Source	IR DD118 HF
η_{df}	drum-frame damping coefficient	N/m	manufacturer	544
K_{df}	drum-frame stiffness coefficient	N/m	manufacturer	3400
m_f	frame mass (@ a single drum)	kg	spec sheet	4225
m_d	drum mass	kg	spec sheet	2371
$m_{ec}e_{ec}$	eccentric moment	kg.m	derived	1.45
ω_{ec}	eccentric rotational frequency	rad/s	measured	314
W	drum width	m	spec sheet	2
A	drum/asphalt contact area	m^2	derived	0.016

3.2.2 Parameters of the Asphalt Pavement

In the simulation results reported in this chapter, it is assumed that the roller is compacting a surface course pavement comprised of 12.5mm (0.5 in.) Nominal Maximum Aggregate Size (NMAS) S4 (76-28 OK) hot mix asphalt (HMA). *In the simulation, the underlying pavement layers are assumed to be stiff and to have negligible influence on the vibratory characteristics of the compactor.* The gradations for the selected mix are shown in Table 3.2. The four parameters ($K_{ma}, \eta_{ma}, K_{ka},$ and η_{ka}) of the asphalt pavement section of the VEP model are estimated indirectly through the measurement of the complex modulus E* of the compacted mix. Laboratory testing according to AASHTO TP-62 standard procedure (AASHTO, 2007b) is first performed to determine the dynamic modulus $|E^*|$and the phase angle ϕ of the mix at different temperatures, air voids contents, and loading frequencies (see Figures 3.1 and 3.2).

Table 3.2 Gradation for mix S4 (PG 76-28 OK)	
Sieve Size	**Job Formula (% Passing)**
1 in.	100
3/4 in.	98
1/2 in.	87
3/8 in.	80
No. 4	62
No.8	40
No.16	27
No.30	20
No.50	12
No.100	5
No.200	2.8

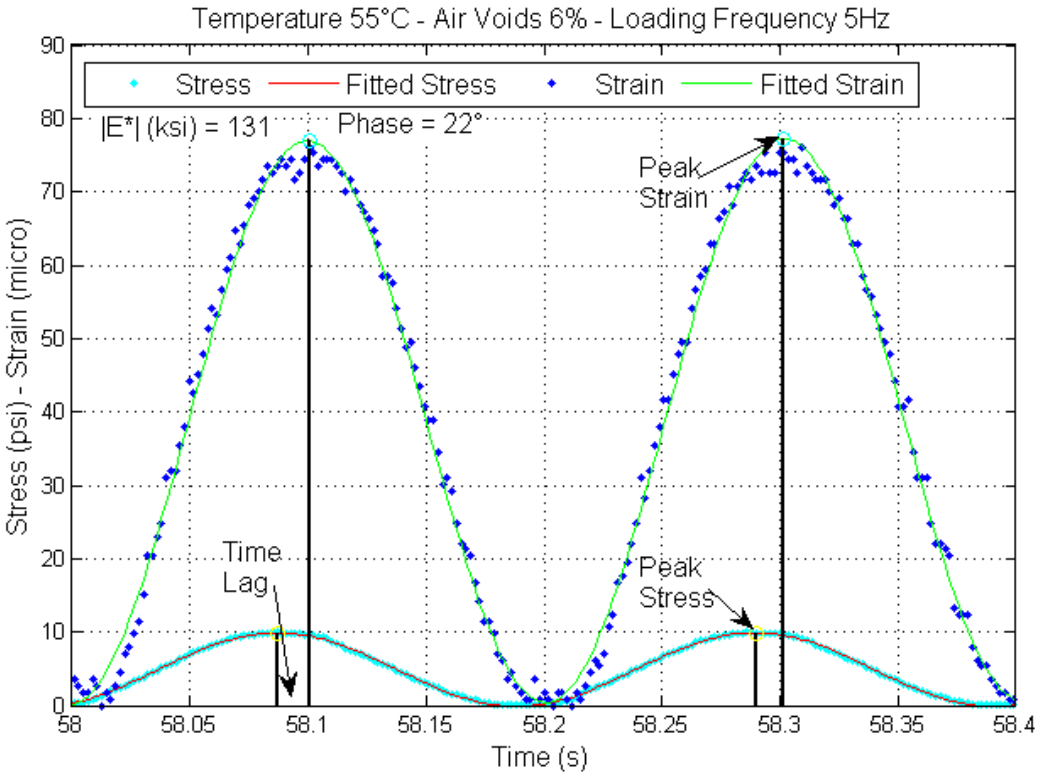

Figure 3.1 Dynamic modulus and phase angle as determined from the stress and strain as measured according to AASHTOO TP-62 standard test.

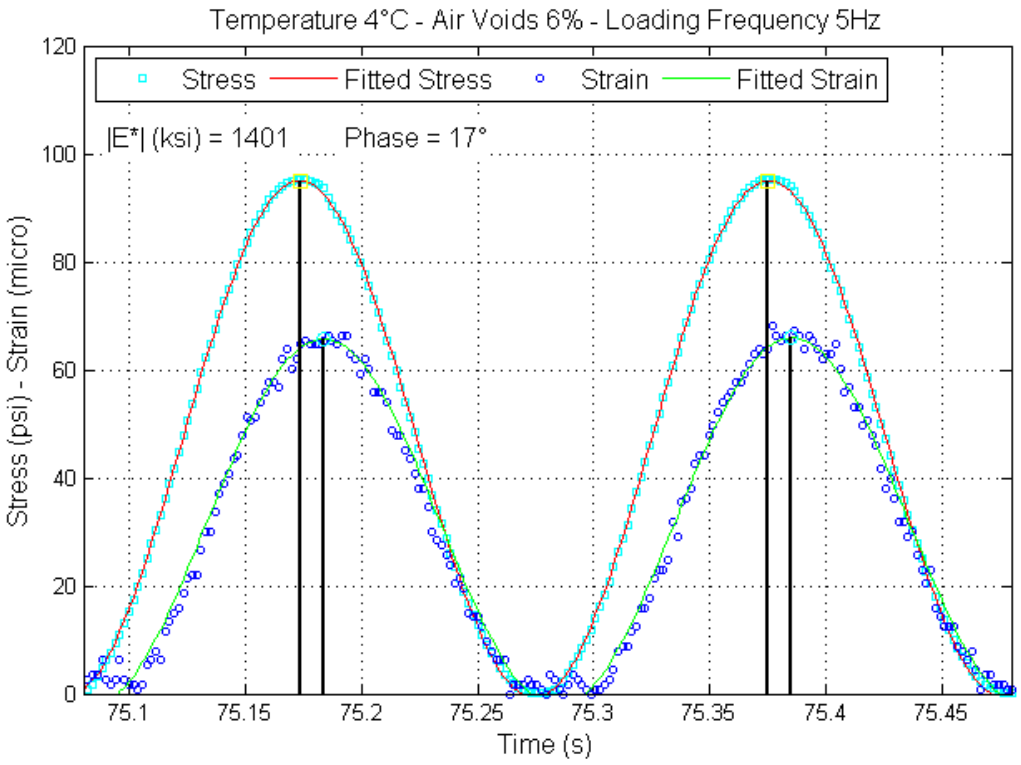

Figure 3.2 Dynamic modulus and phase angle as determined from the stress and strain as measured according to AASHTOO TP-62 standard test.

The parameters , , , and are functions of temperature and air voids content of the asphalt mix. These relationships are determined from the dynamic modulus testing of the asphalt mix according to AASHTO TP-62 test procedure. Following the procedure in Chapter 2, the coefficients in Equation (2.51) were determined for each of the model parameters, , , , and and are expressed as follows:

(3.1)

$$\eta_{ap}(V_a, T) = 7733 + 1656V_a - 144.4T - 138.4{V_a}^2 - 6.8V_aT + 1.1T^2 + 0{V_a}^3 + 0.82{V_a}^2T - 0.025V_aT^2 - 0.0019T^3 \quad (3.2)$$

$$K_{av}(V_a, T) = 4764 - 443.6V_a - 53.5T + 14.4{V_a}^2 + 3.3V_aT + 0.26T^2 + 0{V_a}^3 - 0.079{V_a}^2T - 0.0059V_aT^2 - 0.00049T^3 \quad (3.3)$$

$$\eta_{av}(V_a, T) = 387.7 - 96V_a - 1.3T + 8.7{V_a}^2 + 0.11V_aT + 0.0049T^2 - 0.26{V_a}^3 - 0.0043{V_a}^2T - 0.000096V_aT^2 - 0.0000096T^3 \quad (3.4)$$

Three-dimensional plots of K_{ae}, η_{ap}, K_{av}, and η_{av} are shown in Figures 3.3 and 3.4.

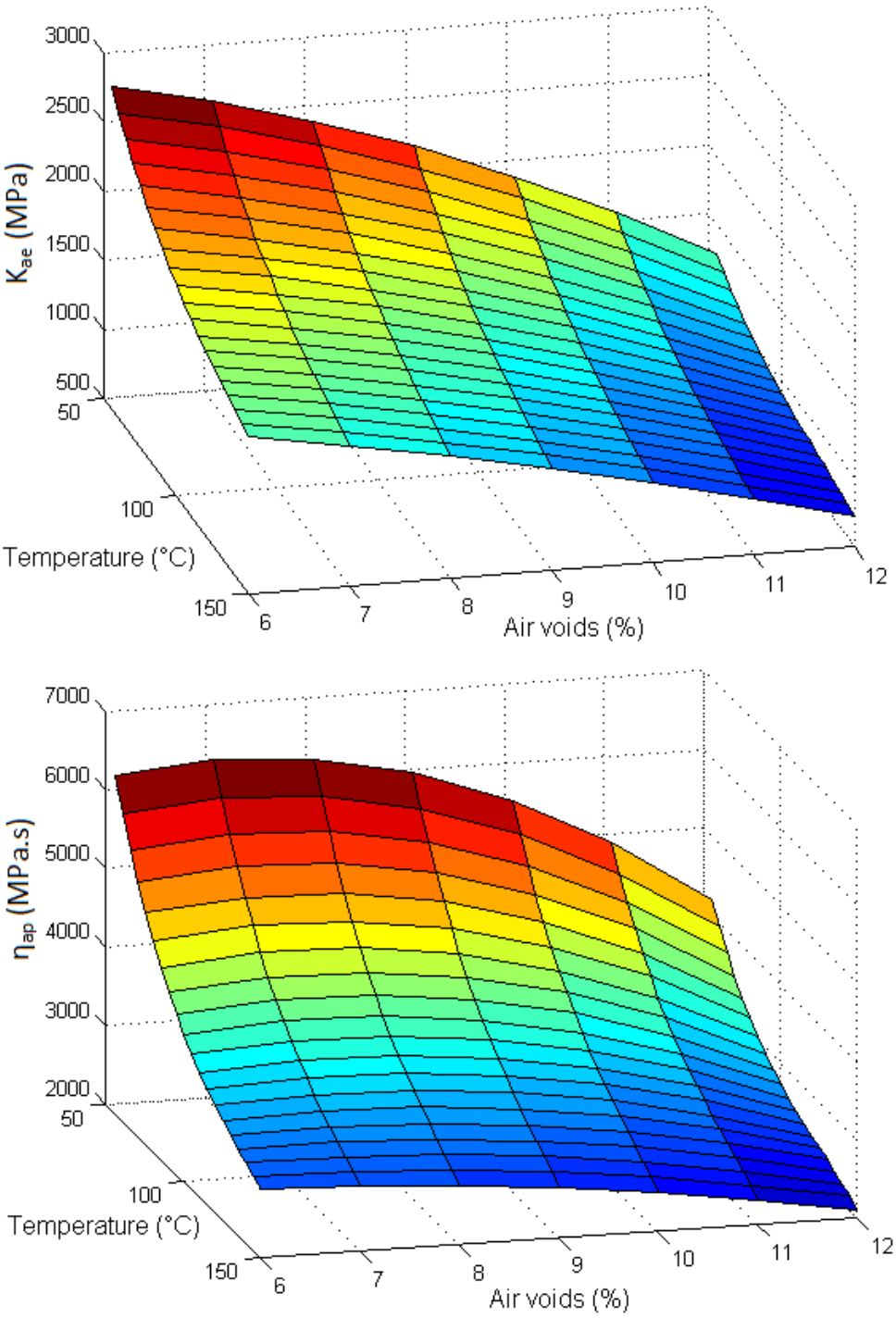

Figure 3.3 Three-dimensional plots of , as function of air voids and temperature.

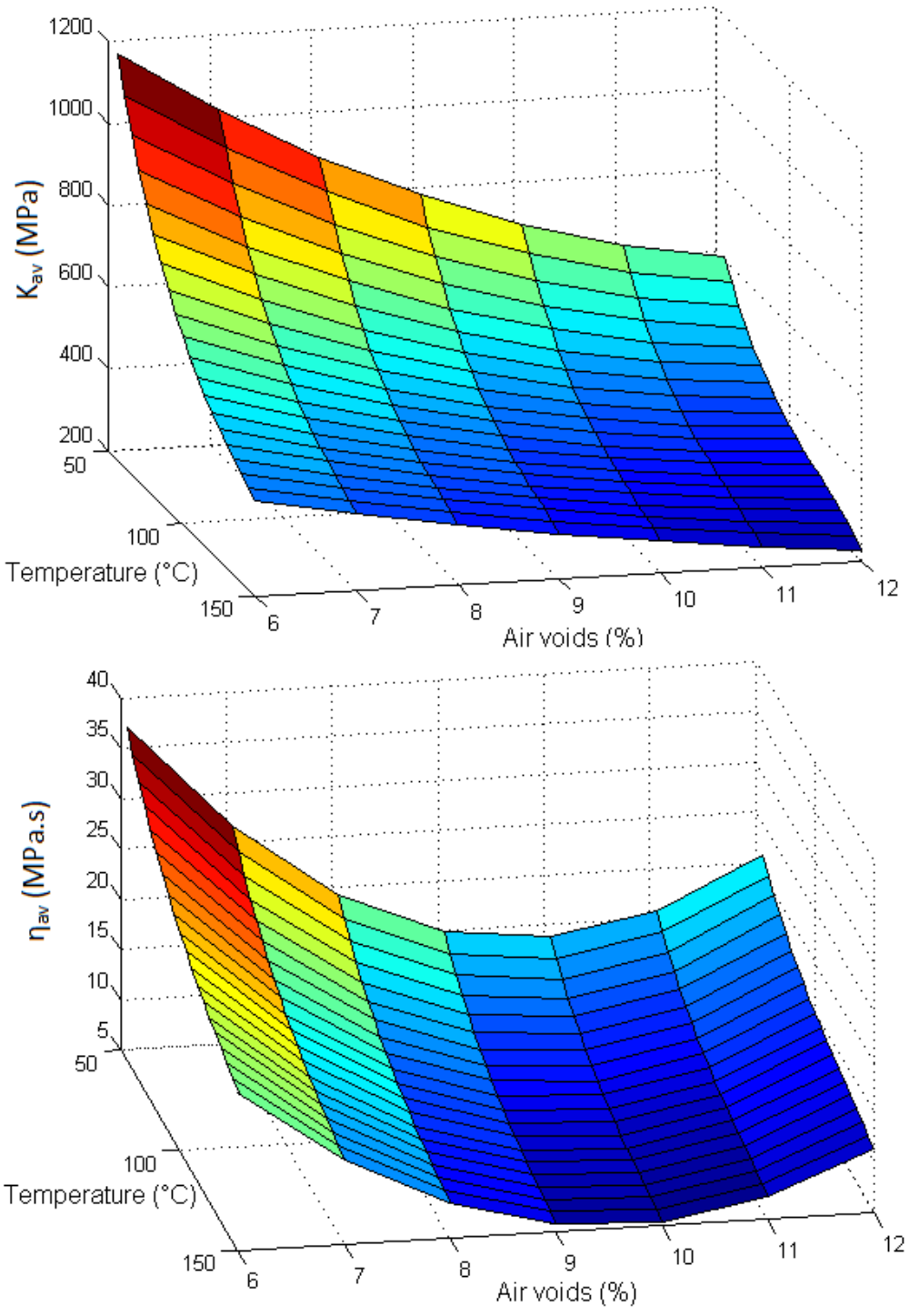

Figure 3.4 Three-dimensional plots of , as function of air voids and temperature.

Tables 3.3 and 3.4 show the effect of the temperature and air voids content on the parameters of the asphalt pavement model. As the temperature increases, the stiffness of the asphalt mix increases. This is reflected in the numerical values of K_{ae} and K_{av}. The viscosity of the binder also increases with an increase in temperature, as seen in the values of η_{ap} and η_{av}.

Table 3.3 Effect of the temperature on the parameters of the asphalt pavement model at 6% air voids content.

T (°C)	**150**	**140**	**130**	**120**	**110**	**100**
K_{ae} (MPa)	1713.1	1778.3	1849.7	1930.5	2024.0	2133.4
η_{ap} (MPa.s)	3063.3	3232.2	3418.1	3632.5	3887.2	4193.8
K_{av} (MPa)	453.9	486.5	522.2	564.1	615.1	678.2
η_{av} (MPa.s)	21.2	22.2	23.2	24.3	25.6	27.2

Table 3.4 Effect of the air voids content on the parameters of the asphalt pavement model at 150°C.

V_a (%)	**12**	**10**	**8**	**6**	**4**
K_{ae} (MPa)	622.4	1034.4	1397.9	1713.1	1980.0
η_{ap} (MPa.s)	1869.2	2385.5	2783.5	3063.3	3224.9
K_{av} (MPa)	214.7	273.7	353.4	453.9	575.1
η_{av} (MPa.s)	10.8	7.3	6.7	21.2	63.2

3.3 Numerical Simulation of the VEP Model

Equations (2.13) to (2.21) from Chapter 2, which describe the dynamics of the coupled system, were implemented as Simulink and Stateflow simulation models in Matlab® (Mathworks, 2009).

3.3.1 Simulation of Static Rolling of HMA Pavement

During the simulation of static rolling, the roller is assumed to be operating at rated speed. This implies that the load on a particular strip of an asphalt mat representing the contact area with the drum (see Figure 2.3) increases from zero to its peak value as the roller approaches the contact strip. The load is at a maximum when the drum is fully in contact with the asphalt strip and reduces to zero as the roller moves away. During compaction, each such strip is subjected to between 6-9 loading cycles depending on the rolling pattern that is adopted.

The results of a simulated finish rolling using a static steel drum roller (Ingersoll Rand DD118HF) are shown in Figure 3.5. It is assumed that the finish rolling is performed on a single layer comprised of 76.2mm (3 in.) asphalt pavement (12.5mm PG 76-28 OK). Figure 3.5(a) shows the loading force (equals weight of drum and frame for static rolling) that the roller applies on the contact strip. The temperature profile of the asphalt mix during rolling process is also shown in Figure 3.5(a). In the simulation, it is assumed that the asphalt mix is laid down at 150°C and subsequently decreases to cessation temperature (50°C). *It is to be noted that the parameters* ($K_{ae}, \eta_{ap}, K_{av},$ and η_{av}) *of the VEP model representing the asphalt pavement change over time based on the temperature profile and air voids content*. This variation is taken into account during the simulation process. The compaction achieved with static rolling and the stiffness of the pavement is shown in Figure 3.5(b). This figure shows the air voids content reduction and dynamic modulus change during rolling

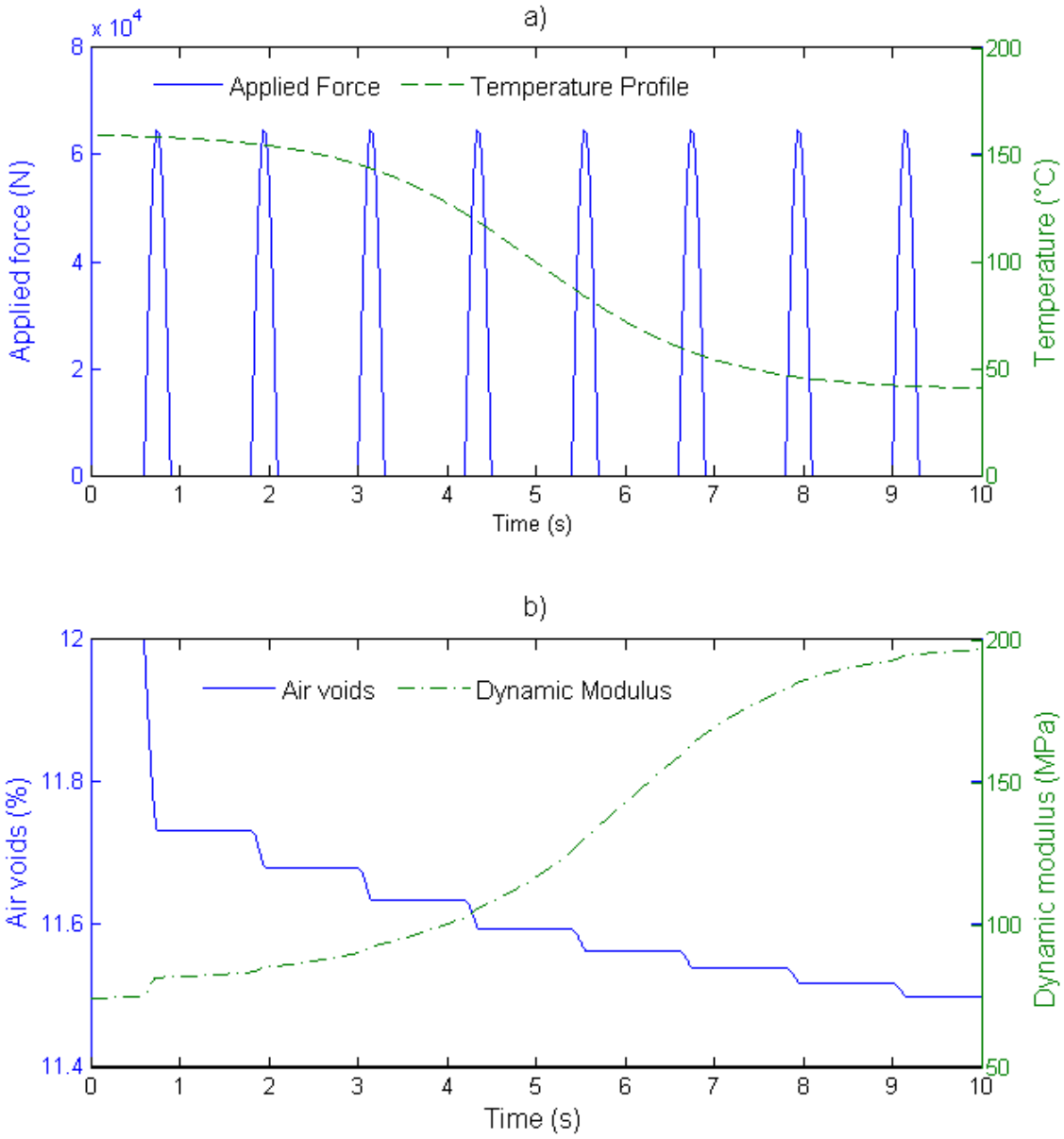

Figure 3.5 Simulation results of field compaction via static loading.

3.3.2 Simulation of Vibratory Compaction of HMA Pavement

It is assumed that the asphalt mix is initially placed at a temperature of 150°C and having 12% air voids. Two temperature profiles are used as follows: i) temperature held constant at 150°C; ii) temperature changing from 150°C to 100°C. The compactor is

assumed to apply impulsive force at a frequency of 50Hz (314 radians/sec). The reduction in air voids in the asphalt mix as a result of compaction is shown in Figure 3.6.

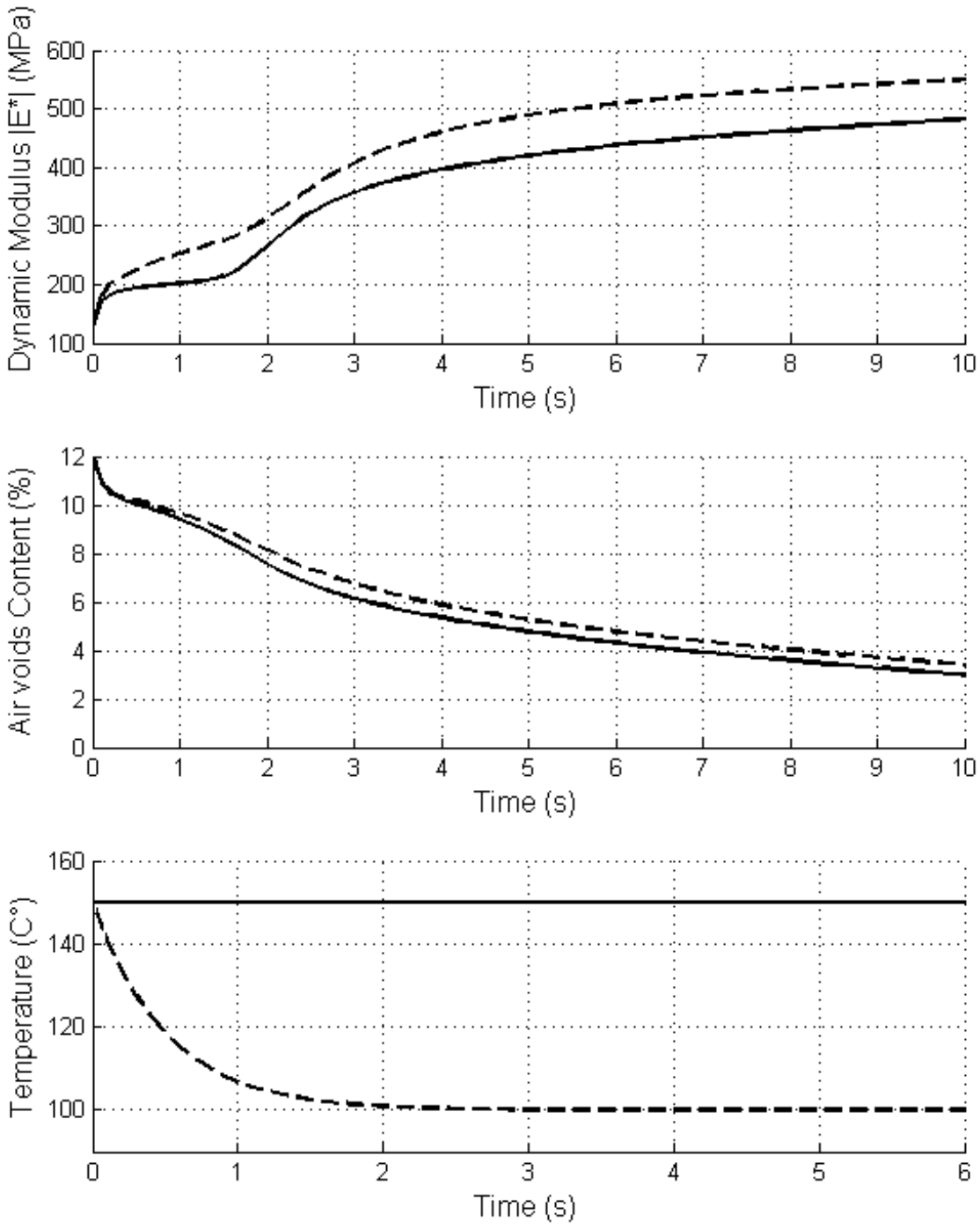

Figure 3.6 Compaction of a 50 mm asphalt surface course using IR DD118HF roller.

3.3.3 Effect of Temperature and Thickness of Asphalt Mat on Compaction

Two sets of simulations are performed to study the effect of the thickness of the pavement layer and its temperature on the vibratory compaction of asphalt mixes. The effect of the lift thickness on the compaction is considered in the first set of simulations. The compaction of a 50.8mm (2 in.) and 76.2mm (3 in.) asphalt pavement comprised of asphalt mix with a NMAS of 12.5mm (0.5 in.) and PG76-28 OK binder is studied first. Similar to the case of static rolling, an IR DD118HF roller is considered and the asphalt mat temperature is assumed to be constant at lay down temperature of 150°C. The roller is assumed to be operating at a frequency of 50Hz and moving at a constant speed of 3.2 kilometers per hour. Thus, each simulation second corresponds to approximately two roller passes on the asphalt mat.

The results of these simulations are shown in Figure 3.7. The reduction in the air voids content is shown in Figure 3.7(a), while the change in the stiffness of the asphalt mat as a result of compaction is shown in Figure 3.7(b).

In the second set of simulations the effect of variation in temperature on the quality of compaction is addressed. The first set of temperature profiles selected is as follows: i) temperature held constant at 160°C; ii) temperature changing from 160°C to 40°C; iii) temperature changing from 120°C to 40°C; and iv) temperature held constant at 40°C. The selected temperature profiles are shown in Figure 3.8(c). The second set of temperature profiles selected is as follows: i) temperature held constant at 160°C; ii) temperature changing from 160°C to 80°C; iii) temperature changing from 120°C to

80°C; and iv) temperature held constant at 80°C. The selected temperature profiles are shown in Figure 3.9(c).

The results of these simulations are shown in Figures 3.8 and 3.9. The reduction in the air voids content in the asphalt mix is shown in Figures 3.8(a) and 3.9(a) while the variation in the dynamic modulus is shown in Figures 3.8(b) and 3.9(b).

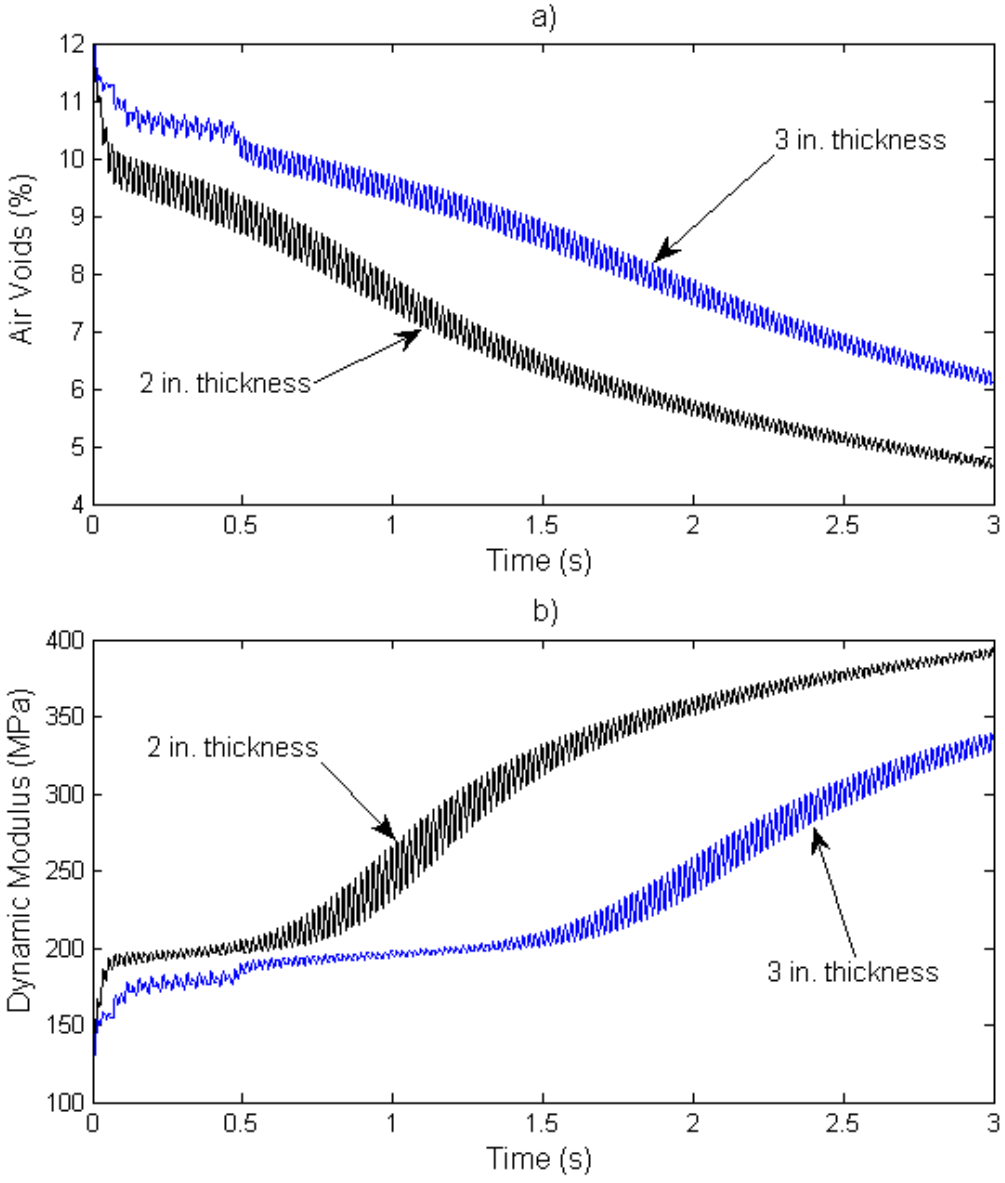

Figure 3.7 Results of vibratory compaction simulation at 150°C.

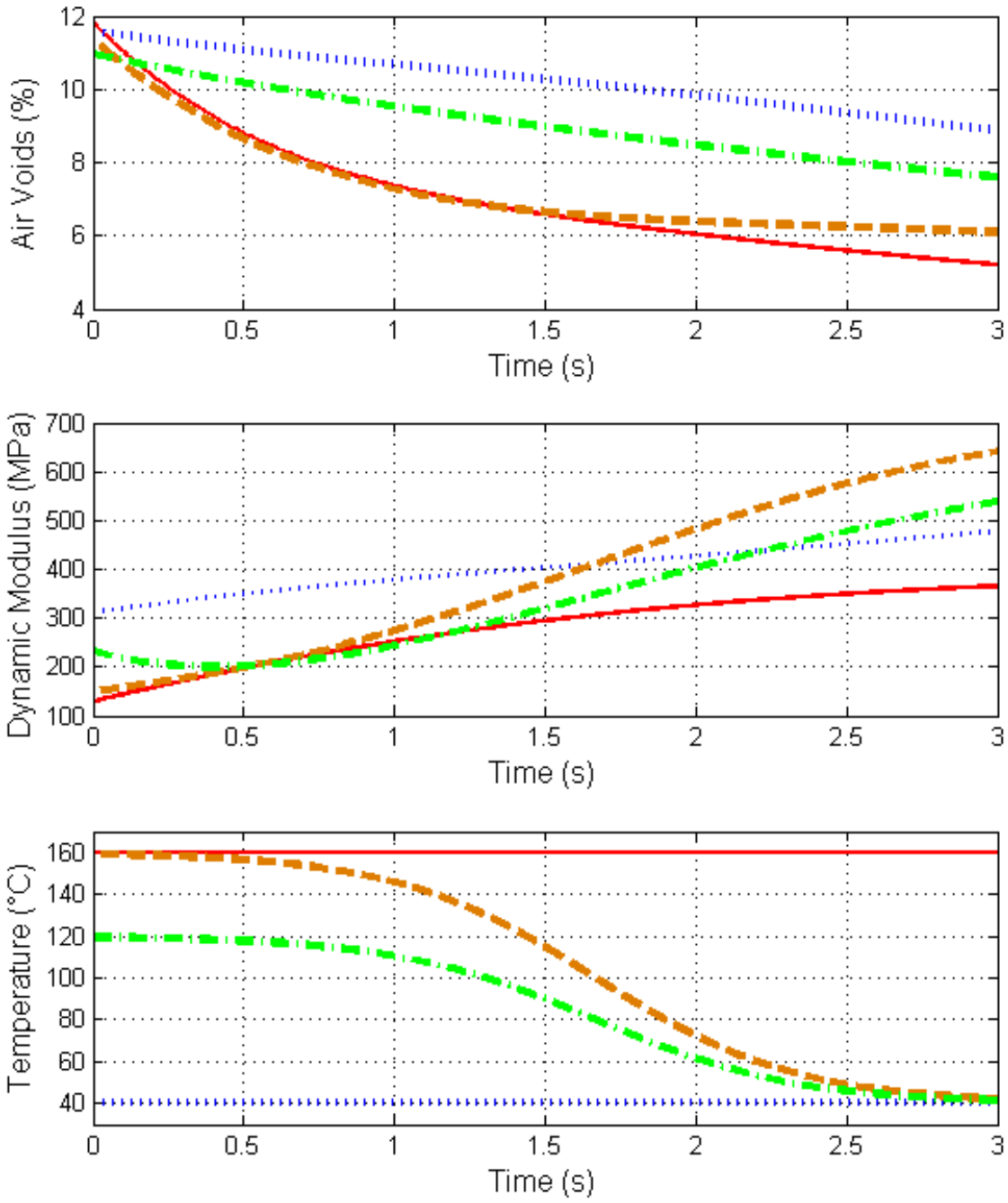

Figure 3.8 Effect of temperature on reduction in the air voids content in the asphalt mix and on the variation in its dynamic modulus during compaction (Simulation).

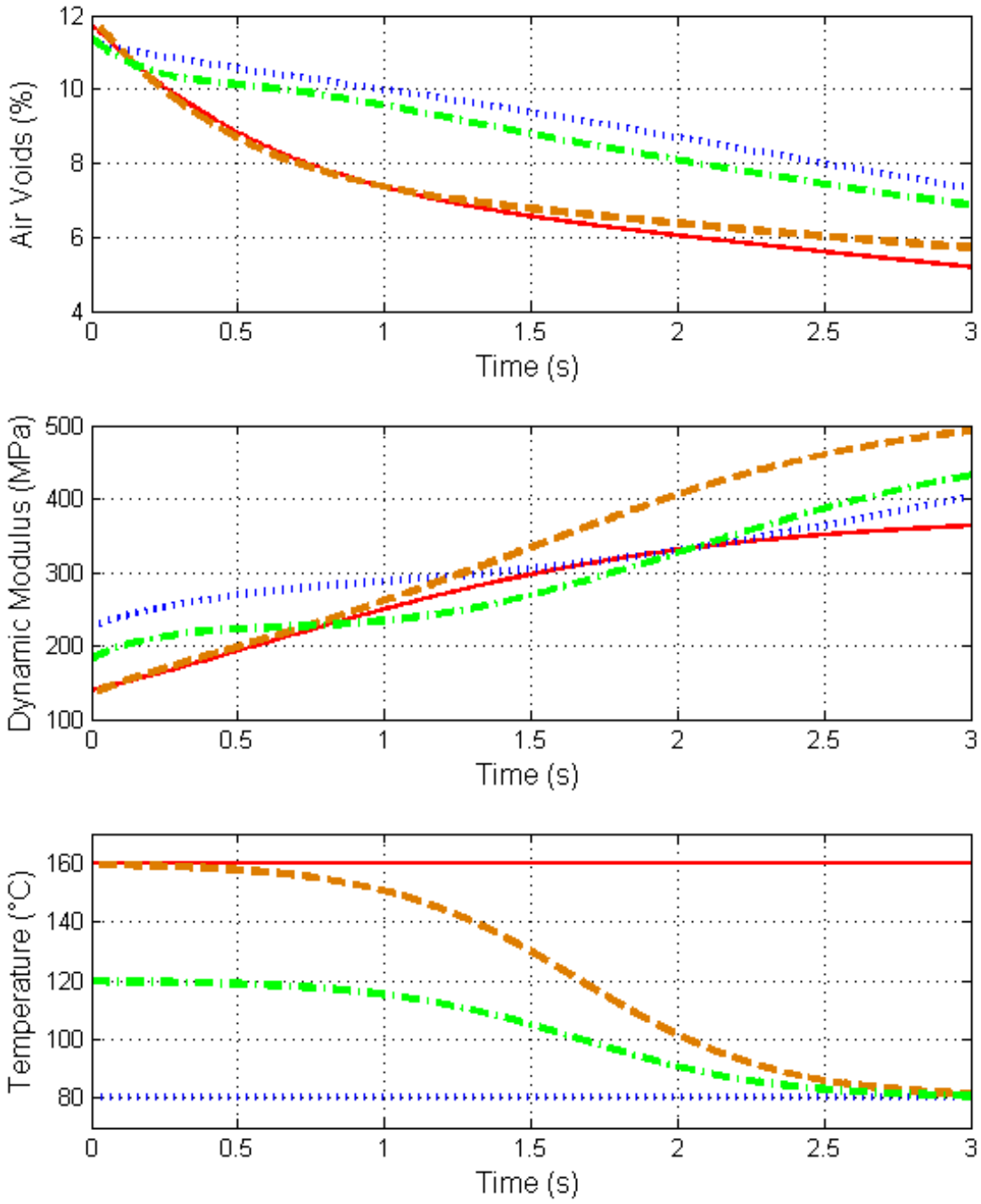

Figure 3.9 Effect of temperature on reduction in the air voids content in the asphalt mix and on the variation in its dynamic modulus during compaction (Simulation).

3.3.4 Discussion of the Results of the Simulations

The simulation results in Figure 3.5 demonstrate that the model is able to capture the behavior of asphalt pavement during static rolling. The use of static rolling during field compaction of an asphalt mix would normally result in minimal reduction in the air voids content. This is clearly seen in Figure 3.5, where less than 1% improvement in air voids is obtained as a result of static rolling. The same holds true for the resulting stiffness of the pavement as a result of static compaction.

The simulation results in Figure 3.6 demonstrate that the model is able to capture the behavior of asphalt pavement during vibratory compaction. *It can be seen from this figure that the air void content of the mix decreases as the total time of compaction increases. Furthermore, the stiffness of the mix also increases with compaction.* It is also seen that the air voids in the asphalt mix reduce by approximately 4% in the first two seconds, 2% during next two seconds, and 2% during seconds 4 - 10 of compaction. This validates the fact that for a given compactive effort, it is harder to achieve compaction as the stiffness of the material increases.

From Figure 3.7 it can be seen that identical effort would result in higher compaction of a thin pavement layer compared to a thicker pavement layer. Experimental results from field compaction validate this observation. In fact, experience shows that higher compaction is usually achieved in thin surface courses as compared to thick base or intermediate pavement layers (Commuri, 2009a).

During compaction in the field, the asphalt mix is produced at the plant and is transferred to the construction site at approximately 160°C. The asphalt mat is laid down

by the paver at approximately 150°C. The roller operator has a limited temperature window (i.e. before the asphalt mix cools down to cessation temperature) during which breakdown rolling has to be completed. The rate at which the asphalt mat cools is determined by factors such as ground temperature, ambient temperature, wind conditions, pavement thickness, etc. The effect of the temperature on the air voids as well as the stiffness of the asphalt mat can be seen in Figures 3.8(a), 3.8(b), 3.9(a), and 3.9(b). It is evident that compaction is most effective at laydown temperature and least effective at temperatures close to cessation temperatures.

3.4 Validation of the VEP Model

The validity of the proposed model is investigated by comparing the simulation results to data collected during the construction of a 50mm (2 in.) surface course on interstate I-35 in Norman, Oklahoma. This construction project involved the expansion of the existing highway, stabilizing the subgrade to a depth of 200mm (8 in.) using 10% cement kiln dust (CKD), followed by 200mm (8 in.) thick aggregate base. The asphalt concrete base layer consisted of 100mm thick asphalt layer of 19mm (0.75 in.) NMAS S3 (64-22 OK), while the second and third layers were constructed with 19mm (0.75 in.) NMAS S3 (76-28 OK) of 100mm (4 in.) and 75mm (3in) thickness, respectively. A 50mm surface course of 12.5mm (0.5 in.) NMAS S4 (76-28 OK) was compacted on top of the three asphalt layers. During the construction of the surface course, the vibrations of the compactor were measured using a 13200C uniaxial accelerometer from Summit Instruments, mounted on the axle of the drum (Summit Instrument 2010). The acceleration of the drum during compaction corresponding to 9%, 8%, 7%, and 6% air voids in the asphalt mix is shown in Figure 3.10. It can be seen from the figure that the

model accurately captures the fundamental frequency of vibrations of the roller. Furthermore, the model correctly predicts the increase in the magnitude of the drum acceleration as the stiffness of the asphalt mat increases.

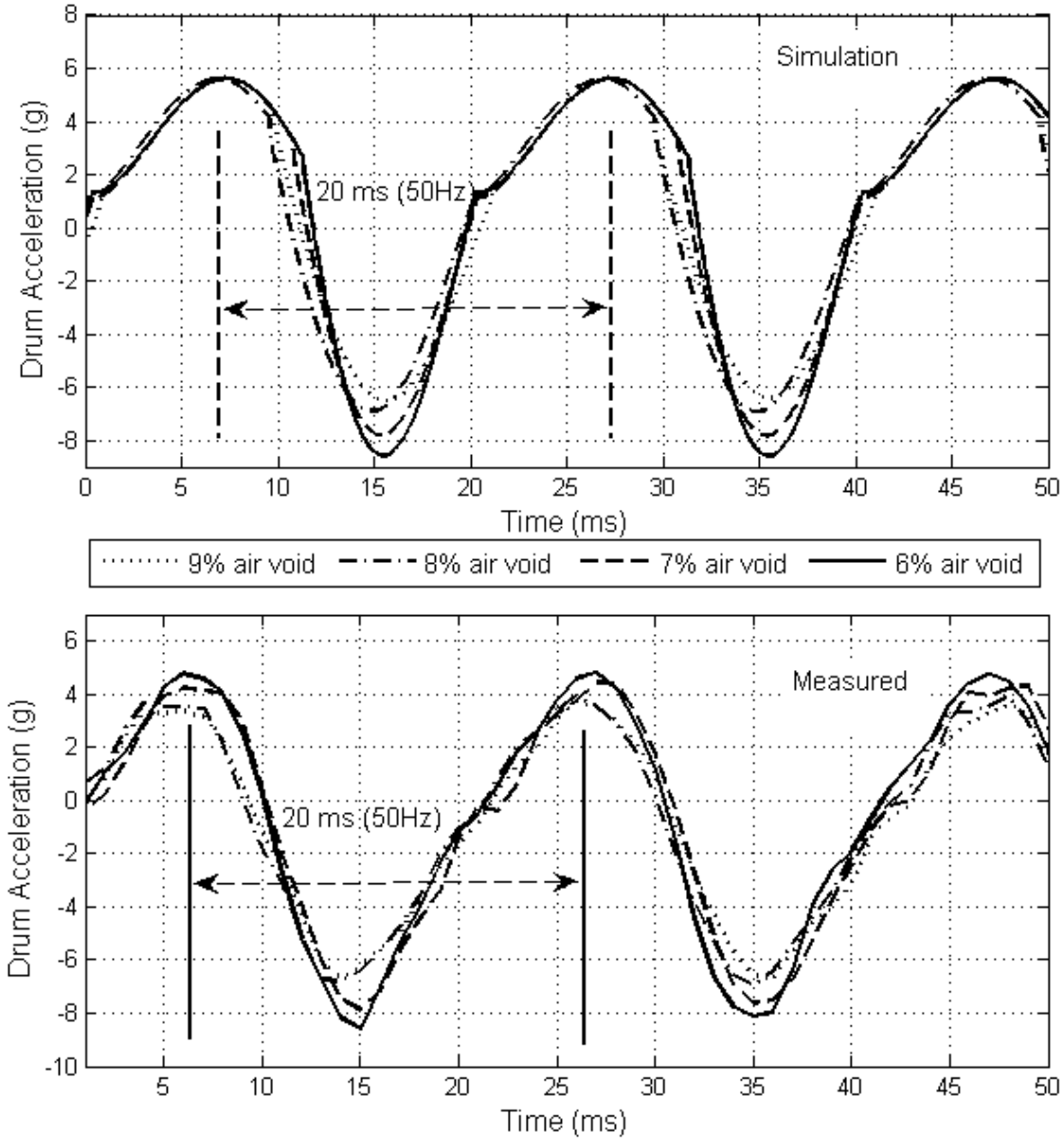

Figure 3.10 The acceleration of the drum during compaction: (a) predicted by the model; (b) measured during field compaction.

Intelligent Compaction methods are based on the hypothesis that the vibratory compactor and the asphalt mat form a coupled system and that the response characteristics of the roller depend on the stiffness of the underlying material. Furthermore, increased stiffness of the asphalt mat results in higher frequency components in the vibrations of the roller. The frequency components of the roller vibrations, measured and simulated, were extracted using Fast Fourier Transform (FFT). Figure 3.11(a) shows the spectrogram of the vibrations of the roller drum as measured in the field during compaction. Figure 3.11(b) shows the spectrogram of the vibrations of the roller drum as recorded during numerical simulations. Analysis of the simulated compaction shows that the power content of the harmonic frequencies increases with an increase in compaction (Figures 3.12 and 3.13). Two temperature profiles are used as follows: i) temperature held constant at 135°C (Figure 3.12); ii) temperature changing from 150°C to 100°C (Figure 3.13). Figure 3.14 shows the power at each of the harmonic frequencies of the roller during the field compaction of the pavement. Finally, it can be seen from Figures 3.11 - 3.14 that the proposed model provides salient information regarding roller dynamics during field compaction. Comparison of the two spectrograms of Figure 3.11(a) and (b) demonstrates that the model adequately represents the field compaction of asphalt mixes. Finally, comparison with the power content of the harmonics in the roller vibrations during actual compaction (Table 3.5) demonstrates that the simulated results are a good representation of the compaction in the field.

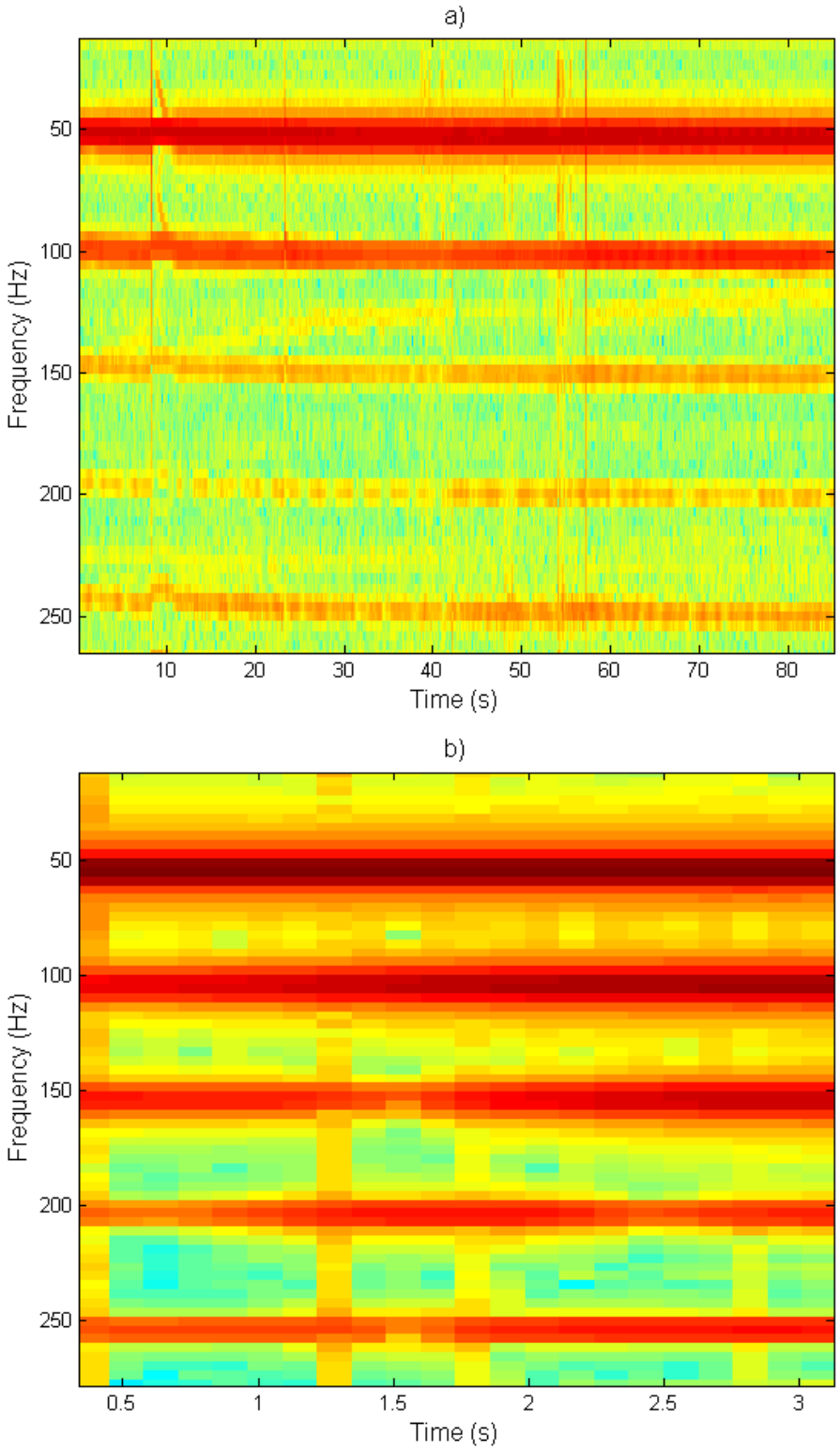

Figure 3.11 a) Measured roller vibrations in the frequency domain b) simulated roller vibrations in the frequency domain.

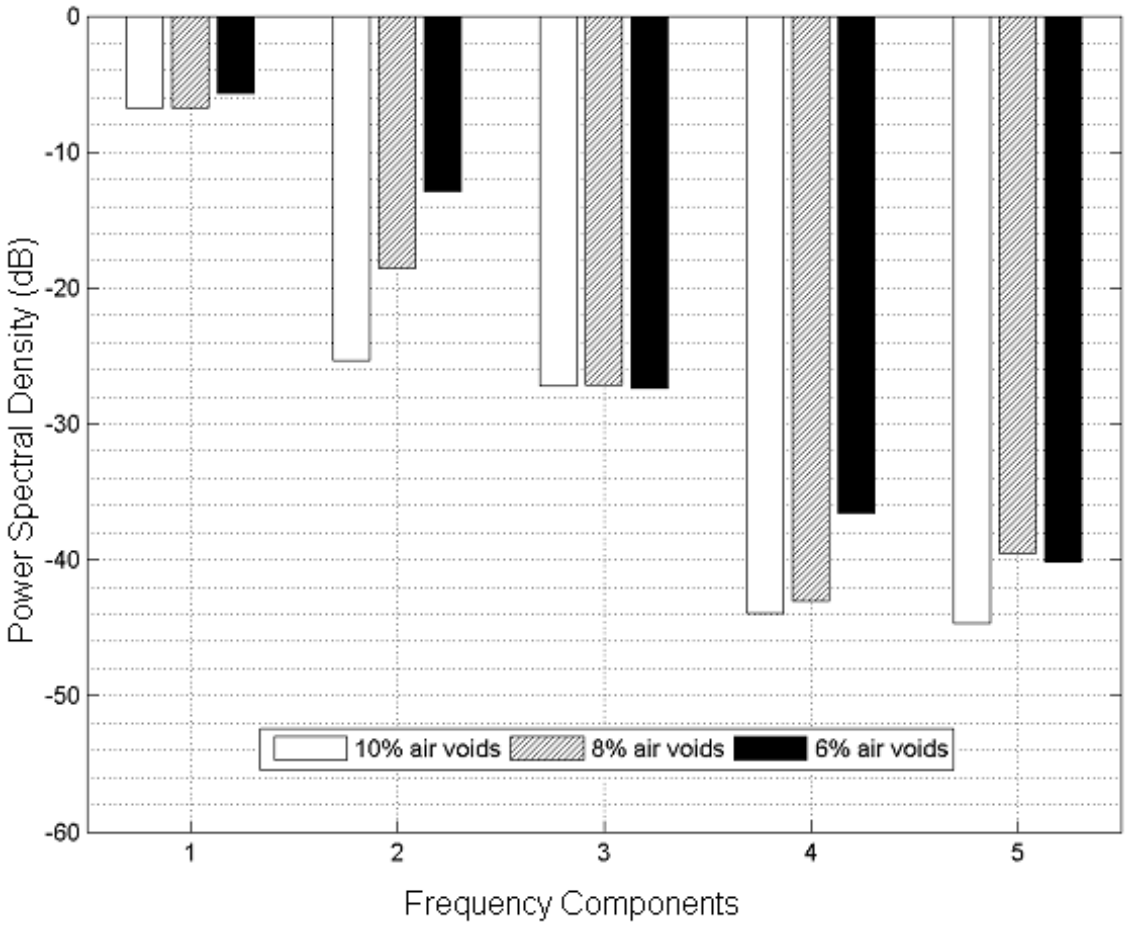

Figure 3.12 Power content in the fundamental frequency and its harmonics at 10%, 8%, and 6% air voids and at constant temperature 135°C (Simulated Dynamics).

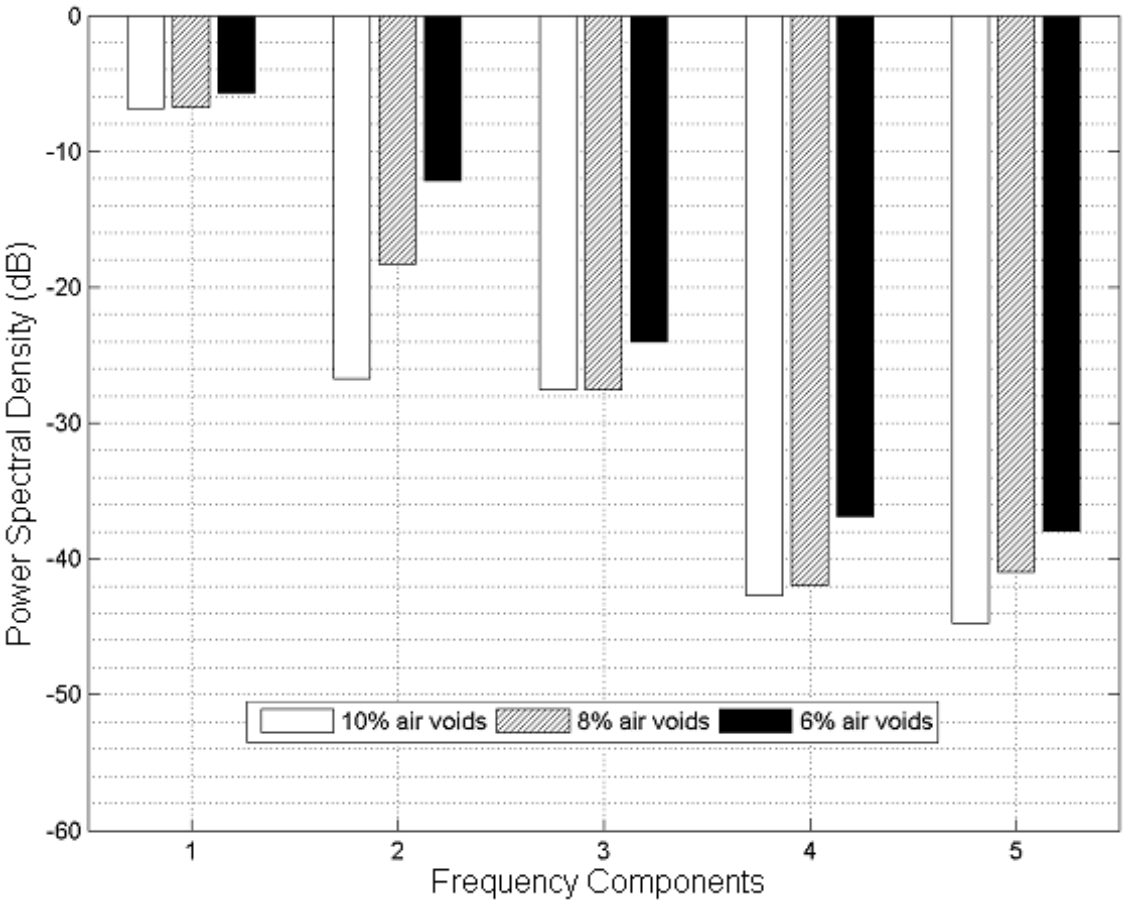

Figure 3.13 Power content in the fundamental frequency and its harmonics at 10%, 8%, and 6% air voids with temperature changing from 150°C to 100°C (Simulated Dynamics).

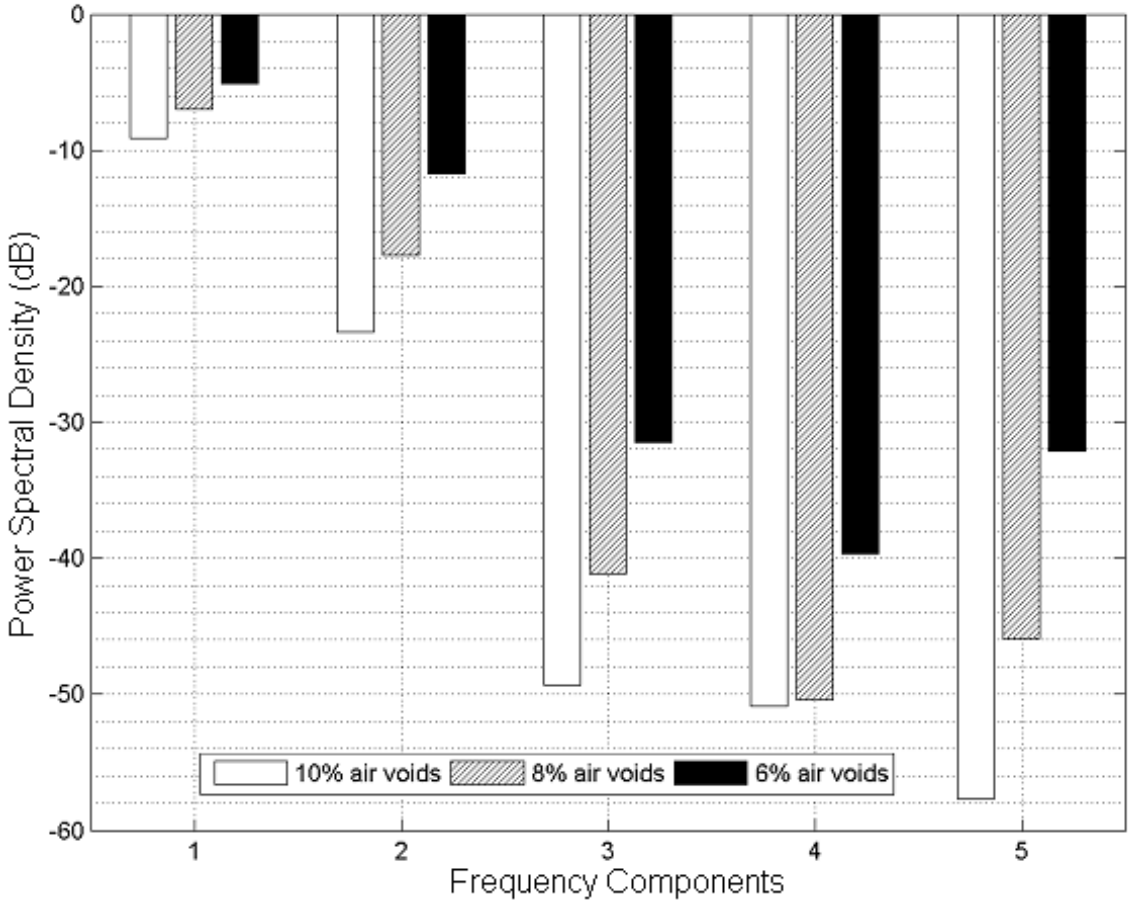

Figure 3.14 Power content in the fundamental frequency and its harmonics at 10%, 8%, and 6% air voids (IR DD118HF roller during field compaction).

Table 3.5 Variation in the power level (in dB) of the harmonics with compaction

Air Voids	Harmonic (Frequency)									
	1st (50Hz)		2nd (100Hz)		3rd (150Hz)		4th (200Hz)		5th (250Hz)	
	Sim.	Meas.	Sim.	Meas.	Sim.	Meas.	Sim.	Meas.	Sim.	Meas.
10%	-7.0	-9.2	-25.8	-23.4	-27.8	-49.3	-42.5	-50.9	-44.9	-57.7
8%	-6.8	-7.0	-18.2	-17.7	-27.8	-41.1	-41.9	-50.4	-41.0	-45.9
6%	-5.8	-5.1	-12.2	-11.7	-24.0	-31.4	-37.0	-39.7	-37.9	-32.2

3.5 Chapter Conclusions

In Chapter 2, a mathematical model was developed with an aim to understand the interaction between an asphalt pavement layer and the vibratory compactor during the construction of asphalt pavements. The model takes into account the visco-elastic-plastic properties of the asphalt mat and the dynamics of the roller in order to predict the effect of compaction on the vibrations of the roller drum. The parameters of the model were shown to be easily derived from the roller specifications and from the material properties of the asphalt mix. In this chapter, simulation results showed that the model accurately predicts the compaction of hot mix asphalt in the field. Numerical simulations of static compaction resulted in minimal reduction in the amount of air voids content, revealing that the model has the basic feature to describe field asphalt compaction. Another set of simulations proved that the model is able to capture the asphalt mat thickness effect on the compaction outcome. Furthermore, additional simulations showed that the model can capture the temperature cooling effect on the compaction process and on the workability of the mix, and the effect of starting compaction at a temperature below optimum. Finally, comparison of the simulation results with data gathered during construction of asphalt pavements indicate that this model lays the theoretical groundwork for the realization of Intelligent Compaction of asphalt pavements.

Chapter 4 INTELLIGENT ASPHALT COMPACTION ANALYZER

4.1 Introduction

The Intelligent Asphalt Compaction Analyzer (IACA) is a non-contact sensor that can measure the density of an asphalt pavement continuously in real-time, over the entire length of pavement during its construction. Quality Control techniques currently used in the field involve the measurement of density at several locations on the completed pavement or the extraction of roadway cores. These methods are usually time consuming and do not reveal the overall quality of the construction. Furthermore, any compaction issues that are identified cannot be easily remedied after the asphalt mat has cooled down. The ability of the IACA to measure the level of compaction of the asphalt pavement during its construction will enable the roller operator to identify and remedy under-compaction of the pavement while avoiding over-compaction.

In recent years, several Intelligent Compaction (IC) technologies have been introduced by manufacturers of vibratory compactors (Arasteh, 2007; Briaud and Seo, 2003; Camargo et al., 2006; CTC, 2006; Wisdom, 2009; Moore, 2006; Petersen, 2005; Peterson and Petersen, 2006; Thompson, 2006). Uniform compaction of both soil and aggregate bases is achieved through the variation of the machine parameters (amplitude and frequency of vibrations, vectoring of the thrust, etc.). Dynamic control of the machine parameters allows for the application of the vibratory energy only to under-compacted areas and thereby preventing over-compaction and ensuring uniform compaction of the soil/aggregate base (Petersen, 2005; Peterson and Petersen, 2006).

These IC techniques hold promise for the future and their performance is being evaluated by several agencies, including the Federal Highway Administration (FHWA) (Chang et al., 2008). However, one of the limitations of these IC technologies is that the measurement values reported by these devices cannot be easily verified through in-situ measurements of density or dynamic modulus.

The IACA is a measurement device that does not control any aspect of the machine behavior. The IACA is a standalone device that can be retrofitted on any existing vibratory compactor. The main utility of the IACA is in providing real-time measurements of the density of the asphalt mat at each location on the pavement under construction. This information can be utilized by the roller operator to ensure uniform compaction, address under-compaction, as well as prevent over-compaction of the pavement.

The rest of this chapter is organized as follows. Overview and operational principle of the IACA technology are discussed in Section 4.2. Overall results of the field evaluation of the IACA are presented in Section 4.3. Finally, detailed descriptions of the field evaluations at different construction sites are presented in Section 4.4.

4.2 Overview and Operational Principle of the IACA

The Intelligent Asphalt Compaction Analyzer (IACA) is based on the hypothesis that a vibratory compactor and the hot mix asphalt (HMA) mat form a coupled system having unique vibration properties that can be identified by analysis of the power spectrum distribution (refer to Chapters 2 and 3). The response of the roller is determined by the frequency of its vibratory motors and the natural vibratory modes of this coupled system.

Compaction of an asphalt mat increases its stiffness and consequently, the vibrations of the compactor (coupled system) are altered. The knowledge of the properties of the asphalt mat and the vibration spectrum of the compactor can therefore be used to estimate the stiffness of the asphalt mat.

Accelerometer measurements are used to extract relevant features from the power spectrum of the vibrations of the roller drum. These features are then classified by frequency and signal power and an Artificial Neural Network (ANN) based pattern recognition approach is used to continuously measure the degree of compaction in real-time. At this time, since the quality specifications are usually specified as percentage air voids content or as a percentage of the Maximum Theoretical Density (MTD) of the asphalt mix, the IACA estimates the compacted density of the pavement rather than the stiffness (Commuri and Zaman, 2007; Commuri, 2009b; Commuri and Zaman, 2010; Commuri et al., 2009; Commuri et al., 2011).

4.2.1 Functional Specifications of the IACA

The functional specifications of the IACA can be categorized into the following sub-groups: Sensing Specifications, Operational Specifications, Calibration Specifications, Display and Recording Specifications, and Training and User Documentation. The overall functional model is shown in Figure 4.1 and the specifications are discussed in the following sections.

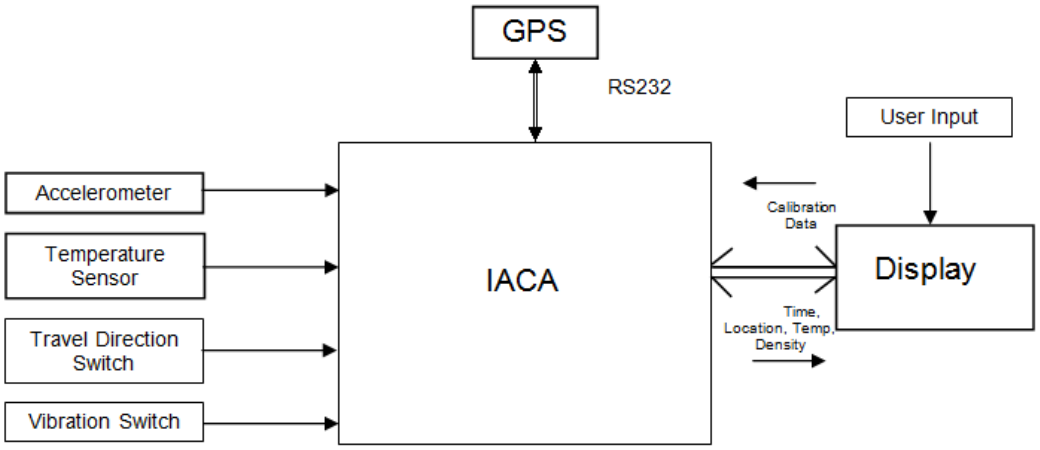

Figure 4.1 Functional Model of the IACA.

4.2.1.1 Sensing Specification

The IACA records the instantaneous spatial position of the compactor on the asphalt mat. The IACA also measures through non-contact means the surface temperature of the asphalt mat. In addition, the IACA is able to detect the state of the vibration motors (ON/OFF) and the direction of travel of the compactor (FORWARD/REVERSE).

1. GPS Sensor. The GPS sensor is capable of sub-meter accuracy in measurement and is capable of providing updates every one second. The interface between IACA and the GPS unit is through RS232 or through a wireless Bluetooth connection. By parsing the NMEA string that is sent by the GPS unit, the IACA is capable of extracting the latitude and longitude of the location of the compactor.

2. Temperature Sensor. A non-contact temperature sensor capable of sensing surface temperatures from -18°C (0°F) to 178°C (350°F) is integrated with the IACA. The temperature is registered at a minimum of once every second. The temperature input

is an analog voltage with a swing between 0 and 5 volts. Calibration routines account for the DC bias and conversion factor of the sensing device.

3. Travel Direction Switch Sensor. The IACA is able to detect the switch status of the roller to determine the direction of travel. This input is typically a digital input to the IACA having discreet logic level (0 or 1) corresponding to Forward/Reverse. Currently, an algorithm has been developed to detect change in the direction of travel using GPS input.

4. Vibration Switch Sensor. The IACA is able to detect the switch status of the roller to determine when the vibration motors are turned on. This input is typically a digital input to the IACA having discreet logic level (0 or 1) corresponding to ON/OFF. Currently, analysis of the vibration of the accelerometer signal is employed to determine the status of the vibration motors.

5. Accelerometer Sensor. The IACA reads the acceleration of the drum through an accelerometer mounted on the frame of the drum. The output of the accelerometer is an analog voltage between 0 and 5 volts. The vertical acceleration of the drum is sampled at a 1000Hz (once every millisecond).

4.2.1.2 Operational Specifications

The IACA reads the sensed vibrations of the drum and estimates the corresponding density of the asphalt mat. The density estimates, along with the location of the roller on the asphalt mat, the current process time, and the asphalt mat temperature, are to be displayed to the user at least once every second. The difference in the estimated density

and the actual density measured from the roadway core are within limits comparable to point wise density measurement tools in use today (accuracy of PQI 301 is within ±1.5 pounds per cubic foot (pcf) and for nuclear density gauge the accuracy is ±2.5 pounds per cubic foot (pcf)). The density is displayed to the user as a numeric value (1 decimal precision), as well as a slider bar that indicates the progress in compaction.

The IACA electronics are housed in a rugged enclosure that is tested for vibration and shock, as well as environmental variables such as temperature and moisture (SAE J 1445 and SAE/TMSC environmental standards).

4.2.1.3 Calibration Specifications

The use of the IACA requires detailed procedures for calibrating the output of the IACA to minimize the error between the estimates and the density measured off roadway cores (refer to Appendix B for more details). The procedure provides calibration in the field using measurements from roadway cores, as well as measurements taken using a non-nuclear density gauge such as PQI 301 or a nuclear density gauge like the Troxler 3450 gauge. The procedure also provides a measure of the calibration accuracy. Once the readings from the field are input into the system, the calibration process is automatic and results in the operational parameters (interconnection weights of the Artificial Neural Network and the calibration constants) being set in the IACA for field use during compaction.

The calibration procedures account for the location of the temperature sensor relative to the ground and provide the user the ability to calibrate the sensor in order to accurately record the surface temperature of the asphalt mat.

4.2.1.4 Display and Recording Specifications

The IACA display provides the user with real-time information on the location of the compactor, the temperature of the asphalt mat, and the estimated density at the location (see Figure 4.2). The density information is displayed both in a numeric format as well as a visual indication of the level of compaction (e.g. a slider bar). The compaction data (time, latitude, longitude, temperature, density) is also stored for retrieval and post processing to generate as-built data maps.

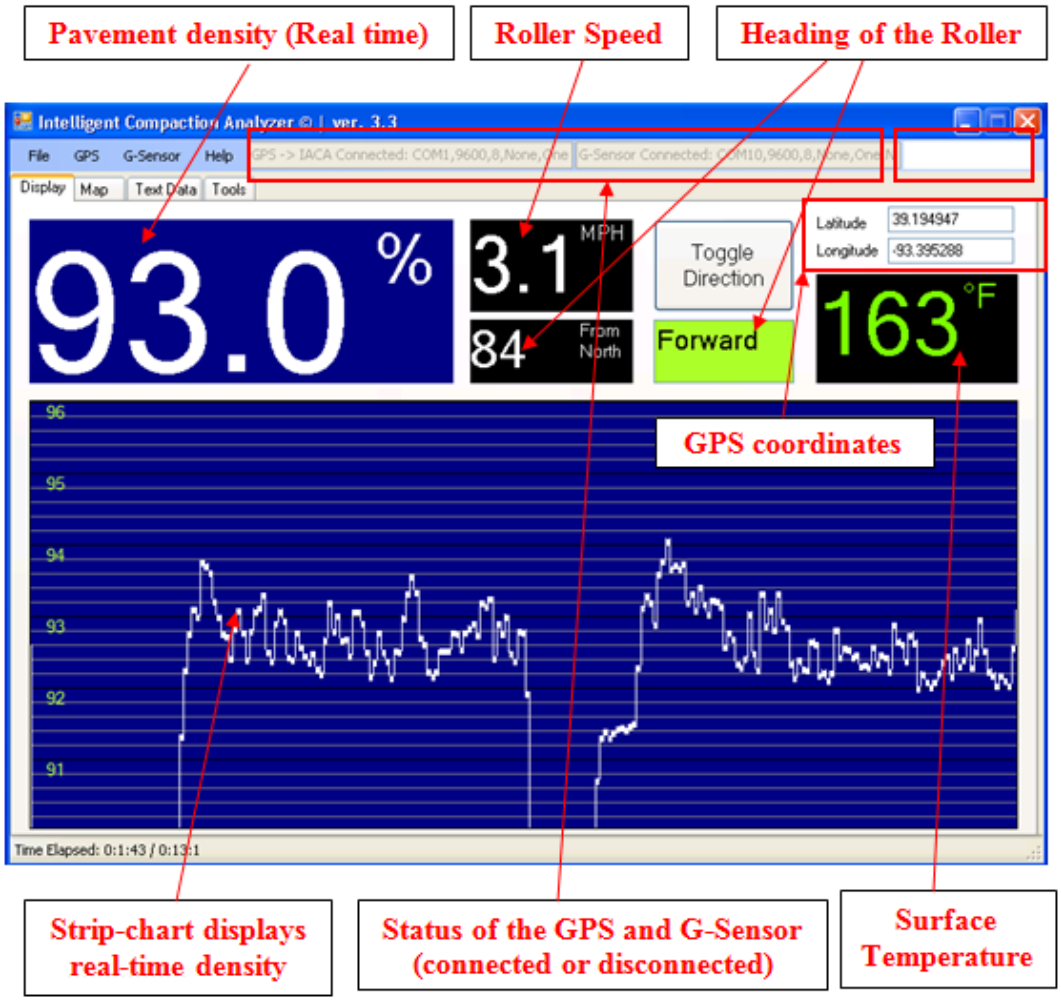

Figure 4.2 IACA display providing real-time information to the roller operator.

The display is crucial to the field validation of the IACA. Validation in the field would require real-time information of the compaction achieved at any location on the pavement. It is anticipated that the readout from the IACA would be used to correlate the spatial location on the pavement with the estimated densities. This would allow verification with densities measured from roadway cores as well as using point-wise density measuring tools.

The display also includes a mechanism for selecting prior calibration data for use during the construction. The selection of the appropriate calibration data would involve the knowledge of the construction characteristics and the mix information.

4.2.2 Principle of Operation of the IACA

Compaction of an asphalt mat is achieved through the application of vibratory energy and pressure by a roller. The asphalt mat and the roller form a coupled system whose response is determined by the frequency of the vibratory motors of the roller and the natural vibratory modes of the coupled system. Compaction of an asphalt mat increases its stiffness and as a consequence, the vibrations of the roller are altered. The knowledge of the properties of the asphalt mat and the vibration spectrum of the roller can therefore be used to estimate the stiffness of the asphalt mat. *Since the quality specification is usually percentage air voids content or percentage of the Maximum Theoretical Density (MTD) of the asphalt mix, the IACA estimates the compacted density of the pavement rather than the stiffness.*

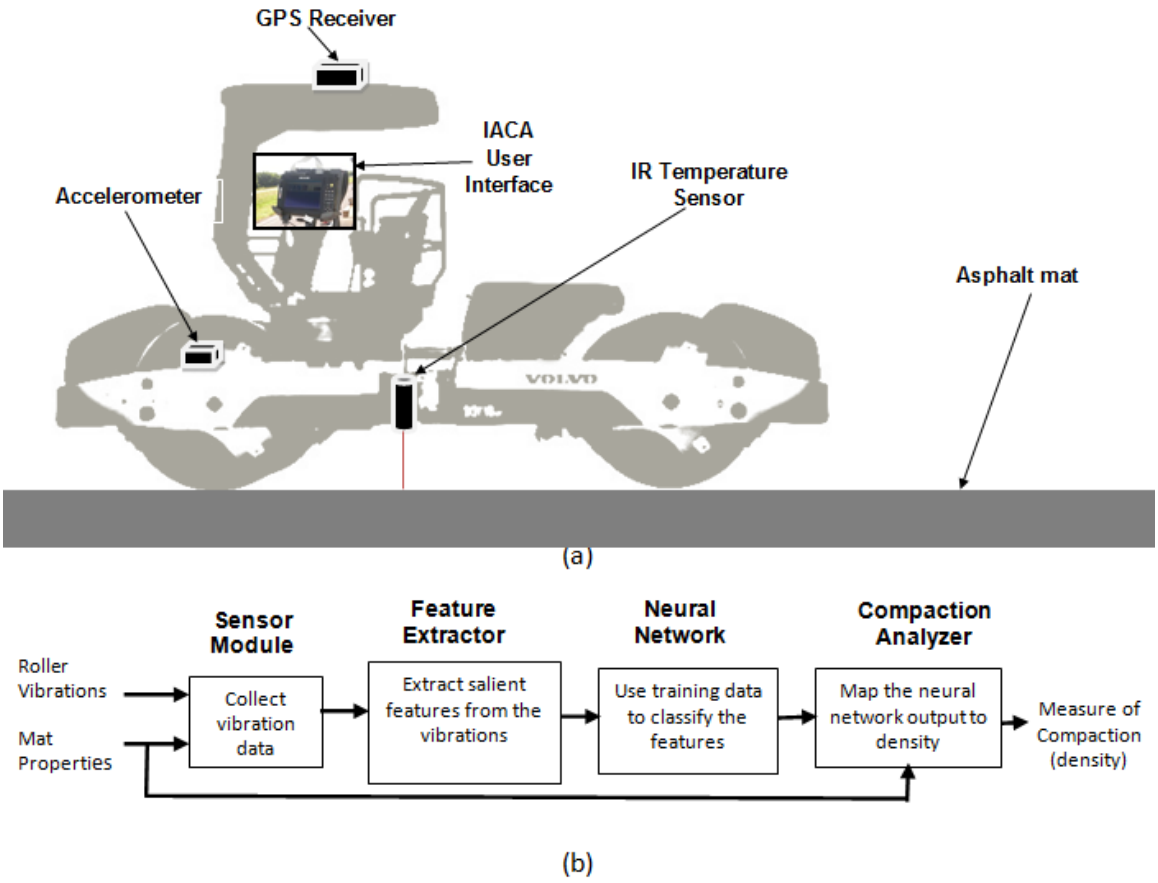

Figure 4.3 Experimental Setup (a) Instrumentation of the compactor; (b) Functional block diagram of the IACA.

A vibratory compactor equipped with IACA is shown in Figure 4.3(a) and the components of the IACA are shown in Figure 4.3(b). The sensor module (SM) in the IACA consists of accelerometers for measuring the vibrations of the compactor during operation, infrared temperature sensors for measuring the surface temperature of the asphalt mat, a user interface for specifying the amplitude and frequency of the vibration motors, and for recording the mix type and lift thickness. The feature extraction (FE) module computes the Fast Fourier Transform (FFT) of the input signal and extracts the features corresponding to vibrations at different salient frequencies. The Artificial Neural Network (ANN) Classifier is a multi-layer ANN that is trained to classify the extracted

features into different vibration patterns specific to a pre-specified level of compaction. The Compaction Analyzer (CA) then post-processes the output of the ANN and estimates the degree of compaction in real time. Details of the IACA and its preferred embodiment are discussed in detail in the IACA patent application (Commuri and Zaman, 2010).

4.2.2.1 Implementation of the IACA

The functional components of the IACA and their operational principles are described in this section.

Sensor Module**.** In the implementation discussed in this section, the Sensor Module of the IACA is comprised of an accelerometer mounted on the frame of a Ingersoll-Rand DD138HFA vibratory compactor, an Intel Pentium based tablet PC to input the asphalt mat properties such as the mix type, binder, pavement layer, layer thickness, target density, etc., and a real-time data acquisition system. The accelerometer used was a 13200C uniaxial rugged accelerometer manufactured by Spectrum Sensors & Controls formerly Summit Instruments, Inc. (SSC, 2010), that is capable of measuring 10g acceleration up to a frequency of 10kHz. The accelerometer measures the vibrations of the roller drum during the compaction process. The surface temperature of the asphalt mat is measured using a Raytek CI3A10L infrared temperature sensor mounted on the frame below the roller (Raytek, 2010). A Trimble Pro XT GPS receiver (Trimble, 2010) is used to record the instantaneous location of the roller.

Feature Extractor Module. Analysis of the vibratory response of the roller requires the extraction of the frequency components of the vibrations and their amplitudes. These characteristic ‘features’ are related to the roller and the underlying pavement layers. As

the pavement layer is compacted, the vibratory response of the roller changes. These changes are visible in the altered spectrum of the roller vibrations as the compaction progresses. The knowledge of these features is then used to determine the density of the pavement layer during its compaction.

The feature extractor module of the IACA implements a Fast Fourier Transform (FFT) to efficiently extract the different frequency components of the roller vibrations. The output of the FFT is a vector with 200 elements, where each element corresponds to the normalized signal power at the corresponding frequency. Since the vibration signal of the roller is sampled at 1kHz, the frequency spectrum is uniformly distributed between 0 and 500Hz. In order to classify these vibrations, the 200 elements corresponding to the fundamental frequency of the roller response and its harmonics are used as input to the classifier.

Classifier Module. The Artificial Neural Network (ANN) classifier implemented in the IACA is a three layer ANN with 200 inputs, 10 nodes in the input layer, 4 nodes in the hidden layer, and 1 node in the output layer. The inputs of the ANN correspond to the outputs of the feature extraction module, (in this case, 200 features in the frequency spectrum). The output corresponds to a signal indicative of the level of compaction reached.

Analyzer Module. The analyzer module uses the mix parameters such as the mix type, binder, pavement layer, layer thickness, and the target density, and the calibration data to convert the output of the classifier to a value representing the density of the asphalt mat at the current location of the roller. The calibration data consists of a slope

parameter and an offset parameter that is used to convert the output of the neural network, a number between 0 and 4, to a density value between 0 and 100 (typically between 85 and 96). The density estimated by the IACA is the density of the pavement layer beneath the drum expressed as a percent of the theoretical maximum density of the asphalt mix.

4.2.2.2 Training of the Neural Network

Central to the functioning of the IACA is the Artificial Neural Network that is used to classify the observed vibrations of the compactor into classes representing different levels of compaction. In order to accomplish this, the output of the feature extractor module is analyzed over several roller passes during the calibration process and the total power content in the vibration signal is calculated at each instant in time. Five equally spaced power levels are identified, and the features corresponding to these power levels are used to train the Neural Network. During compaction, the ANN observes the features of the roller vibration and classifies these features as those corresponding to one of the levels of compaction. Figure 4.4 shows the features corresponding to five different compaction levels, with the lowest level corresponding to the case where the roller is operating with the vibration motors turned off and the highest level corresponding to the case where the maximum vibrations observed.

4.2.2.3 Calibration of the Analyzer

The calibration of the Analyzer is a two-step process. In the first step, ideal compaction is assumed with the expectation that the analyzer would encounter ‘Lay

Down' density of the asphalt mat during the first roller pass and a density corresponding to the 'target' density during the final pass of the roller.

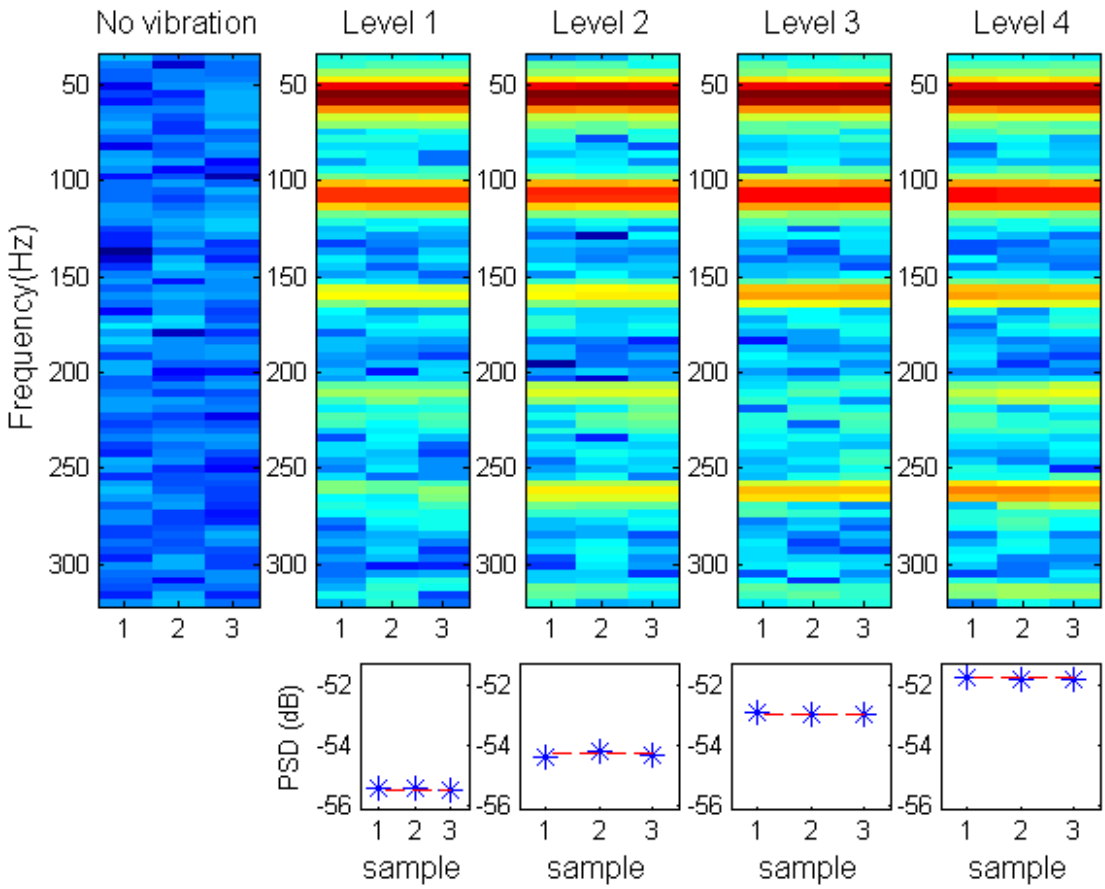

Figure 4.4 Spectral features corresponding to five levels of compaction.*

During the calibration process, a 9.1m (30 ft.) section of the road is first identified and the vibration data is collected during successive roller passes over this stretch. The features extracted from this vibration data (Figure 4.5) are used to train the ANN in the classifier module. After the completion of the training process, the Classifier can recognize five levels of compaction labeled from '0' through '4' (Figure 4.4). Level 0

* This figure was automatically produced by the IACA.

corresponds to the situation when the vibratory motors are turned off. The initial calibration assumes that 'Level 1' of the vibrations corresponds to the "lay down" density of the asphalt mat and 'Level 4' of the vibrations corresponds to the target density specified for the mix. While the target density for Superpave mixes is 96%, the actual density achieved during the testing of the mix in a Superpave Gyratory Compactor after a specified number of gyrations (N_{Des}) is reported in the Quality Control sheets from the asphalt plant. This actual density is an indicator of the maximum compaction that is achievable during field compaction of the asphalt mix and is selected as the target density for IACA calibration.

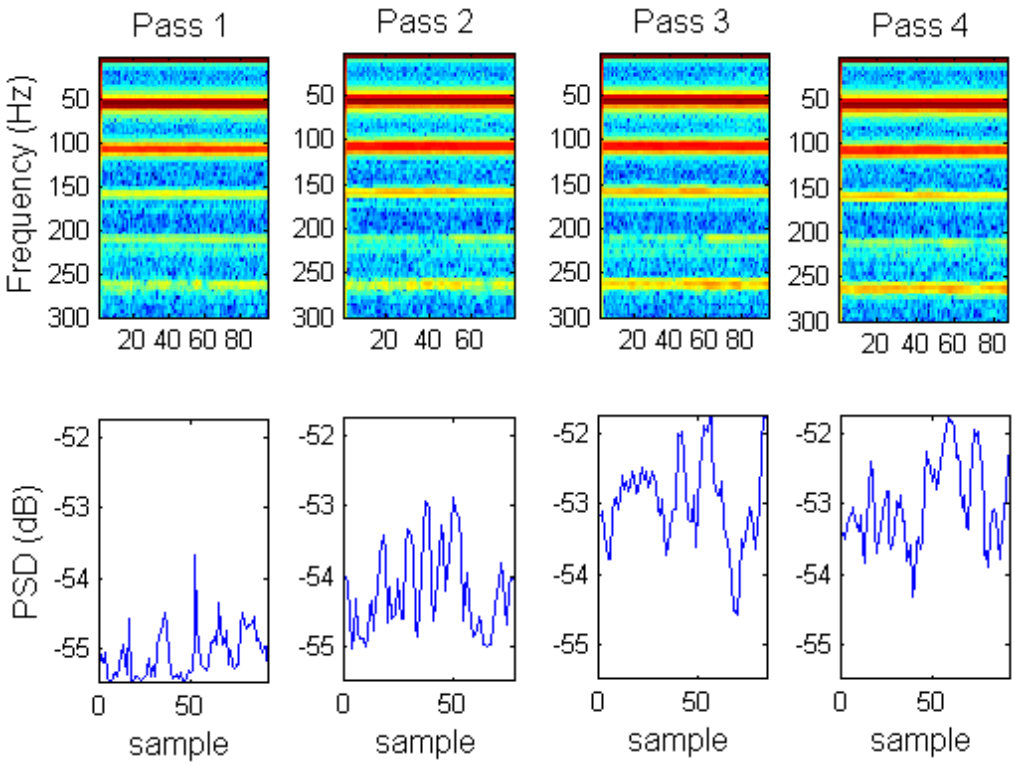

Figure 4.5 Power content of the vibration signal during successive roller passes.[†]

[†] This figure was automatically produced by the IACA.

After the compaction of the 'calibration stretch', three roadway cores are extracted from known locations on the compacted pavement and their density is measured in the laboratory according to AASHTO T-166 method (AASHTO, 2007a). The offset and slope constants for the compaction analyzer are determined to minimize the mean square error between the estimated density and the density measured from the cores (Allen et al., 2003).

4.2.2.4 Validation of the Analyzer

In order to validate the functioning of the analyzer, core locations are marked at random on the completed pavement and the location of the cores is measured using a GPS sensor. The cores are then extracted and their density is measured in the lab. The GPS readings are used to determine the density estimated by the IACA at these locations during the final compaction pass of the roller. The error between the measured and estimated densities is then studied to determine the statistical measures of performance.

4.2.2.5 Procedure for calibrating the IACA during the compaction of an asphalt pavement

The calibration stretch is shown in Figure 4.6 and the procedure for calibration is described below (refer to Appendix B for more details on the calibration process).

1. The vibration data for calibration of the IACA is first acquired during the construction of a control strip. The control strip is 33m (100 ft.) long and 3.6m (12 ft.) wide. A 9.1m (30 ft.) 'test section' is selected in the middle of the control strip and the

GPS sensor is used to trigger the collection of the vibration data as the roller compacts this 'test section.'

2. Using the GPS sensor, the coordinates at the beginning and at the end of the test section are obtained by taking measurements at the center of the lane. These coordinates are used to automatically start and stop the collection of the vibration signals as the roller passes over the test strip.
3. Three test locations at the center of the lane, 1.6m (5 ft.), 5m (15 ft.) and 8.33m (25 ft.) from the beginning of the test section are marked.
4. Using a device similar to a 3450 Troxler Nuclear Density Gauge or a TransTech PQI 301 non-nuclear density gauge, the density of the pavement is measured after each roller pass at each of the test locations marked in step (iii).
5. The compaction process is stopped when no appreciable increase in the density is noticed after the roller pass or when roll over (i.e., reduction in measured density is observed). The core locations are marked from the center of the final roller pass at each of the test locations in step (iv). The GPS locations of the cores, as well as the density at the core and in the immediate vicinity of the core are recorded.
6. The cores marked in the previous step are extracted and their density is measured in accordance with the AASHTO T-166 method.
7. The density measurements taken after each roller pass and the densities of the extracted cores are used to train and calibrate the IACA.

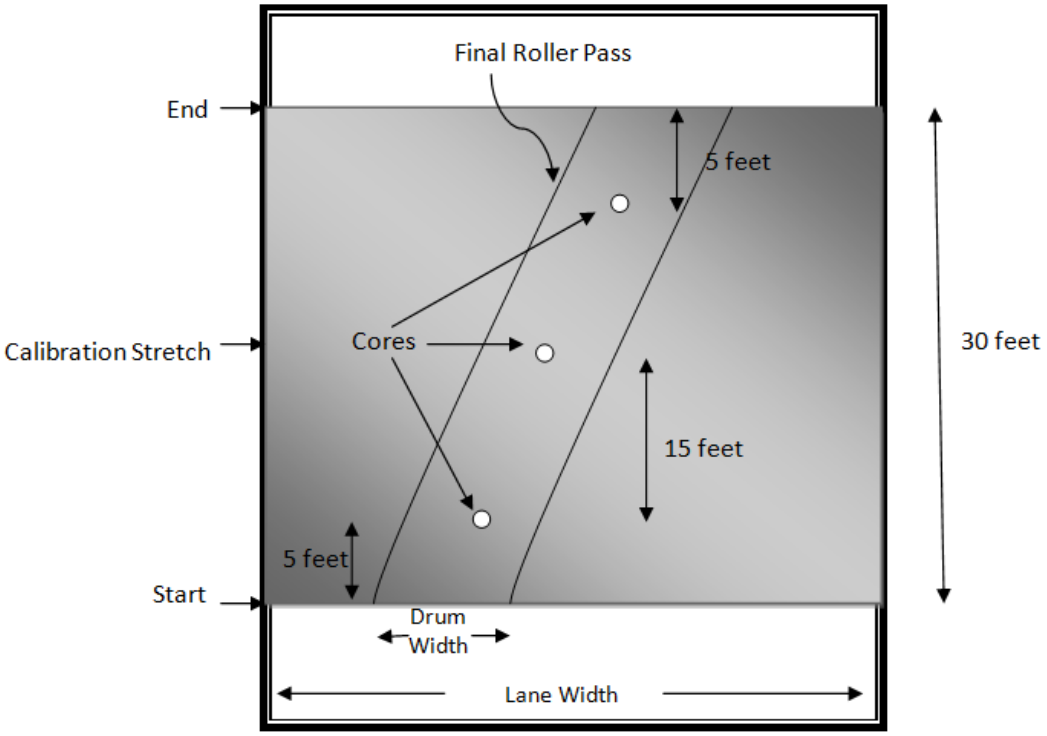

Figure 4.6 Selection of core locations after the final pass of the roller.

4.3 Results of Field Demonstrations

The field evaluation that is reported in this section was carried out at six different construction sites between June 2009 and April 2010. During the field demonstration of the IACA technology discussed in this section, the installation of the IACA was performed by the research team with the assistance of the performing contractors. The cores for calibration and validation of the IACA were marked and extracted by the contractor and their density independently was verified either by material testing facilities or the contractor. The density of the cores was determined by the AASHTO T-166 method, which specifies the procedure for the determination of the bulk specific gravity of compacted specimens (G_{mb}) from pavement cores. This value is used to determine the

density of the compacted specimen, and is used for comparison between roadway compaction tests and the IACA estimated density values.

4.3.1 Accuracy of IACA Measurements

The IACA measurements reflected the quality of compaction during the field validations that were conducted. In all, 180 roadway cores were extracted at random from the completed pavements at the test sites selected for this dissertation and their densities measured using the AASHTO T-166 method. The comparison of the densities of the roadway cores from the compacted pavements with the density estimated by the IACA at the location of the cores is shown in Table 4.1. *The mean density of the cores was 93.1% (standard deviation of 1.4), corresponding to a mean air void level of 6.9%. The IACA measurements at these locations show a mean density of 93.1% (standard deviation of 1.5), corresponding to a mean air voids level of 6.9%.* Null hypothesis testing showed that there is no significant statistical difference between the density measurements from the cores and the density estimated by the IACA.

It is seen from Table 4.1 that the overall compaction that was achieved during asphalt overlay was significantly higher than that achieved during the construction of full-depth asphalt pavement (mean density of 93% versus a mean density of 92.3%). Furthermore, significant variation in the density was observed during the compaction of the Asphalt Concrete (AC) base layers, both for full depth as well as for asphalt overlays (standard deviations of 1.6 and 1.5 respectively). Also, low compaction and high variability was seen during the construction of Full Depth Pavement.

Table 4.1 Summary of compaction data

Pavement Type	AC base (Full Depth)	Intermediate (Full Depth)	Surface (Full Depth)	AC base & Intermediate (HMA Overlay)	Surface (HMA Overlay)
Total Cores	25	27	15	49	64
Mean Density* (Cores)	92.3	93.2	92.1	93.0	93.8
Std. dev (Cores)	1.62	0.9	0.87	1.53	1.04
Mean Density* (IACA)	92.2	93.1	92.1	92.9	93.8
Std. dev (IACA)	1.4	1.1	1.0	1.6	1.1
Error (IACA vs. Core)	-0.1	-0.1	-0.0	-0.1	0.1
Std. dev Error†	0.5	0.7	0.6	0.6	0.8
Max Error (IACA)	1.7	-1.3	-1.2	-1.5	-2.2
R^2	0.83	0.63	0.63	0.83	0.54

* Mean density (%) of the cores extracted after the compaction of the pavement
† Error between the measured density and the density estimated by the IACA

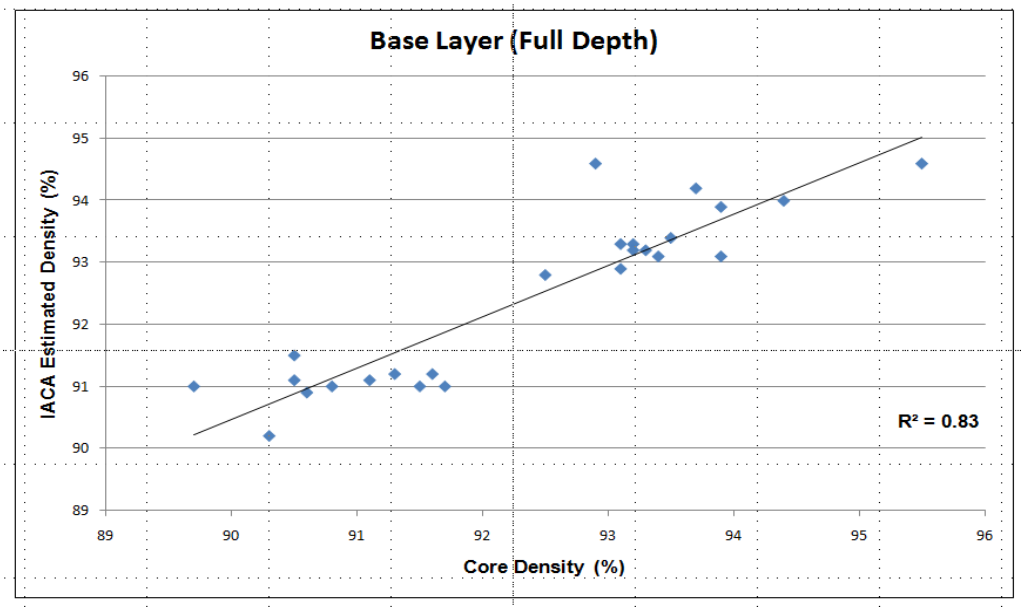

Figure 4.7 Comparison of the IACA estimated density with density determined from cores extracted from AC base layer (Full Depth construction).

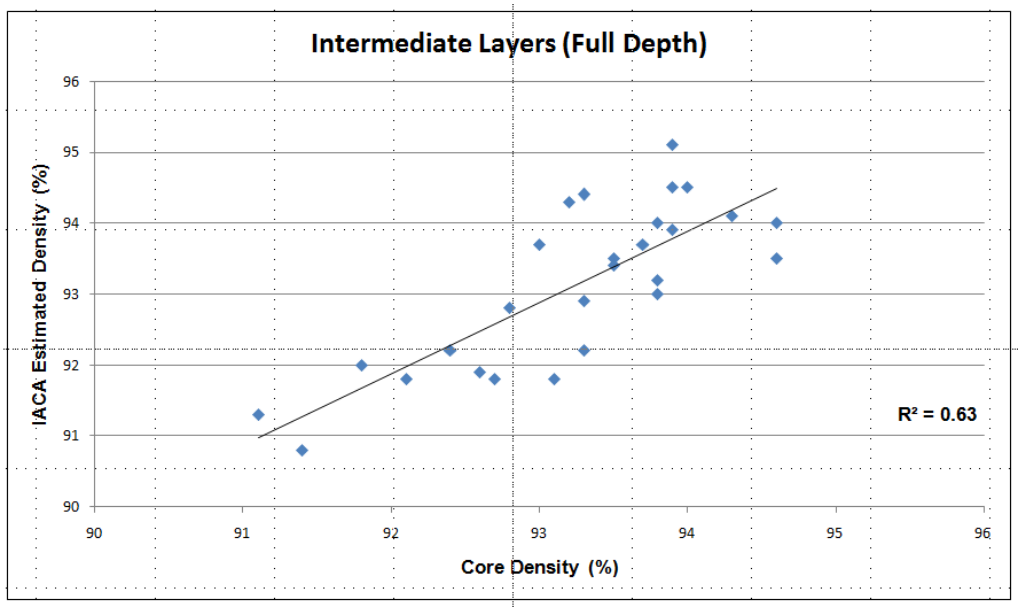

Figure 4.8 Comparison of the IACA estimated density with density determined from cores extracted from AC intermediate layers (Full Depth construction).

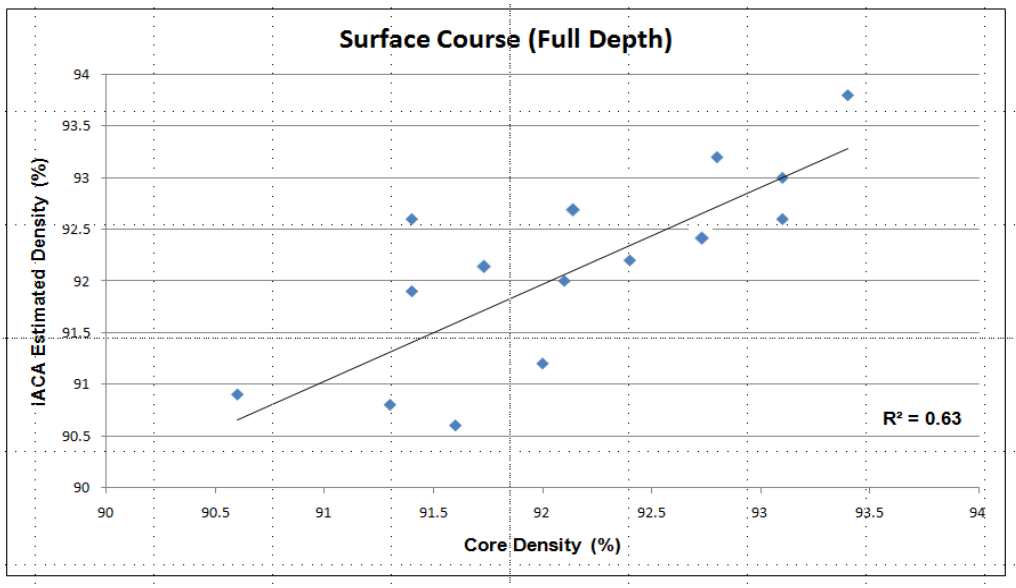

Figure 4.9 Comparison of the IACA estimated density with density determined from cores extracted from surface layers (Full Depth construction).

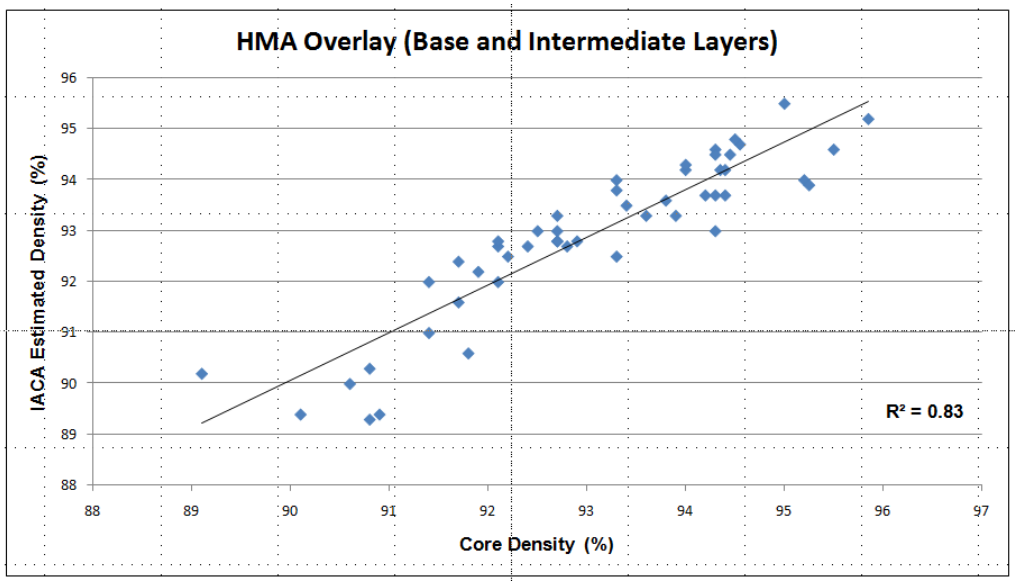

Figure 4.10 Comparison of the IACA estimated density with density determined from cores extracted from AC base and intermediate layers (HMA overlay).

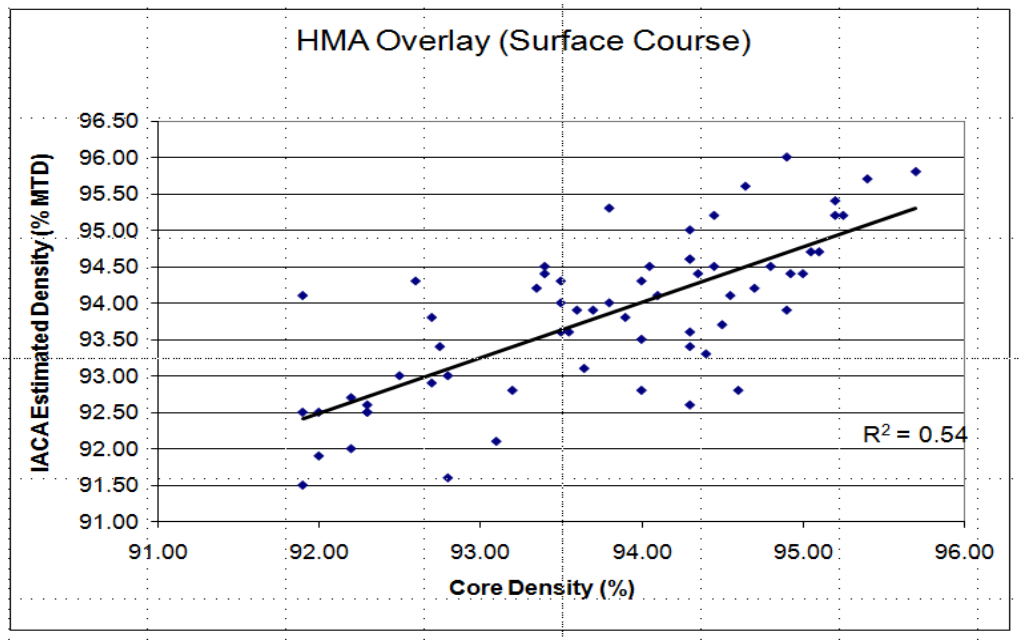

Figure 4.11 Comparison of the IACA estimated density with density determined from cores extracted from surface course (HMA overlay).

During the field tests, the IACA was observed to be able to estimate the density of the asphalt pavement layer with good accuracy. The results in Table 4.1 show that there is little statistical difference in the density estimated by the IACA as compared to the density measured from the roadway cores. Furthermore, Figures 4.7 and 4.10 demonstrate that the IACA estimates for the AC base layers and the core measurements are strongly correlated (coefficient of determination = 0.83). Figures 4.8 and 4.9 also indicate that in the case of full depth pavement, the IACA performance is not influenced by the asphalt layer (similar mean and variance as the density measured from the core and identical coefficient of determination). However, in the case on HMA overlay on exiting pavement, thin overlays on existing pavement resulted in larger estimation errors and a lower coefficient of determination (0.5) between estimated densities and the density measured from cores.

4.3.2 Installation and calibration of the IACA

During each of the field evaluations, the installation of the IACA on the vibratory compactor was completed within fifteen minutes and the training and calibration of the IACA was accomplished within two minutes of the completion of the calibration stretch (refer to Appendix B for the IACA user manual). Figures 4.12, 4.13, and 4.14 show the IACA installed on a contractor owned Ingersoll Rand DD90 vibratory a compactor and a Volvo owned DD118HFA vibratory compactor. At each site, calibration was performed for each layer of asphalt. The validation results presented in this dissertation were obtained by comparing the density of randomly selected roadway cores with the IACA estimated density at the core locations. Recalibration of the IACA was not found to be necessary during the course of the project.

The operator feedback on the ease of installation and calibration was positive. The displayed information was also well received. However, the research team found that the roller operator primarily paid attention to adhering to the rolling pattern that was established and not to the quality of compaction that was being achieved. The roller operator would seldom look at the display or pay attention to the density estimates and the as-built density maps. Therefore, it was not possible to evaluate the benefits that could result in the uniformity of compaction or the productivity through the use of IACA technology.

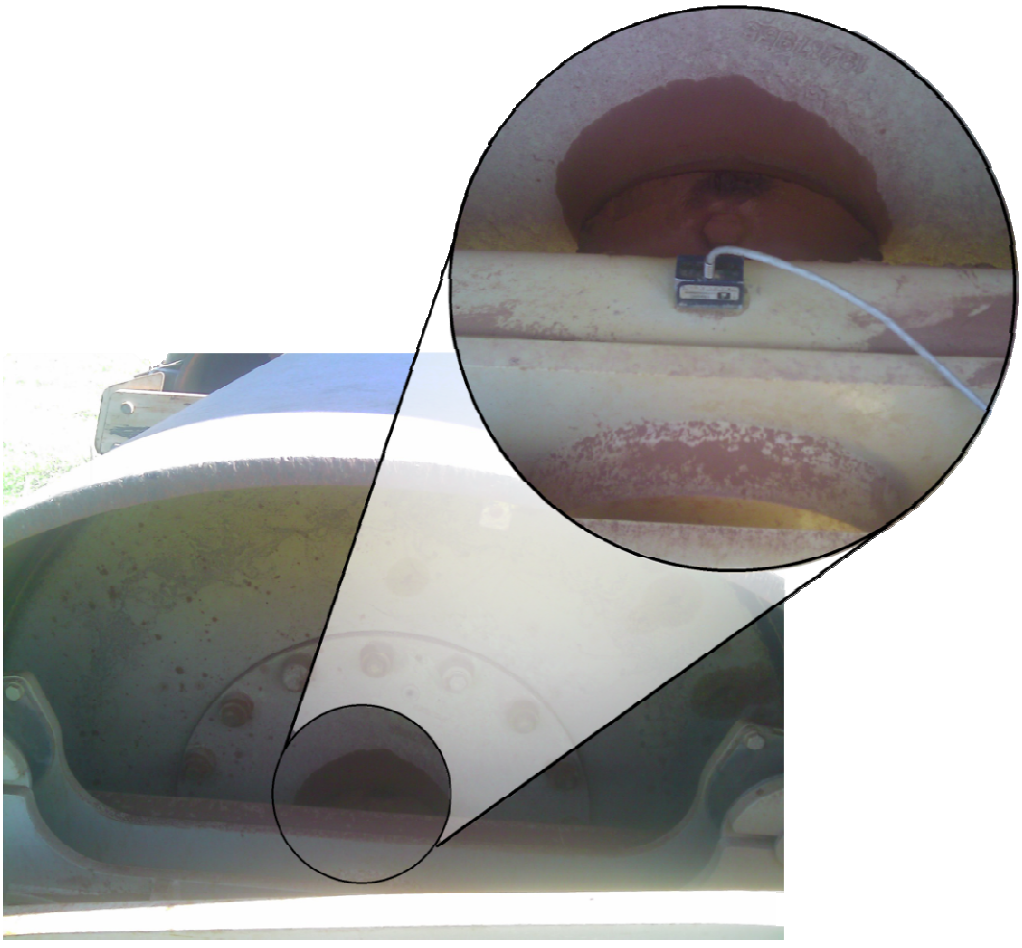

Figure 4.12 Accelerometer mounted on the drum axle of an Ingersoll Rand DD138HFA vibratory compactor.

Figure 4.13 Installed view of the IACA on an Ingersoll Rand DD90 vibratory compactor.

(a)

(b)

Figure 4.14 (a) Installation of the IACA on a Volvo DD118HFA roller; (b) IACA in use.

4.4 Details of Field Demonstrations of the IACA

4.4.1 Field Demonstration - Reading, Pennsylvania

(June 01 - 05, 2009)

The performance of the IACA was observed during the overlay of asphalt pavement on highway US-222 near Reading, PA. Remediation of the existing pavement involved milling and removal of 4 kilometers (2.54 miles) of existing pavement and the construction of 50mm (2 in.) of 12.5mm (0.5 in.) Nominal Maximum Aggregate Size (NMAS) asphalt mix on top of the Jointed Plain Concrete Pavement (JPCP) base. Compaction was achieved using an Ingersoll Rand DD110 dual drum vibratory compactor. Finish rolling was done using a static steel drum roller Ingersoll Rand DD110 roller. Quality Control in the field was performed using a Troxler 3450 Nuclear Density Gauge (NDG). The location of the site is shown in Figure 4.15 and the site details are given in Table 4.2. The accelerometer sensor was located on the axle of the front drum and the GPS receiver was located on the roof of the compactor. The offset in Table 4.2 indicated the lateral separation between the accelerometer and the GPS receiver and was used to relate the GPS measurement to the location of the drum.

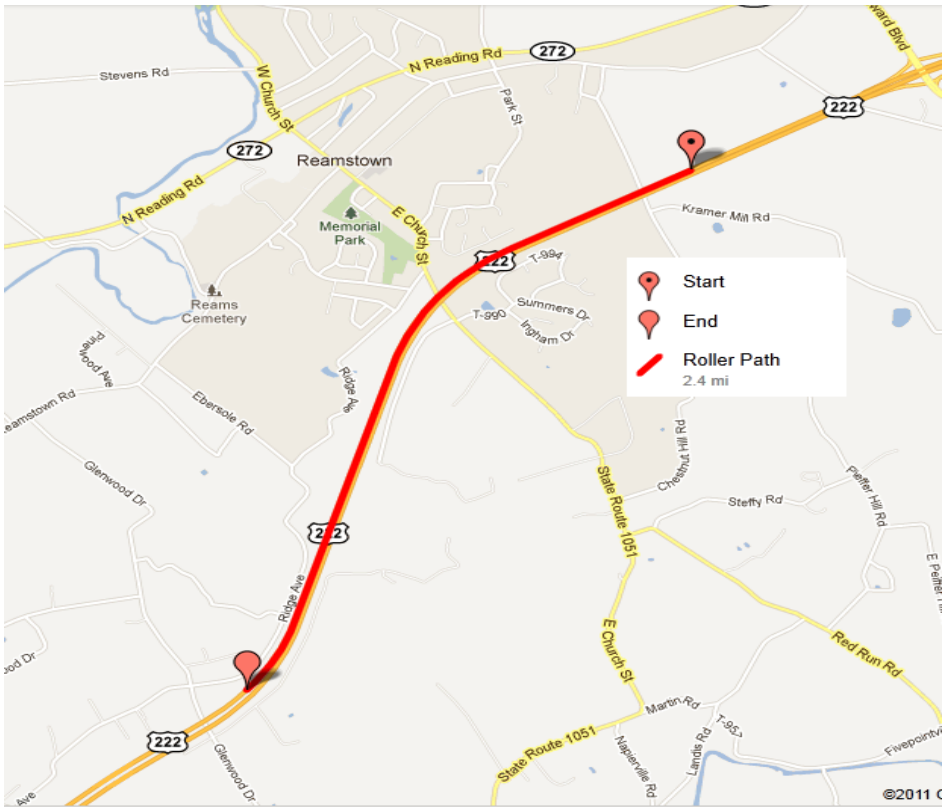

Figure 4.15 Site location on US-222 near Reading, PA.

Table 4.2 Machine and site information (US-222)	
Date	**June 01, 2009**
Location	Reading, PA
Construction type	Mill & Overlay
Lift	Top
Mix	12.5 mm
Thickness	50.8mm
Roller	Ingersoll Rand DD110
Calibration (using NDG)	3 cores
Validation (using NDG)	12 cores
Settings	
Accelerometer location	front
Offset from GPS receiver (ft.)	0
Drum width (ft.)	6.5

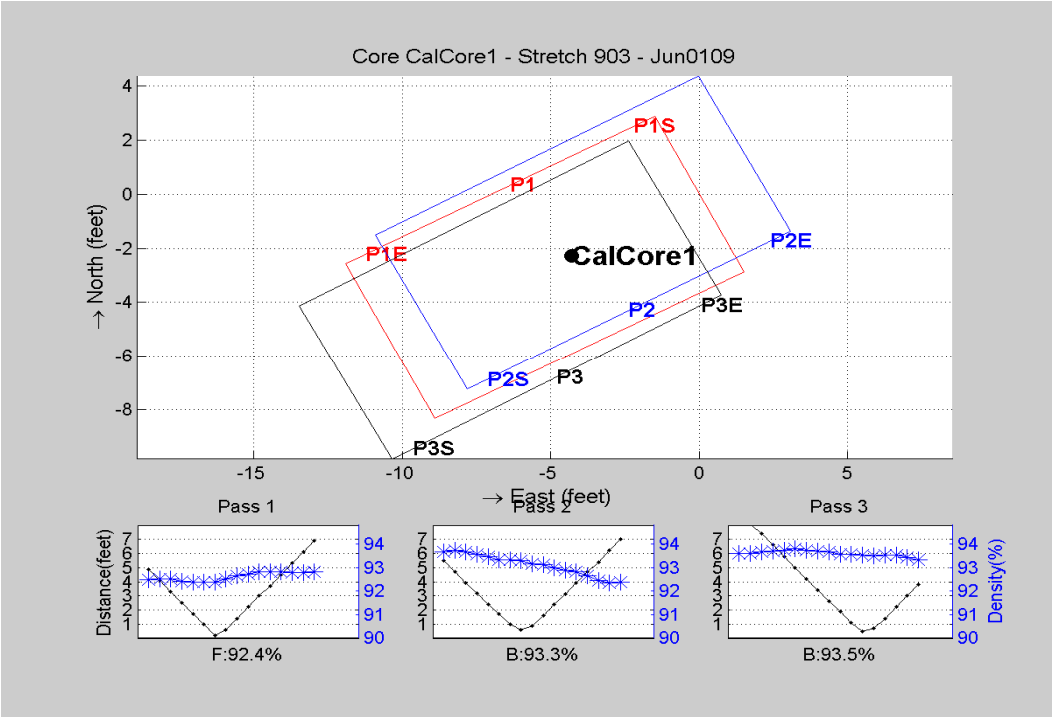

Figure 4.16 Roller path and estimated densities at core location C1, Reading, PA.[‡]

4.4.1.1 Discussion of Results

On the day of the validation, the project team installed the IACA on the contractor's IR DD110 compactor. The calibration of the IACA was performed by comparing the IACA estimated density with the density measured using the contractor's calibrated Nuclear Density Gauge (NDG). The IACA estimated density at the calibration location 'CalCore 1' during each roller pass is shown in Figure 4.16. In this figure, P1, P2, and P3 represent three consecutive roller passes over the calibration location. P1 and P3 denote the forward movement of the roller while P2 indicates the backward movement of the roller. For each pass, the starting point is designated by 'S' and the termination of the pass

[‡] The figure was automatically produced by the IACA.

is designated by 'E'. For example, P1S represents the starting point for Pass 1 and P1E indicates the terminal point of Pass 1. The graph in the lower panel depicts the variation of the IACA measured density in the vicinity of the calibration location. From this figure, the operator can verify the increase in density after each roller pass and the uniformity of the compaction at the calibration location.

Table 4.3 Validation results from US-222, Reading, PA

Core Location	Core Density (NDG)	Estimated Density (IACA)	Estimation Error (IACA-NDG)
C1	93.6	93.5	-0.1
C2	91.8	93.5	1.7
C3	94.9	93.1	-1.8
M4	93.3	91.3	-2.0
M5	94.5	94.3	-0.2
M6	94.5	92.3	-2.2
M7	93.9	94.0	0.1
M8	93.4	94.2	0.8
M9	92.9	94.3	1.4
M10	92.8	93.9	1.1
M11	91.8	94.0	2.2
M12	91.7	93.9	2.2
M13	91.8	92.9	1.1
M14	92.8	93.3	0.5
M15	93.5	93.5	0.0

After the IACA was calibrated, several locations were randomly marked on the compacted pavement and the density at each of these locations was measured using the nuclear gauge. The GPS coordinates of these locations were also measured and the IACA estimated density was recorded. The measured and estimated densities are shown in Table 4.3. The results from these tests indicate that the mean estimation error (i.e., mean of the difference between NDG measured density and IACA estimated density) is 0.3 with a corresponding standard deviation of 1.4. Furthermore, the 95% confidence interval

for the estimation error is [-0.4, 1.1] which implies that the IACA measurements are statistically similar to the measurements obtained using a nuclear density gauge.

4.4.2 Field Demonstration - I-40, Hinton, OK

(June 10- July 10, 2009)

The performance of the IACA was observed during the overlay of asphalt pavement on Interstate I-40 near Hinton, OK (Figures 4.17 - 4.19). Remediation of the existing pavement involved the milling and removal of 9.6 kilometers (6 miles) of existing pavement and then compacting a 75mm (3 in.) lift of 19mm (0.75 in.) NMAS asphalt mix followed by a second lift of 50mm (2 in.) using the same mix (Table 4.4). Compaction was achieved using a Dynapac and an Ingersoll Rand DD138HF dual drum vibratory compactors operating in tandem. Finish rolling was done using an Ingersoll Rand DD118 roller operating in static mode.

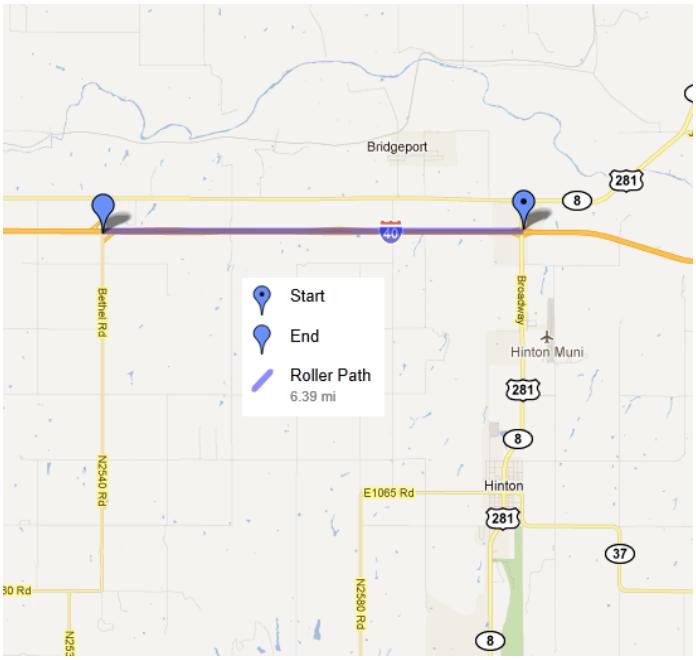

Figure 4.17 Site location on I-40 (West bound) at Hinton, OK.

Figure 4.18 Calibration region on East bound I-40 (Hinton, OK).

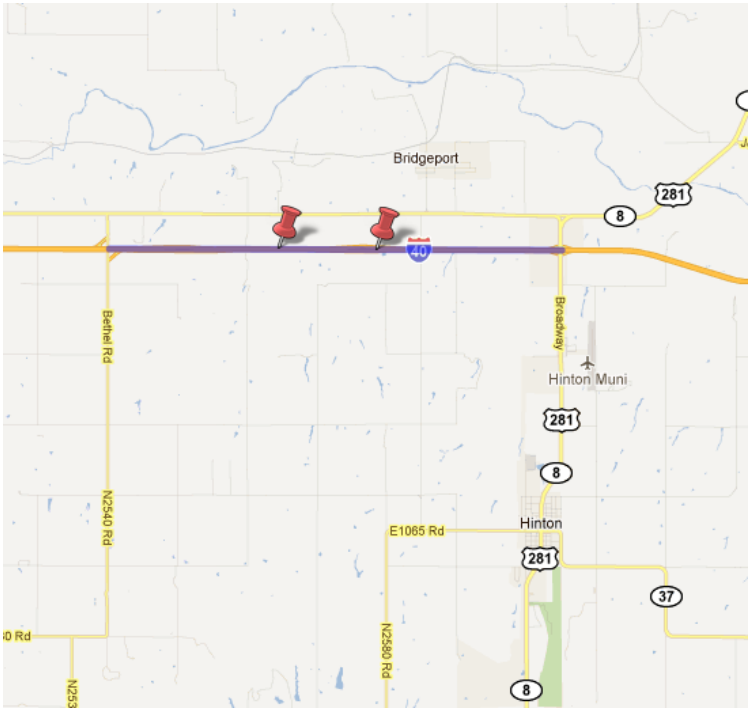

Figure 4.19 Validation region on East bound I-40 (Hinton, OK).

Table 4.4 Site and machine information, I-40 at Hinton, OK					
Date	**Jun1009**	**Jun1109**	**Jun1209**	**Jun2609**	**Jul1009**
Location	Hinton OK	Hinton OK	Hinton OK	Hinton OK	Hinton OK
Construction type	Mill & Overlay	Mill & Overlay	Overlay	Mill & Overlay	Mill & Overlay
Lift	1st	1st	2nd	2nd	2nd
Mix	19 mm S3 PG-76-28	19mm S3 PG-76-28	12.5mm S4 PG-76-28	12.5mm S4 PG-76-28	12.5mm S4 PG-76-28
Thickness	3 in.	3 in.	2 in.	2 in.	2 in.
Roller	Ingersoll Rand DD138HF	Ingersoll Rand DD138HF	Ingersoll Rand DD138HF	Ingersoll Rand DD138HF	Ingersoll Rand DD138HF
Calibration Cores	0	3	0	3	0
Validation Cores	3	3	6	0	3
Settings					
Accelerometer location	front	front	front	front	front
Offset from GPS receiver (ft.)	0	0	0	0	0
Drum width (ft.)	7	7	7	7	7

4.4.2.1 Discussion of Results

The calibration and validation of the IACA was performed for both asphalt layers as described in the previous section. Comparison of the density estimated by the IACA and the actual density measured from the roadway cores are shown in Table 4.5 and 4.6. The results from these tests indicate that in the case of the AC base layer, the mean estimation error (i.e., mean of the difference between core density and IACA estimated density) is 0.4% with a corresponding standard deviation of 0.8. Furthermore, the 95% confidence

interval for the estimation error is [-0.2, 1]. In the case of the second asphalt layer, the mean of the difference between core density and IACA estimated density was found to be 0.5% with a corresponding standard deviation of 0.2. Furthermore, the 95% confidence interval for the estimation error is [0.3, 0.7]. These results also indicate that the IACA measurements are statistically close to the measurements obtained using a roadway cores.

Table 4.5 Validation results for the first lift I-40, Hinton, OK

Core Location	Core Density (Core)	Estimated Density (IACA)	Estimation Error (IACA-Core)
5210+32	96.2	97.9	1.8
5158+52	94.5	94.0	-0.5
5158+91	93.3	93.4	0.1
Calcore1	95.4	94.7	-0.7
Calcore2	95.1	95.5	0.4
Calcore3	94.5	94.6	0.1
5157+64	95.4	96.5	1.1
5240+86	94.4	95.5	1.1

Table 4.6 Validation results for the second lift I-40, Hinton, OK

Core Location	Core Density (Core)	Estimated Density (IACA)	Estimation Error (IACA-Core)
Calcore1	95.0	94.4	0.6
Calcore2	94.3	94.6	0.3
CalCore3	94.3	94.6	0.3
5273+61	93.6	93.1	0.5
5262+14	94.9	94.4	0.5
5268+98	94.6	95.6	0.1

4.4.3 Field Demonstration - I-86, Howard, NY

(July 22-24, 2009)

Field testing of the IACA system was conducted on Interstate I-86 near Hornell, New York (Figure 4.20). The rehabilitation of the pavement was undertaken by first milling

and removing a thin lift of Nova Chip 15mm (0.6 in.) from some of the pavement. Then, the pavement was paved with a 60mm (2.5 in.) lift of a 25mm (1 in.) mix, two 50mm (2 in.) lifts of 19mm (0.75 in.), and then a 40mm (1.6 in.) lift of 9.5mm (0.4 in.) asphalt mix. The IACA data was collected during the construction of the second lift of the 19mm (0.75 in.) mix. The mix was trucked to the location by trucks and laid down using a Vogele 2219w paver. Compaction was then achieved using a Hamm HD-130-HV and a Volvo DD118HFA dual drum vibratory compactors operating in tandem. Finish rolling was done using the same Volvo roller but operating in static mode (see Table 4.7).

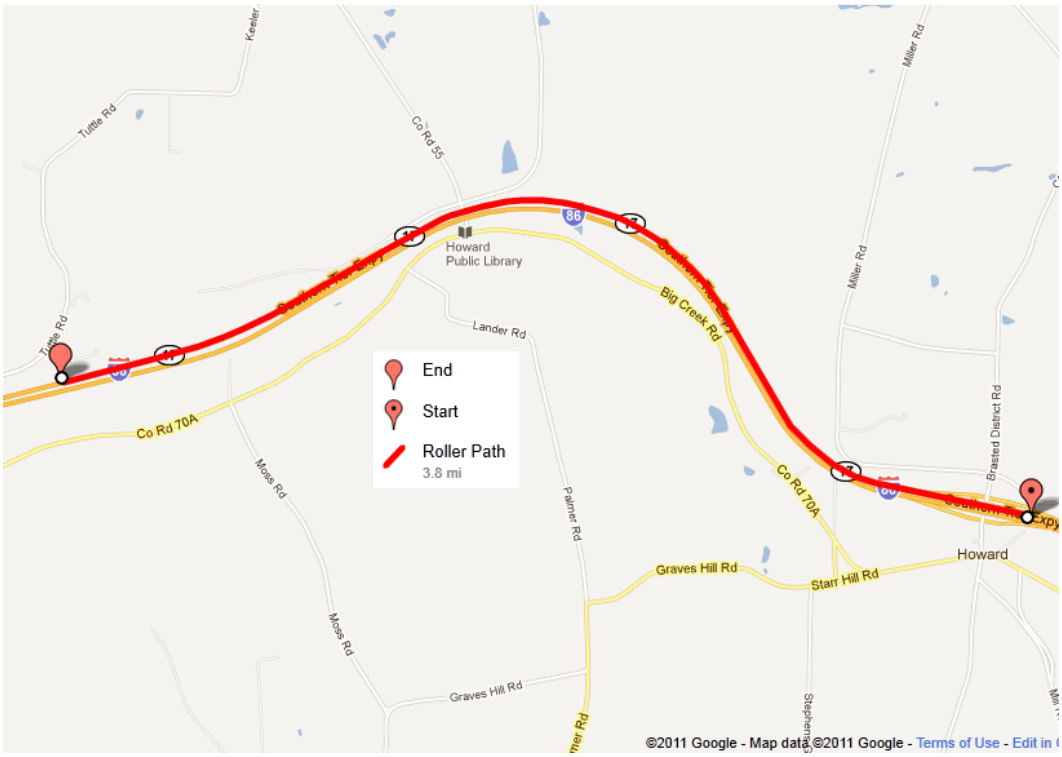

Figure 4.20 Site location on I86 near Howard, NY (3.8 miles).

Table 4.7 Site and machine information, I-86 near Howard, NY	
Date	**July 22,2009**
Location	Howard, NY
Construction type	Mill & Overlay
Lift	Top
Mix	19mm PG 64-22
Thickness	2 in.
Roller	DD118HFA
Calibration Cores #	3
Validation Cores #	7
Settings	
Accelerometer location	front
Offset from the GPS receiver (ft.)	0
Drum width (ft.)	6.5

4.4.3.1 Discussion of Results

The calibration and validation of the IACA was performed as described in the previous section. Comparison of the density estimated by the IACA and the actual density measured from the roadway cores is shown in Table 4.8. The results from these tests indicate that the mean estimation error (i.e., mean of the difference between core density and IACA estimated density) is 0.1% with a corresponding standard deviation of 0.8. Furthermore, the 95% confidence interval for the estimation error is [-0.4, 0.7].

Table 4.8 Validation results from I-86, Howard, NY

Core Location	Core Density (Core)	Estimated Density (IACA)	Estimation Error (IACA-Core)
Calcore1	94.9	93.50	-1.40
Calcore2	94.30	94.80	0.50
Calcore3	94.10	94.50	0.40
WC4	94.45	95.10	0.65
WC5	94.35	93.40	-0.95
WC6	95.25	94.60	-0.65
F1	94.30	94.40	0.10
F2	94.55	95.60	1.05
F3	95.85	96.30	0.45
F4	94.30	95.40	1.10

4.4.4 Field Demonstration - HWY 386, Cohocton, NY

(August 12-17, 2009)

Field testing of the IACA system was conducted on Interstate HWY 386 near Cohocton, New York (Figure 4.21). The rehabilitation of the pavement was undertaken by first milling and removing a thin lift of Nova Chip 15mm (0.6 in) from some of the pavement. The rest was the existing, very faulted concrete pavement. The concrete pavement was rubbelized and then proof rolled. Any soft areas were undercut by excavating the pavement and offending sub-base and then replacing it with screened gravel and a lift of 25mm (1 in.) mix. Then the pavement (either rubbelized or undercut) was paved with a 60mm (2.5 in.) lift of a 25mm (1 in.) mix, two 50mm (2 in.) lifts of 19mm (0.75 in.), and then a 40mm (1.6 in.) lift of 9.5mm (0.38 in.) in asphalt mix. The IACA data was collected during the construction of the second lift of the 19mm mix. The mix was trucked to the location by trucks and laid down using a Vogele 2219w paver. Compaction was then achieved using a Hamm HD-130 HV and a Volvo DD118HFA dual drum vibratory compactors operating in tandem. Finish rolling was done using the same Volvo roller but operating in static mode.

4.4.4.1 Discussion of Results

The calibration and validation of the IACA was performed as described in the previous section. Comparison of the density estimated by the IACA and the actual density measured from the roadway cores is shown in Table 4.9. The results from these tests indicate that the mean estimation error (i.e., mean of the difference between core

density and IACA estimated density) is 0% with a corresponding standard deviation of 0.9. Furthermore, the 95% confidence interval for the estimation error is [-0.4, 0.4].

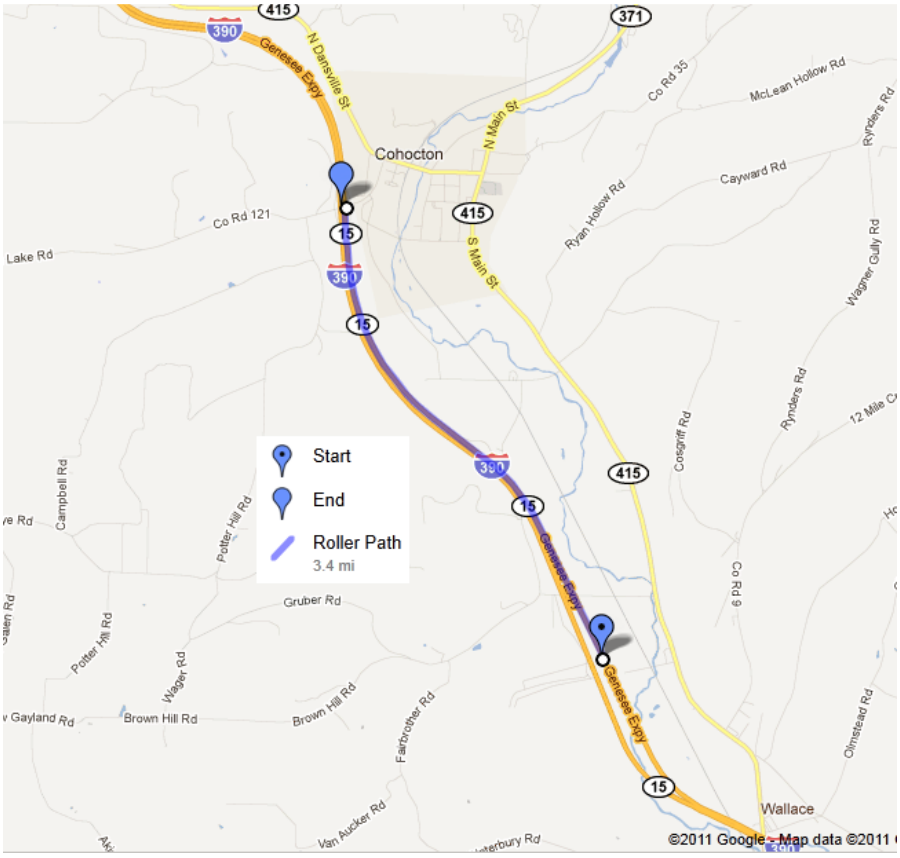

Figure 4.21 Site location on HWY 386 near Cohocton, NY (3.7 miles).

Table 4.9 Validation results from HWY 386, Cohocton, NY

Core Location	Core Density (Core)	Estimated Density (IACA)	Estimation Error (IACA-Core)
Calcore1	94.7	94.0	-0.7
Calcore2	94.0	93.4	-0.6
CalCore3	93.4	94.5	1.1
C1	95.0	93.3	-1.7
C2	94.4	93.4	-1.0
C3	94.5	93.9	-0.6
C4	91.9	93.8	1.9
C5	93.5	94.0	0.5
C6	93.4	94.5	1.1
C7	93.5	92.8	-0.7
Calcore1	94.3	93.7	-0.6
Calcore2	93.7	93.6	-0.1
CalCore3	92.6	93.4	0.8
C4	92.7	93.9	1.2
C5	92.7	93.4	0.7
C7	93.3	92.7	-0.6
C2	94.5	93.8	-0.7
C3	92.8	92.9	0.1
C4	92.2	92.5	0.3

4.4.5 Field Demonstration - I-35, Norman, OK

(June 17, 2009 - April 21, 2010)

The use of the IACA in estimating the stiffness of a multi-layer HMA pavement was investigated during the construction of Interstate I-35 in Norman, OK (Figure 4.22). This project involved the expansion of the existing highway, stabilizing the subgrade to a depth of 200mm (8 in.) using 10% cement kiln dust (CKD), followed by 200mm (8 in.) thick aggregate base. The asphalt concrete base layer consisted of 100mm (4 in.) thick asphalt layer of 19 mm (0.75 in.) Nominal Maximum Aggregate Size (NMAS) S3 (64-22 OK), while the second and third layers were constructed with 19 mm (0.75 in.) NMAS S3 (76-28 OK) of 100mm (4 in.) and 75 mm (3 in.) thickness, respectively. A 50mm (2 in.)

surface course of 12.5mm (0.5 in.) NMAS S4 (76-28 OK) was compacted on top of the three asphalt layers. During the course of the project, the project team had installed the IACA on a contractor owned and operated Ingersoll Rand DD110 roller. The research team helped calibrate the IACA for each pavement layer by verifying the IACA estimated density against 3 calibration cores extracted from the finished pavement. The contractor was allowed to use the IACA instrumented roller and validate the performance of the device.

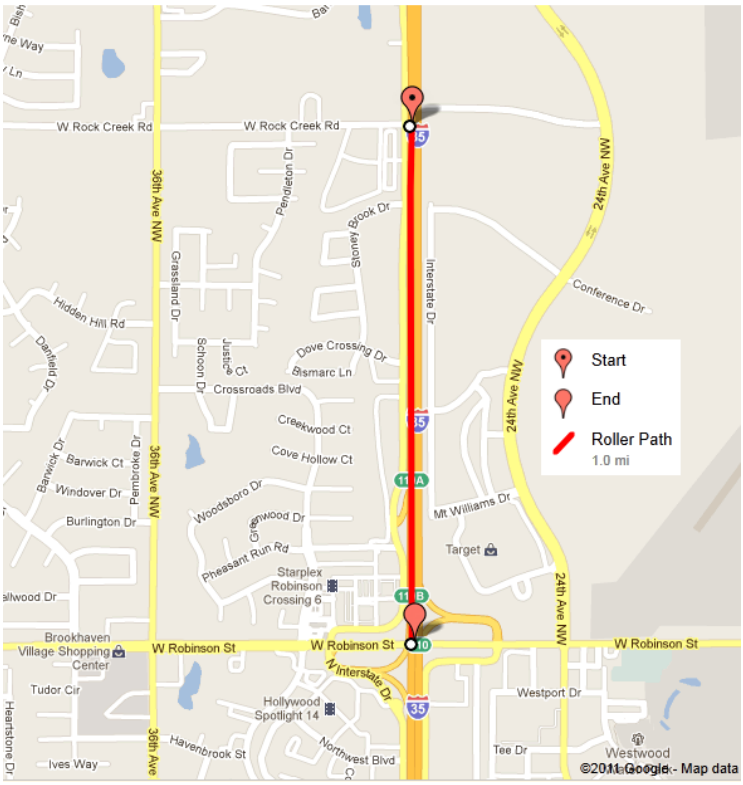

Figure 4.22 Site location on I-35 in Norman, OK.

Table 4.10 Site and machine information, I-35 in Norman, OK

Date	**6/17/09**	**6/18/09**	**6/22/09**	**3/15/10**
Location	I 35 Norman	I 35 Norman	I 35 Norman	I 35 Norman
Construction type	Full depth	Full depth	Full depth	Full depth
Lift	AC base	2nd	3nd	4th
Mix	S3 64-22 OK	S3 76-28 OK	S3 76-28 OK	S4 76-28 OK
Thickness	4"	3"	3"	2"
Roller	IR DD110	IR DD110	IR DD110	IR DD110
Calibration Cores #	3	3	3	3
Validation Cores #	2	3	6	15
	Settings			
Accelerometer location	front	front	front	front
Offset from GPS	0	0	0	0
Drum width (ft.)	6.5	6.5	6.5	6.5

4.4.5.1 Discussion of Results

The calibration and validation of the IACA was performed as described in the previous section. For the AC base layer, the tests indicate that the mean estimation error (i.e., mean of the difference between core density and IACA estimated density) is -0.2% with a corresponding standard deviation of 0.4. Furthermore, the 95% confidence interval for the estimation error is [-0.5, 0.1].

For the second layer of the asphalt pavement, the tests indicate that the mean estimation error is -1 % with a corresponding standard deviation of 1.22. Furthermore, the 95% confidence interval for the estimation error is [-2, -0.1].

For the third layer of the asphalt pavement, the tests indicate that the mean estimation error is -0.7% with a corresponding standard deviation of 0.8. Furthermore, the 95% confidence interval for the estimation error is [-1.3, -0.2].

For the final layer of the asphalt pavement, the tests indicate that the mean estimation error is 0.1% with a corresponding standard deviation of 0.8. Furthermore, the 95% confidence interval for the estimation error is [0.1, 0.4].

4.4.6 Field Demonstration - I-35, Ardmore, OK

(July 01 - 31, 2009)

The performance of the IACA was observed during the overlay of asphalt pavement on Interstate I-35 near Ardmore, OK (Figures 4.23 - 4.24). Remediation of the existing pavement involved milling and removal of 9.65 kilometers (6 miles) of existing pavement and then compacting a 50mm (2 in.) lift of 19mm (0.75 in.) NMAS asphalt mix followed by a second lift of 45mm (1.75 in.) using the same mix. Compaction was achieved using an Ingersoll Rand DD90 dual drum vibratory compactor. Finish rolling was done using Ingersoll Rand DD90 roller operating in static mode.

Figure 4.23 Site location on I-35 near Ardmore, OK (July 01, 2009).

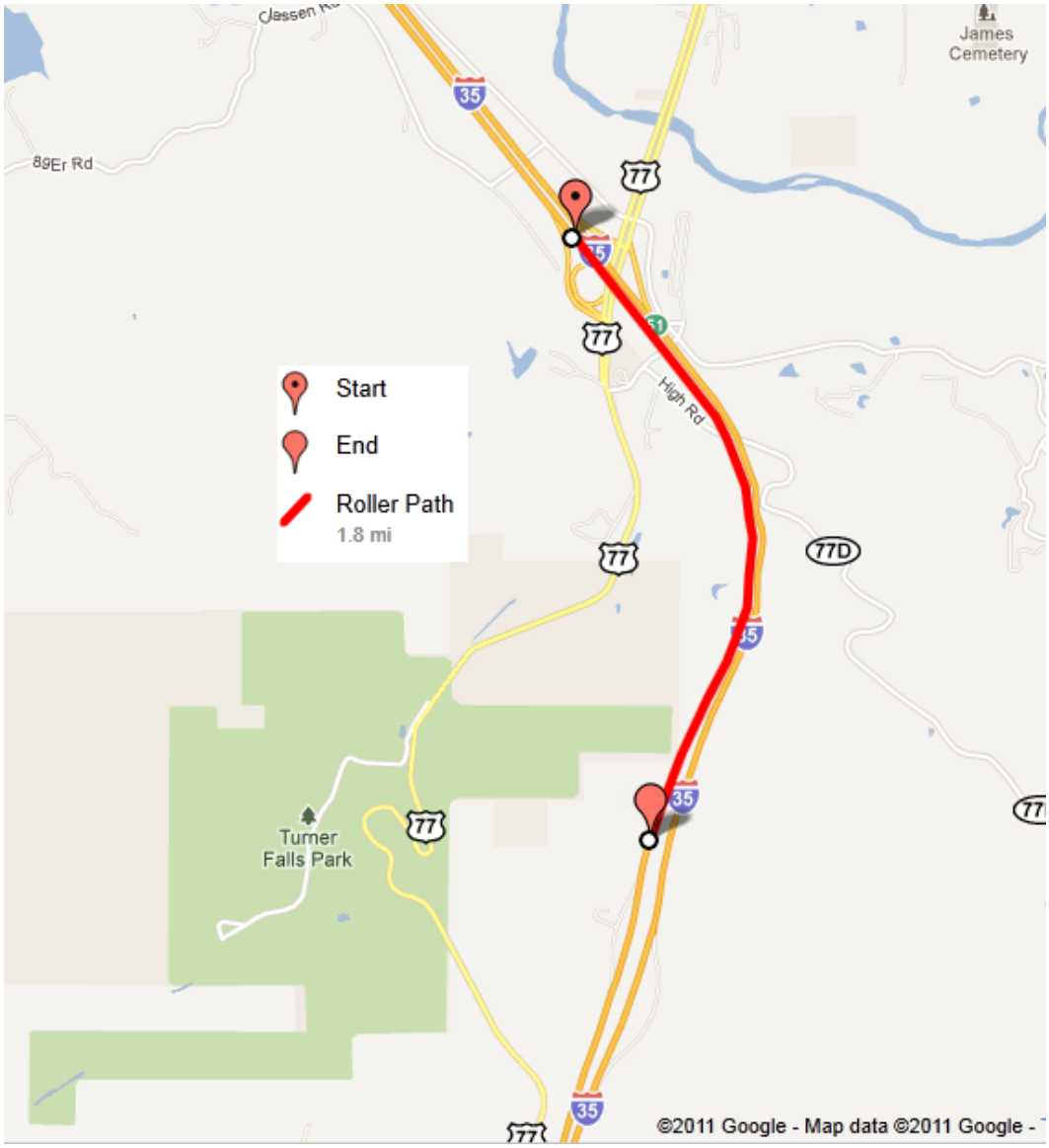

Figure 4.24 Site location on I-35near Ardmore, OK (July 07, 2009).

4.4.6.1 Discussion of Results

Table 4.11 Validation results from I-35 near Ardmore, OK

Layer Thickness	Core Location	Core Density (Core)	Estimated Density (IACA)	Estimation Error (IACA-Core)
2.5"	Calcore1	92.5	93.0	-0.5
	Calcore2	92.7	92.9	-0.2
	CalCore3	92.8	91.6	1.2
	W4	94.1	90.7	3.4
	W5	94.6	92.8	1.8
1.75"	Calcore1	94.0	93.5	0.5
	Calcore2	93.6	93.9	-0.3
	CalCore3	93.8	94.0	-0.2
	T4	94.3	92.6	1.7
	T5	93.1	90.7	2.4

The project team installed the IACA on the contractor owned Ingersoll Rand DD90 vibratory compactor and trained the operator on the operation of the IACA and its installation/removal each day after its use. The calibration and validation of the IACA for each of the asphalt layers was accomplished by the crew. The IACA device was provided to the contractor for a period of two months (duration of the project). During this time, the operator diligently used the IACA each day during the compaction of the pavement. However, the roller operator did not mark any validation cores on the completed pavement. Therefore, the validation of the IACA was accomplished only at the locations marked by the research team at the beginning of the project (Table 4.11).

4.5 Chapter Conclusions

The overview and operational principle of a commercial prototype of the Intelligent Asphalt Compaction Analyzer (IACA) were addressed in this chapter. A rugged

electronic computational platform was selected and the IACA application was ported to this computer. A sensor suite and the associated wiring harness were also developed. Installation procedures for retrofitting vibratory compactors with the IACA were demonstrated on a variety of vibratory asphalt compactors. The accuracy and repeatability of the IACA measurements were demonstrated during the construction of asphalt pavements at six different construction sites.

Chapter 5 QUALITY ASSURANCE OF HOT MIX ASPHALT PAVEMENTS USING THE INTELLIGENT ASPHALT COMPACTION ANALYZER

5.1 Introduction

Adequate compaction of asphalt pavements during their construction is essential to the long-term performance of the pavement. Current Quality Control techniques determine the quality at a limited number of points and are not indicative of the overall quality of the pavement. In this chapter, the Intelligent Asphalt Compaction Analyzer (IACA) is used to estimate the density of an asphalt pavement during its construction and thereby determine the overall quality of compaction. Comparison of these estimates with the Percent Within Limits (PWL) calculations based on roadway cores demonstrates that the IACA can be effectively used as a non-destructive Quality Assurance (QA) tool. Furthermore, since the IACA continuously estimates the density of the asphalt in real-time, inadequate compaction can be addressed during the construction, thereby improving the overall quality of pavement. Thus, the IACA can also serve as a valuable Quality Control (QC) tool during construction.

Currently, QC procedures commonly used during the construction of asphalt pavements require the extraction of roadway cores from the finished pavement and may additionally require several measurements using a point-wise density measurement tool similar to a Nuclear Density Gauge (NDG). While the density measured from the cores provide an accurate indication of the quality, these tests are destructive in nature and are the source of some of the performance issues, such as potholes, that reduce the useful life

of the pavement. Spot tests using nuclear or non-nuclear density gauges provide a quick measurement of the level of compaction, but have inherent limitations that reduce their effectiveness as QC methods. Some of the limitations of QC procedures currently used during compaction are enumerated below (Briaud and Seo, 2003; White et al., 2006; Maupin, 2007).

1. Spot tests cover only a small portion of the compaction area (typically 1:1,000,000).

2. Density tests from roadway cores are time consuming and require several days to complete. While the result is a true indication of the compaction at the test location, it is not an accurate indicator of the quality of the overall pavement. Furthermore, some of these tests are destructive in nature.

3. The test procedure and the analysis of the test data can be time consuming and can result in delays in the construction.

4. Personnel being in the vicinity of heavy equipment can create a potentially unsafe environment.

Table 5.1 summarizes the currently available quality measurements devices (Sebesta et al., 2003; Allen et al., 2003; Schmitt et al., 2006; Sebesta et al., 2006; AASHTO, 2007a; Quintus et al., 2009).

Table 5.1 Tools commonly used for determining compaction quality

Test Name	Operator	Time required for each Reading	Destructive	Portable	Miscellaneous
Nuclear Density Gauge (NDG)	DOT radioactive materials license/ Operator certification	3-4 mins.	No	Yes	- contains hazardous material, - firm contact with the surface is required
Core Density (AASHTO T-166)	Special Training/ Technician or Engineer	12 hours	Yes	No	- requires additional equipment like core drill, coolant, saw etc.
GeoGauge	Basic training required	1.25 min.	No	Yes	
Falling Weight Deflectometer (FWD)	Technical and sophisticated training	2 mins.	No	No	- Large, expensive apparatus that is mounted on a trailer. - 30 minutes to configure the trailer and the data acquisition program
Light Weight Deflectometer (LWD)	Basic training required	1-6 mins.	No	Yes	- Same theory as the FWD
Dynamic Cone Penetrometer (DCP)	Basic training required and physically demanding	10 mins.	Yes	Yes	- Destructive testing - Device prone to jamming and can be dangerous.
Pavement Quality Indicator (PQI)	Basic training required	Instantaneous	No	Yes	- Adjustable for moisture variations and mix type
PaveTracker	Basic training required	Instantaneous	No	Yes	- Measuring the uniformity of HMA

In Chapter 4, the Intelligent Asphalt Compaction Analyzer (IACA) was introduced and its ability to estimate the density of the pavement was demonstrated during compaction in the field. Recently, several agencies in the United States have launched programs to evaluate the technology and determine its suitability as an official (QA)/ (QC) process (CTC, 2006). When properly implemented, Intelligent Compaction can have beneficial effects in the overall quality of the pavements. These benefits include (Briaud and Seo, 2003; Petersen, 2005; Camargo et al., 2006; Peterson and Petersen, 2006; White et al., 2006; Zambrano et al., 2006; Maupin, 2007):

- providing a complete coverage of the compaction area,
- ensuring uniform compaction,
- reducing the overall cost of construction,
- reducing the life-cycle cost by increasing the service life of the pavements,
- providing the quality results in real-time, thereby aiding the management and control of the compaction process, and
- providing mapped and stored information for later use in forensic analysis and long-term pavement management.

In this chapter, the utility of using IACA for Quality Control during the compaction of Hot Mix Asphalt (HMA) pavement is demonstrated. The results show that the IACA estimated density has a statistically significant correlation with the density measurements obtained from roadway cores. Furthermore, the estimated density has a mean error with a 95% confidence interval [$-0.4 \leq 0.1 \leq 0.6$] in terms of air voids in the compacted pavement. Statistical analysis of the IACA data shows that the IACA estimated density has a range comparable to that measured from the roadway cores. The results of the field tests disclosed in this chapter justify the use of IACA for QC during field compaction as well as for computing the PWL for determining the pay factors.

The rest of the chapter is organized as follows. First, statistical QA using PWL calculations based on roadway cores is discussed. After that, the test protocol and the results of the field tests are discussed and conclusions are drawn.

5.2 Statistical QA Using Roadway Cores

The construction of an asphalt pavement typically involves the compaction of multiple lanes over several miles of the roadway. Ideally, the Quality Assurance (QA) would require the measurement of the density over the entire extent of the pavement. However, such a measurement is infeasible both from a time and cost standpoint. As a consequence, QA in the field is restricted to taking only a finite number of measurements at randomly selected locations. Depending on the contracting agency, QA would also include statistical techniques to estimate the overall quality based on this set of finite measurements. Currently, most state agencies employ Statistical QA (SQA) specifications to some degree. The acceptance criteria in these specifications address at least the following three items: i) the quality level desired by the agency; ii) the procedure to determine the quality; and iii) the pay factors and the penalty for not meeting the prescribed quality. Depending on the contracting agency, such a penalty could result in a simple pass/fail decision with pursuant adjustments in the contract payment. Percent Within Limit (PWL) is the SQA method that the Federal Highway Administration (FHWA) has recommended for ensuring the quality of HMA pavements (Burati et al., 2003; Gee, 2004). This technique was designed to encourage and reward contractors to achieve uniform, consistent compaction of HMA pavements. PWL technique enables the awarding agency and the contractor to use a small number of spot tests on the completed pavement to statistically estimate the overall quality of the pavement (FHWA, 2006b).

The PWL method is based on the assumption that the density of the compacted asphalt pavement is normally distributed about a mean density (Burati et al., 2003; Burati

et al., 2004). The variance of the measurements is an indicator of the uniformity of the compaction - the larger the variance, the greater is the variability of the density about the mean. For example, if four spot tests of density on a mile of compacted asphalt pavement reveal a mean density of 94% (6% air voids) and a standard deviation ( ) of 1%, then it can be construed that 68% of the pavement is within 1 standard deviation of the mean density. In other words, about 68% of the pavement is likely to be compacted between 93-95% of the maximum theoretical density (5-7% air voids). The graph of a normal distribution with a mean ( ) and a standard deviation ( ) is shown in Figure 5.1.

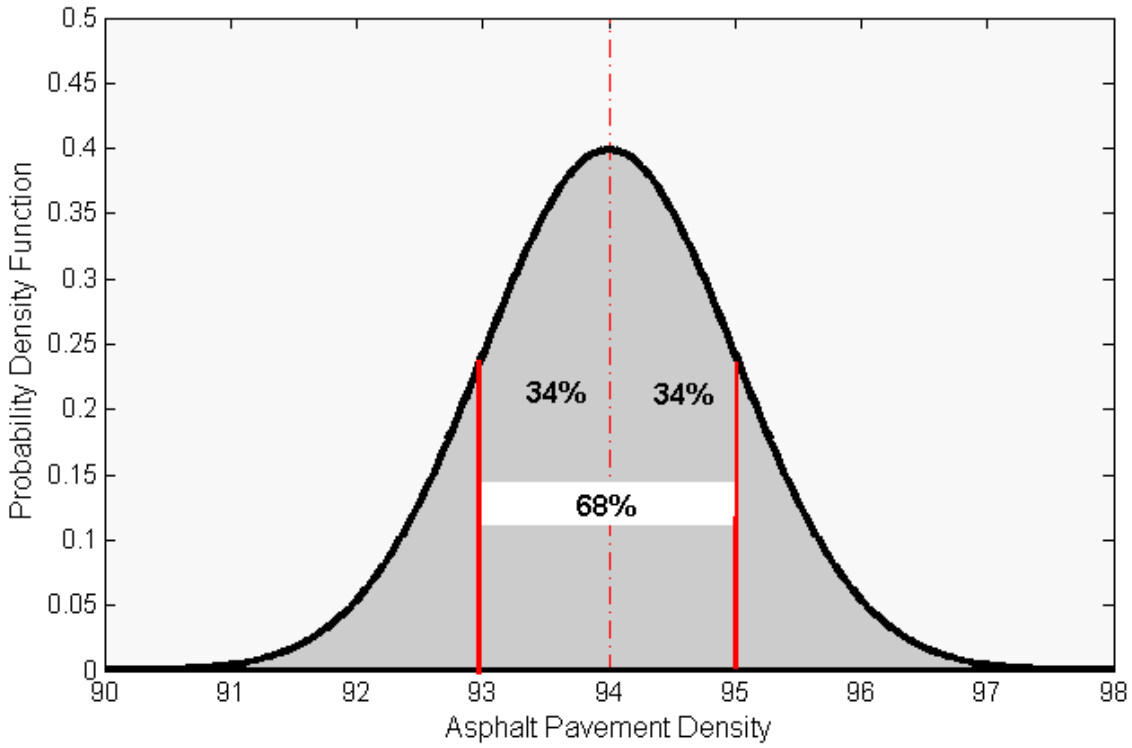

Figure 5.1 Probability density function of a normally distributed data with mean μ = 94 and standard deviation σ = 1.0.

According to (TRB, 2005), PWL is the percentage of the compacted pavement whose density lies between the Lower Specification Limit (LSL) and the Upper Specification

Limit (USL). These limits determine the acceptable quality and the corresponding pay factors (FHWA, 2006b). In this dissertation, the PWL is calculated as follows (Materials Bureau, 2001):

1. Four core locations are marked at random for every 1000 tons of asphalt that is laid and compacted.

2. The cores are extracted and the density of each core is measured according to the AASHTO T-166 method. The mean (μ) and standard deviation (σ) for the entire days' production are calculated.

3. The mean (μ) and the standard deviation (σ) are computed as follows:

$$\mu = \frac{\sum_{i=1}^{n} x_i}{n}, \tag{5.1}$$

$$\sigma = \sqrt{\frac{\sum_{1}^{n}(x_i - \mu)^2}{n}}, \tag{5.2}$$

where 'n' indicates the total number of core samples; and x_i indicates the density of the i^{th} core sample.

4. The Lower Quality Index (Q_L) and Upper Quality Index (Q_U) are computed as follows:

$$Q_L = \frac{[\mu - L]}{\sigma}, \tag{5.3}$$

$$Q_U = \frac{[U - \mu]}{\sigma}, \tag{5.4}$$

where L is the lower specification limit and U is the upper specification limit.

Table 5.2 The percentage of material between the lower (L) and upper (U) specification limits (PWL).

Percent Material							Positive Values QU or QL
Above PL or Below PU	Above PL or Below PU	Above PL or Below PU	Above PL or Below PU	Above PL or Below PU	Above PL or Below PU	Above PL or Below PU	
25	0.75	50	0.00	50	0.00	75	0.75
24	0.78	49	0.03	51	0.03	76	0.78
23	0.81	48	0.06	52	0.06	77	0.81
22	0.84	47	0.09	53	0.09	78	0.84
21	0.87	46	0.12	54	0.12	79	0.87
20	0.90	45	0.15	55	0.15	80	0.90
19	0.93	44	0.18	56	0.18	81	0.93
18	0.96	43	0.21	57	0.21	82	0.96
17	0.99	42	0.24	58	0.24	83	0.99
16	1.02	41	0.27	59	0.27	84	1.02
15	1.05	40	0.3	60	0.30	85	1.05
14	1.08	39	0.33	61	0.33	86	1.08
13	1.11	38	0.36	62	0.36	87	1.11
12	1.14	37	0.39	63	0.39	88	1.14
11	1.17	36	0.42	64	0.42	89	1.17
10	1.20	35	0.45	65	0.45	90	1.20
9	1.23	34	0.48	66	0.48	91	1.23
8	1.26	33	0.51	67	0.51	92	1.26
7	1.29	32	0.54	68	0.54	93	1.29
6	1.32	31	0.57	69	0.57	94	1.32
5	1.35	30	0.60	70	0.60	95	1.35
4	1.38	29	0.63	71	0.63	96	1.38
3	1.41	28	0.66	72	0.66	97	1.41
2	1.44	27	0.69	73	0.69	98	1.44
1	1.47	26	0.72	74	0.72	99	1.47

5. PWL between U and L is finally calculated as follows:

$$PWL = [P_U + P_L] - 100, \quad (5.5)$$

where P_U and P_L are obtained from Table 5.2 that was derived from the procedure for statistically determining the density of the HMA pavement (Materials Bureau, 2001).

5.3 Results and Discussions

5.3.1 Setup

Field testing of the IACA system was conducted during the construction of HMA pavement on interstate I-86 near Hornell, New York. The existing asphalt pavement had a concrete base that was severely fractured at a number of locations. The rehabilitation of the pavement was undertaken by first milling and removing 15mm (0.6 in.) of Nova Chip from the pavement where the support was adequate. The remainder of the pavement was rubblized and then proof rolled. Any soft areas were undercut by excavating the pavement and the sub-base and then replacing it with screened gravel and a lift of 25mm (1 in.) asphalt mix. The pavement (either rubblized or undercut) was then paved with a 63mm (2.5 in.) lift using a 25mm (1 in.) mix, two 50mm (2 in.) lifts of 19mm (0.75 in.) asphalt mix, followed by a 40mm (1.6 in.) lift using 9.5mm (0.38 in.) asphalt mix. The IACA data was collected during the construction of the second lift of the 19mm (0.75 in.) mix. The mix was trucked to the location by trucks and laid down using a Vogele 2219W paver. Compaction was then achieved using a Hamm HD-130 HV and a Volvo DD118HFA dual drum vibratory compactors operating in tandem. Finish rolling was performed by the Volvo roller operating in static mode (see Table 5.3). The breakdown

roller (Volvo DD118HFA) was instrumented with the IACA and the IACA was calibrated during the construction of a control strip. The estimated density of the pavement, instantaneous location of the roller, asphalt mat temperature etc., were recorded during the compaction process.

Table 5.3 Pavement Information

Project Location	Description		Type	Lift Thickness	Mix	Machine
I-86 Hornell, NY	Extent	5.75 Km	Mill & Overlay	50.8 mm	19mm PG-64-22	Volvo DD118HFA HAMM HD130HV
	# Lanes	1				
	# Lifts	1				

5.3.2 Data Collection

The performance of the IACA was studied during the construction of 5.75 kilometers (3.6 miles) of I-86 on July 22th and July 24th of 2009. Three cores, C1 - C3, were first used to calibrate the. At the end of each day, four core locations were marked by the New York Department of Transportation (NyDOT) inspector (see Figure 5.2), according to the random sampling procedure specified in (Materials Bureau, 2001). Five density readings were taken at each marked location using a calibrated Non-Nuclear Density Gauge (NNDG). The GPS coordinates of these locations were also noted. Then two adjacent cores, labeled Department of Transportation core (DOT core) and Companion core (CMP core) in Figure 5.2, were extracted from each marked location. The DOT cores were tested at the NyDOT laboratory and the CMP cores were tested by the contractor according to the AASHTO T-166 method for determining the bulk specific gravity of compacted bituminous specimens.

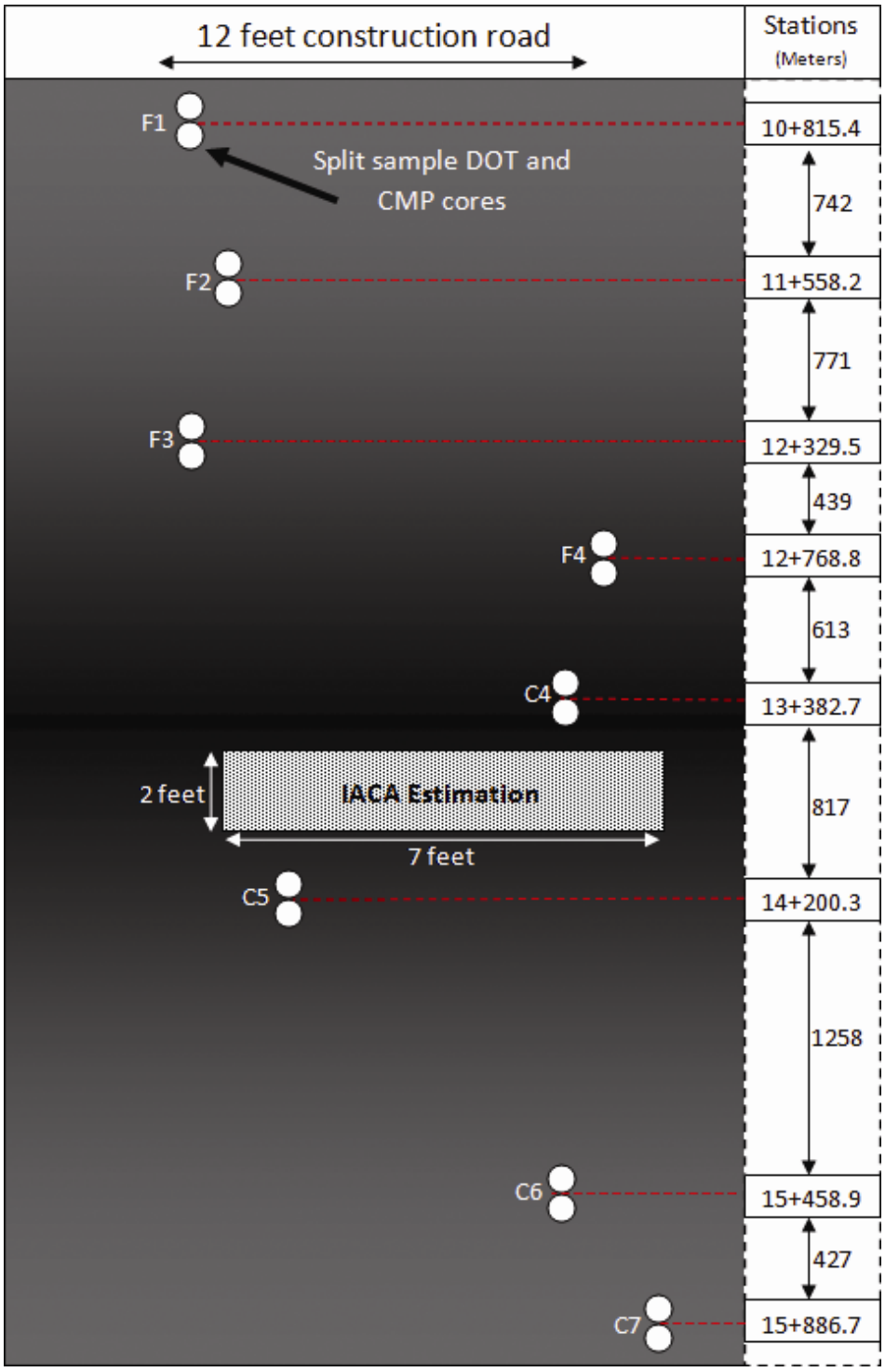

Figure 5.2 Illustration of marked cores and IACA estimation strip.

5.3.3 Interpretation of the Data

The IACA estimated density, roller GPS data, and the asphalt mat temperature were then processed to generate an as-built map showing the compaction achieved over the entire pavement. Figure 5.3 shows the density estimated by the IACA during the final roller pass during both days. The comparison of the IACA estimated density with the actual core densities and NNDG density measurements at the random locations (C4-C7 and F1-F4) tested by the NyDOT personnel is shown in Table 5.4.

Table 5.4 IACA estimation results compared to actual core densities and NNDG measurements.

Measured Location	Density			Error			
	DOT Core	CMP Core	IACA Estimation	DOT vs. CMP	Cores vs. NNDG	Cores vs. IACA	NNDG vs. IACA
C1	N/A	94.9	94.1	N/A	1.3	0.8	-0.5
C2	N/A	94.3	93.7	N/A	0.7	0.6	-0.1
C3	N/A	94.1	94.6	N/A	0.4	-0.5	-0.9
C4	93.6	95.3	94.5	-1.7	0.5	-0.0	-0.5
C5	94.3	94.4	94.2	-0.1	0.6	0.1	-0.4
C6	95.3	95.2	93.9	0.1	1.7	1.3	-0.4
C7	94.1	93.9	94.3	0.2	0.9	-0.3	-1.2
F1	94.1	93.9	94.5	0.2	0.1	-0.5	-0.6
F2	95.9	95.6	94.7	0.3	1.0	1.0	0.1
F3	94.6	93.0	95.2	1.6	-0.5	-1.4	-0.9
F4	94.2	93.0	93.6	1.2	-0.5	0.0	0.5
μ	94.5	94.3	94.3	0.2	0.6	0.1	-0.4
σ	0.7	0.9	0.5	1.0	0.7	0.8	0.5

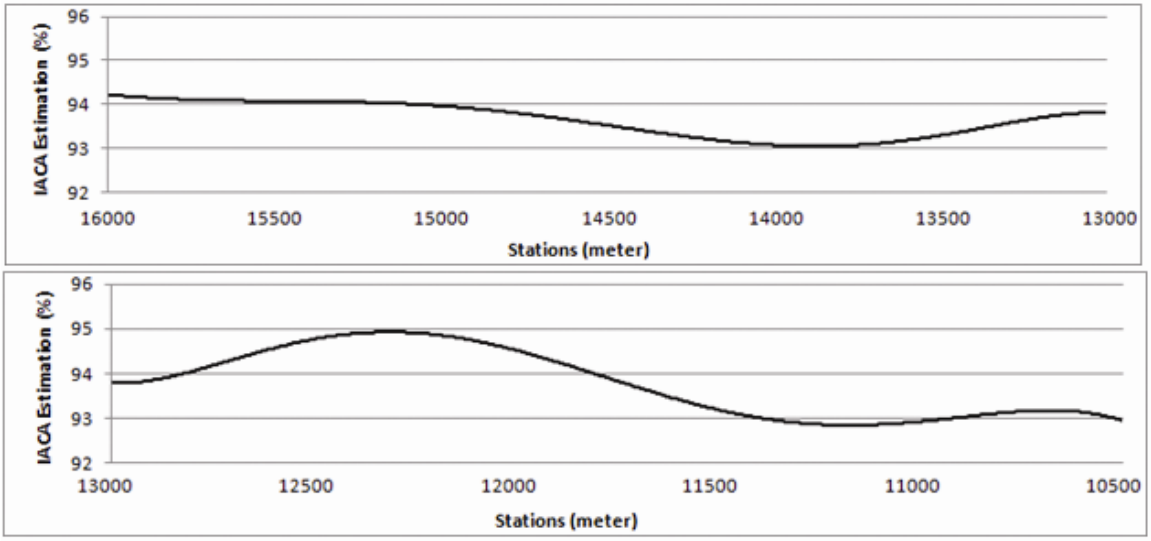

Figure 5.3 Density estimation of the final roller pass during both days.

A comparison of the IACA estimates with the density measured from the cores reveals that the mean and standard deviation of the IACA estimated density (94.3, 0.5) is comparable to the corresponding values of the actual densities (94.5, 0.7). In addition, the mean and standard deviation of the error between IACA estimations and the actual average densities of the corresponding cores is less than the error between DOT and CMP cores. As noted earlier, the DOT and CMP cores belong to the same split core sample and are a few inches apart. However, the densities of these cores have been observed to vary by as much as 1.7%. The GPS reading of the IACA is updated once every second. Taking into account the width of the roller drum (2133mm (7 ft.)), the speed of the roller (approximately 3.2 kilometers per hour (2 miles per hour)), and the IACA display rate of 2Hz, it can easily be verified that the IACA estimated density is the average density observed in a 2.1m (7 ft.) by 0.6m (2 ft.) rectangle surrounding the core (see Figure 5.2). Thus, while the density of distinct locations on the asphalt mat could generally vary, the

IACA tracks the average density of the pavement with reasonable accuracy (see also Table 5.5).

Table 5.5 Variation in density laterally across the drum at a given location on the pavement

Core Location	Density			
	Left	Right	Difference (Left-Right)	IACA Estimate
Base #1	90.9	92.0	-1.1	91.1
Base #2	92.3	93.6	-1.3	92.7
II Lift #1	90.6	91.6	-1.0	90.9
II Lift #2	92.3	90.5	1.8	91.8
II Lift #3	91.7	91.8	-0.1	91.5
III Lift #1	92.3	92.2	0.1	92.4
III Lift #2	91.6	90.2	1.4	92.0
III Lift #3	92.2	92.5	-0.3	92.4
Surface #1	90.6	91.4	-0.8	90.5
Surface #2	91.4	92.4	-0.8	91.9
Surface #3	91.9	91.6	0.3	91.4

5.3.4 Statistical Analysis of the IACA Estimated Density

Observing the mean and variance of two sets of data is usually not enough to determine if the two populations represented by these samples are statistically similar. This is especially true if the number of samples is small (Ledolter and Hogg, 2008). Since a finite number of core samples are extracted per lane mile of the completed pavement, comparison of the mean and variance of the IACA estimates with the corresponding values obtained from the core samples cannot determine if the observed deviations are significant. Null hypothesis tests are therefore conducted to determine if the observed differences in the mean and variance are significant. A paired t-test, recommended by FHWA (Gee, 2004), was used to compare the means of the average core densities versus

estimated IACA densities. After the normality of the distributions of both data samples was checked by the application of the Kolmogorov-Smirnov (K-S) test, a paired t-test was applied. The K-S test showed that the data is consistent with a normal distribution with a 'P' value of 0.66, thereby indicating that that *the difference in the mean of the IACA estimates and the mean of the core densities is not statistically significant*. Furthermore, the 95% confidence interval for the error in the mean densities observed was found to be [-0.4 ← 0.1 → 0.6]. Following the procedure outlined in (Gee, 2004), the F-ratio was 1.9, $F_{critical}$ was 2.9, and the corresponding 'P' value was 0.2. These values demonstrate that *the difference in the variances of the estimated and measured densities is also statistically insignificant*. Together, these results show that the difference between the IACA estimated densities and the densities measured from roadway cores is statistically insignificant.

These results along with the results noted in the overview section show that the IACA can estimate the density of asphalt pavements with a measurement error of less than 2 pounds per cubic foot (pcf) corresponding to an error less than 1.2%. It is well known (Quintus et al., 2009) that the measurement accuracy of nuclear density gauges is typically in the range of 2.5 - 4.0 pounds per cubic foot (pcf). This translates to a measurement error in the range of 1.5 - 2.5% air voids for standard asphalt mixes. In contrast, the IACA has a measurement accuracy of better than 1.2% (95% confidence interval) with the associated benefits of complete coverage of the pavement in real-time.

5.3.5 QA using the IACA

Performing the PWL analysis based on the density measurements from the DOT cores, it was estimated that 100% of the I-86 pavement was compacted between a density of 93% and 96% (Table 5.6). Likewise, for the construction on Hwy-386, it was estimated that 100% of the Hwy-386 pavement was compacted between a density of 93% and 96% (Table 5.6). On the other hand, using the IACA estimated density, one could conclude that 100% of the constructed pavement on I-86 and 98% of the constructed pavement on Hwy 386 was between 93% and 96% compaction. Table 5.7 shows the actual density estimated during the final roller pass during compaction at both these sites. The data reiterates the fact that the majority of the construction was of very high quality and less than 1% of the completed pavement was under-compacted.

Table 5.6 PWL calculation using core densities and IACA estimations.

Density Range	22-Jul		24-Jul	
	Using Core	Using IACA	Using Core	Using IACA
	PWL for DR			
DR ≤ 88	0	0	0	0
88 < DR ≤ 89	0	0	0	0
89 < DR ≤ 90	0	0	0	0
90 < DR ≤ 91	0	0	0	0
91 < DR ≤ 92	0	0	0	0
92 < DR ≤ 93	0	0	0	2
93 < DR ≤ 96	100	100	100	98
96 < DR ≤ 97	0	0	0	0
97 < DR ≤ 98	0	0	0	0
98 < DR ≤ 99	0	0	0	0
DR > 99	0	0	0	0

During the preparation of the I-86 site, the contractor had noted the existence of soft spots in the AC base between stations 13500 and 15500 and between stations 10500 and 11500. These stretches corresponded to the sections of the highway under a bridge and remediation of the AC base was not considered feasible. Reconstruction of the as-built maps from IACA estimates show that an average density of 93% was achieved on this stretch in contrast to densities between 94 - 95% at other locations on the completed pavement.

Table 5.7 IACA tabulated frequencies (percent)

Density Range	22-Jul Percentage	24-Jul Percentage
DR ≤ 88	0%	0%
88 < DR ≤ 89	0%	0%
89 < DR ≤ 90	0%	0%
90 < DR ≤ 91	0%	0%
91 < DR ≤ 92	1%	1%
92 < DR ≤ 93	12%	14%
93 < DR ≤ 96	86%	80%
96 < DR ≤ 97	1%	5%
97 < DR ≤ 98	0%	0%
98 < DR ≤ 99	0%	0%
DR > 99	0%	0%

5.3.6 IACA vs. Traditional Methods

There are three traditional methods that are commonly used in the determination of the density of an asphalt pavement: a) lab measurement of extracted roadway cores; b) Nuclear Density Gauge (NDG) measurements; and c) Non-Nuclear Density Gauge (NNDG) measurements. On one hand, all traditional methods are spot tests and do not adequately reflect the overall quality of the pavement. On the other hand, Intelligent Compaction technologies, like the IACA, can provide a complete assessment of the

quality of the pavement and aid both in Quality Control as well as in Quality Assurance. Furthermore, since the IACA estimates the density in real-time during the compaction process, over- or under-compaction of the pavement can be detected and avoided. While under-compaction can be detected using traditional methods, the testing is infeasible from a cost and time standpoint. Over-compaction on the other hand, can only be detected after the construction is complete, at which time the pavement cannot be easily rectified.

The rolling pattern for a particular compaction job is established by the contractor in cooperation with the representative of the contracting agency at the beginning of the job. During the compaction of a test pavement, the density achieved after each roller pass is measured using a handheld gauge. Compaction is stopped when no further increase in density is observed. Cores are extracted at random from the completed pavement and their density is measured in the laboratory to ensure that compaction targets are met. Once a rolling pattern is established, the contractor periodically verifies the final density but does not usually verify the variations in density after each pass or alter the rolling pattern unless necessitated by quality issues. While this process may be adequate to obtain passing quality during the compaction of asphalt pavements, it is not ideal for attaining optimum quality during compaction. The ability of the IACA to determine the density during compaction can be used to address over/under compaction of the asphalt pavement as demonstrated in the following two case studies.

Case Study 1. The performance of the IACA was observed during the overlay of asphalt pavement on Interstate I-40 near Hinton, OK. Remediation of the existing pavement involved milling and removal of 9.6 kilometers (6 miles) of existing pavement and then compacting a 76.2mm (3 in.) lift of 19mm asphalt mix followed by a second lift

of 50.4mm (2 in.) using the same mix. Compaction was achieved using a Dynapac and an Ingersoll Rand DD138HF dual drum vibratory compactors operating in tandem. Finish rolling was done using an Ingersoll Rand DD118 roller operating in static mode. The density during successive roller passes is shown in Figure 5.4. It can be seen from the figure that significant compaction was already achieved during the first pass of the roller. Since the two breakdown rollers are operating in tandem, the achieved compaction is higher than in the case where only one roller is used. However, it can be seen from the figure that the additional roller passes actually have a detrimental effect in the sense that the mix is over-compacted and the final compaction that is achieved (92.3%) is far lower than the maximum compaction that was obtained at the completion of the second pass (94.6%). Thus, having access to the IACA estimates can avoid over compaction of the asphalt pavement and result in better quality of compaction.

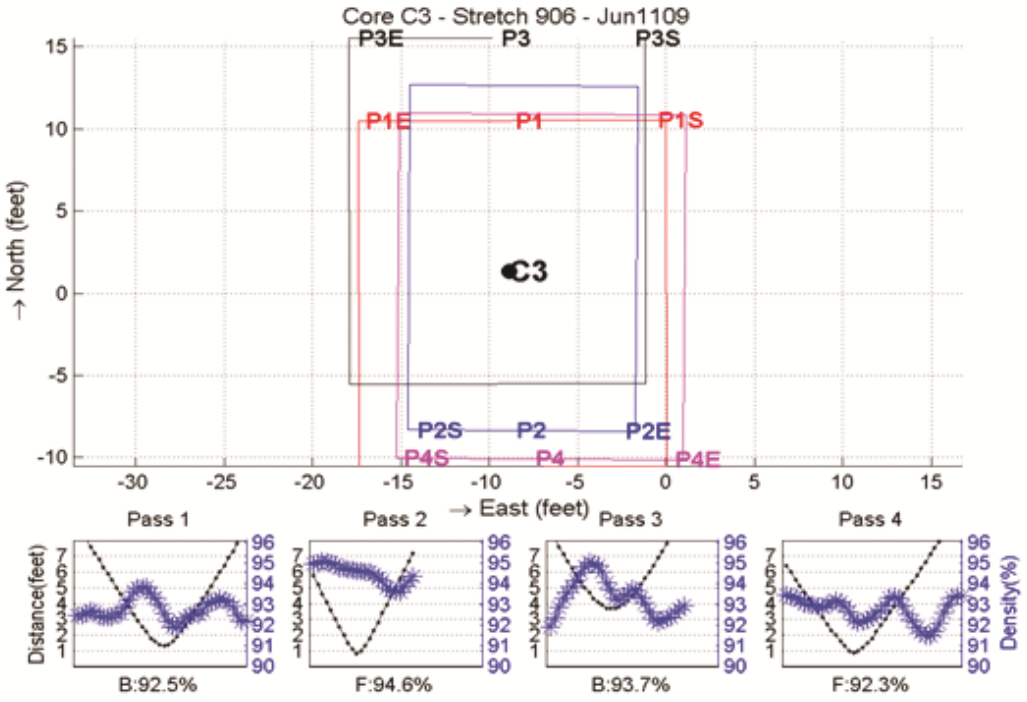

Figure 5.4 Reduction in density as a result of over-compaction of the asphalt pavement.

Case Study 2. The ability of the IACA to detect under-compaction of an asphalt pavement was observed during the construction of 2.7 kilometers (1.7 miles) of US Highway 62, near Blanchard in McClain County, Oklahoma. The project involved the construction of a full-depth asphalt pavement consisting of four driving lanes, a turn lane, and 2.5m (8 ft.) shoulders on either side of the road. The existing pavement was first removed and the soil sub-grade was stabilized to a depth of 200mm (8 in.) using 15% fly ash. Using a 19mm (0.75 in.) asphalt mix, a 75mm (3 in.) base layer was first constructed on top of the compacted sub-grade. This is followed by two additional lifts of 75mm (3 in.) using the same mix. A 50mm (2 in.) surface course was then laid using a 12.5mm (0.5 in.) asphalt mix.

Twelve test locations were marked 3m (10 ft.) apart at the center of each lane after the final pass of the breakdown roller. The density at each of the test locations (labeled L1 - L12 in Table 5.8) was noted using a calibrated nuclear density gauge as well as the IACA. At each location roadway cores were also extracted and their density was measured in the laboratory according to AASHTO T-166 specification. Table 5.8 summarizes all three measurements at each location. The core densities of these locations turned out to be relatively low indicating an under-compaction that might be caused by one or more of the following: soft soil sub-base, problem with the mix production, and/or insufficient compaction. The NNDG measured high densities at these locations, whereas the IACA system estimated low densities with a small estimation error from the actual densities that were measured in the laboratory. The results demonstrate that the IACA could detect under-compaction issues that were not detected traditional Quality Control tools.

Table 5.8 Under-compaction detection using IACA system

Measured Location	Density			Error	
	NNDG (%)	Core (%)	IACA (%)	NNDG – Core (%)	IACA – Core (%)
L1	92.1	90.3	90.2	1.8	-0.1
L2	92.7	90.6	90.9	2.1	0.3
L3	93.4	91.7	91.0	1.7	-0.7
L4	93.2	92.2	90.1	1.0	-2.1
L5	92.9	91.5	91.0	1.4	-0.5
L6	92.1	89.7	91.0	2.4	1.3
L7	92.8	90.8	91.0	2.0	0.2
L8	93.2	90.5	91.5	2.7	1.0
L9	93.5	91.6	91.2	1.9	-0.4
L10	93.4	91.3	91.2	2.1	-0.1
L11	93.4	90.5	91.1	2.9	0.6
L12	93.8	91.1	91.1	2.7	0.0

5.3.7 Discussion on the Use of the IACA

One of the attractive features of the IACA technology is its applicability to vibratory compaction of both asphalt pavements and soil sub-grades. The IACA has been successfully retrofitted on several different vibratory compactors and the performance was reported in (Commuri, 2009a). The extension of the IACA to estimate the stiffness (modulus) of asphalt pavements has been reported in (Singh et al., 2010).

The accuracy of the IACA density estimates depends on the proper calibration of the device. While calibration using roadway cores is preferred, the calibration can be performed using density results obtained using a nuclear density gauge. In this case, the accuracy of the IACA would degrade and be comparable to that of a nuclear density gauge (Commuri, 2009a).

The commercial implementation of the IACA is currently underway (Commuri, 2010). While the cost of the device to the end user is unclear at this time, it is expected

that this device will be of comparable cost to other commercially available Intelligent Compaction technologies. These technologies typically cost between $20,000 - 50,000 and have a return on the investment of less than 1 year in terms of reduced personnel costs and penalties, increased efficiency, and improved workplace safety.

5.4 Chapter Conclusions

In this chapter, the IACA was used to estimate the quality of compaction of asphalt pavement during its construction. Comparison of the pavement density estimated by the IACA with the density of the roadway cores show that there is no statistically significant difference between the two sets of measurements. Comparison of the IACA readings with the PWL calculations based on roadway cores demonstrated that the IACA can be used for determining the overall quality based on PWL. Furthermore, since the IACA provides these measurements during the compaction of the asphalt mat, the IACA can be used to improve the overall quality of compaction, thereby serving as a QC tool. Analysis of the density estimated by the IACA during the construction at two different sites demonstrate that the IACA can detect over-compaction as well as under-compaction of asphalt pavements during their construction.

The IACA data reported in this chapter has shown that the IACA measurements are comparable to the current Quality Control techniques in terms of measuring accuracy. In addition, the IACA provides a complete coverage of the compaction area and stores mapped information for later use in forensic analysis and long-term pavement management. Furthermore, IACA provides real-time density measurements that can be used to manage and control the compaction process that would improve quality due to

more uniform compaction. As a result, compaction costs are reduced resulting in significant savings in the overall cost of construction maintenance of this critical infrastructure. The extension of the IACA to estimate the stiffness of asphalt pavement layers as well as cohesive soils and granular materials is currently underway.

Chapter 6 CONCLUSIONS AND SCOPE OF FUTURE WORK

In this dissertation, a non-contact sensor capable of determining the quality of asphalt pavements during their construction was developed. Adequate compaction of an asphalt mat during its construction is necessary for the proper functioning of the pavement over its designed lifetime. Excessive rutting, cracking, potholes etc., that are signs of failure in asphalt pavement can be avoided by ensuring proper compaction through the use of Quality Control tools and via the adoption of better construction practices. Current Quality Control technologies allow only point-wise measurements of density during the construction of asphalt pavements. This manual process of measurement is time consuming and results in avoidable delays in the construction and does not reflect the overall quality of the pavement. While the mechanism of pavement failure is well understood, there are no accepted tools that can determine the quality of the entire pavement during its construction. *Thus, there is a need for integrating sensors into vibratory rollers and to develop automated systems that can control the compaction process to achieve the target levels of compaction.*

In the past decade, several Intelligent Compaction (IC) models were introduced commercially. However, these systems do not report measurements of any physical quantity that is associated with the pavement and cannot be verified through in-situ measurements. Since there is minor theoretical or mechanics background in the development of these techniques, little insight can be gained into the compaction of asphalt pavements. While there have been a few studies on the compaction using these

techniques, such studies have focused on soil compaction and very little research addressed the compaction of asphalt pavements.

6.1 Contributions

While it is generally understood that the quality of asphalt pavements during construction can be improved using Intelligent Compaction techniques, some fundamental modeling and control issues have to be addressed before such techniques can be proven successful. A closed-loop control strategy for the roller cannot be developed without a proper understanding of the underlying dynamics and the ability to feedback required information in real-time. *In this dissertation, the dynamics of the interaction between the roller and asphalt mat were first determined through the development of the Visco-Elastic-Plastic (VEP) model. A sensing technology that can estimate the level of compaction (density or stiffness) of the asphalt mat in real-time during construction was then developed.*

6.1.1 Visco-Elastic-Plastic Model

A summary of the contributions is as follows:

- The dynamic equations representing the behavior of the VEP model were shown to be computationally tractable and in a form that is conductive to numerical simulation.
- It was also shown that the parameters in these equations are dependent on the roller and the properties of the asphalt mix.
- It was shown that these parameters can be calculated from experimental results in a straightforward fashion.

- Simulation results showed that the model accurately predicts the compaction of hot mix asphalt in the field.
- Numerical simulations of static compaction resulted in minimal reduction in the amount of air voids content (0.5%), revealing that the model has the basic features to describe field asphalt compaction.
- During numerical simulations of vibratory compaction, the fundamental frequency of the vibrations of an IR DD118 compactor matched the measured value of 50Hz.
- Another set of simulations proved that the model is able to capture the asphalt mat thickness effect on the compaction outcome.
- Additional simulations showed that the model can capture the temperature cooling effect on the compaction process and on the workability of the mix, and the effect of starting compaction at a below optimum temperature.
- Comparison of the simulation results with data gathered during construction of asphalt pavements indicate that this model lays the theoretical groundwork for the realization of Intelligent Compaction of asphalt pavements.

6.1.2 Intelligent Asphalt Compaction Analyzer

A summary of the contributions is as follows:

- The experimental verification of the intelligent sensing that is proposed in this dissertation was accomplished through the development of a rugged, real-time Intelligent Asphalt Compaction Analyzer (IACA).

- The prototype IACA is easily installable on any vibratory compactor, and is able to estimate the compaction with accuracy suitable for its use in Quality Control and Quality Assurance.
- The performance of the IACA prototype was evaluated during the construction of both full-depth and overlays of asphalt pavements.
- The IACA was able to measure the density of the compacted pavement with a mean error of 0.1 percent (of the Theoretical Maximum Density) and a standard deviation of 0.8.
- Results showed that the IACA is suitable for use as a Quality Control tool during the construction of asphalt pavements.
- The utility of using IACA for Quality Assurance was also demonstrated at two different construction sites.
- The estimated density had a mean error of 0.1 with a 95 percent confidence interval [-0.4, 0.6] in terms of air voids in the compacted pavement.
- Such a technology would not only result in better quality and longer lasting pavement, but will also result in increased productivity of the construction crew, shorter construction times, and reduced construction costs.

6.2 Scope of Future Work

Adequate control of the compaction process via the adjustment of the compactive effort would help eliminate under-compaction and prevent over-compaction of an asphalt mat. Settings of a vibratory roller, such as the frequency and amplitude of the eccentric force, could be altered in ordered to adapt the compactive effort. The findings of this

dissertation can be used as a foundation to extend the IACA system so it can control the machine behavior.

The long-term performance of an asphalt pavement is directly related to its load bearing capability and is determined by the stiffness achieved during the construction process. Early deterioration of pavements due to rutting, fatigue cracking, and other types of distresses can be traced to inadequate stiffness. While dependence of pavement performance on stiffness is well known, this parameter is rarely measured during construction. Instead, current Quality Control in the field during the construction of asphalt pavements focuses on the measurement of density of the finished pavement at specific locations. Therefore, the use of the IACA in determining the dynamic modulus |E*| of the entire pavement under construction is being explored.

The proposed VEP model is shown to be computationally tractable and in a form that is conductive to numerical simulation. However, the performance of the model in capturing the behavior of the roller and asphalt pavement during compaction can be improved by addressing the following:

a) Extension of the model to consider the effect of pavement layers and subbase on the compaction process.
b) Consideration of the shear stress and strain during the compaction process.
c) A solution to estimate the contact area between the drum and the pavement surface.
d) Investigation of the effect of changing amplitude and frequency of the drum eccentrics on compaction.

REFERENCES

American Association of State Highway and Transportation Officials (AASHTO) (2007a). *AASHTO T-166: Bulk Specific Gravity Of Compacted Bituminous Mixtures Using Saturated Surface-Dry Specimens.* Standard Method, Washington, DC: American Association of State Highway and Transportation Officials.

American Association of State Highway and Transportation Officials (AASHTO) (2007b). *AASHTO TP 62: Standard Method of Test for Determining Dynamic Modulus of Hot Mix Asphalt (HMA).* Standard Method, Washington, DC: American Association of State Highway and Transportation Officials.

Åkesson, F. (2008). *Dynapac Compaction Analyzer and Optimizer,* Presentation, Dynapac, Dallas, TX: Transportation Pooled Fund Intelligent Compaction Systems initial-Task Working Group meeting.

Allen, D.; Schultz, D.; and Willett, D. (2003). *Evaluation of Non-Nuclear Density Gauges.* Lexington, KY: Kentucky Transportation Center.

Anderegg, R.; and Kaufmann, K. (2004). "Intelligent Compaction with Vibratory Rollers: Feedback Control Systems in Automatic Compaction and Compaction Control." *Soil Mechanics 2004* (Transportation Research Record), no. 1868, pp. 124-134.

Anderegg, R.; Von, D.; and Kaufmann, K. (2006). "Compaction Monitoring Using Intelligent Soil Compactors." *GeoCongress 2006: ASCE Geotechnical Engineering in the Information Technology Age.* Atlanta, GA.

Andregg, R. (2008). *Intelligent Compaction GPS-based Compaction Control.* Presentation, Ammann/Case, Dallas, TX: Transportation Pooled Fund Intelligent Compaction Systems initial-Task Working Group meeting.

Arambula, E.; Massad, E.; and Martin, A. (2007). "Influence of Air Void Distribution on the Moisture Susceptibility of Asphalt Mixes." *ASCE Journal of Materials in Civil Engineering*, vol. 19, no. 8, pp. 655-664.

Arasteh, M. (2007). "Innovations in Compaction Control and Testing." *Intelligent Compaction 2007 Construction Conference,* Federal Highway Administration, Bishmark, ND.

American Trucking Association (ATA) (2008). *Trucking and the Economy.* Arlington, VA: American Trucking Association.

Beainy, F.; Commuri, S.; and Musharraf, Z. (2010). "Asphalt Compaction Quality Control Using Artificial Neural Network." *IEEE 49th Conference on Decision and Control (CDC)*, pp. 4643-4648, Atlanta, GA.

Beainy, F.; Commuri, S.; and Musharraf, Z. (2011). "Quality Assurance of Hot Mix Asphalt Pavements Using the Intelligent Asphalt Compaction Analyzer." *ASCE Journal of construction Engineering and Management*, posted ahead of print May 21th.

Bohuslav, T. (2008). *Pavement Design Guide.* Austin, TX: Texas Department of Transportation.

Bonaquist, R.; and Christensen, D. (2005). "Practical Procedure for Developing Dynamic Modulus Master Curves for Pavement Structural Design." *Journal of the Transportation Research Board* (Transportation Research Board of the National Academies), no. 1929, pp. 208-217.

Briaud, J.; and Seo, J. (2003). *Intelligent Compaction Overview and Research Needs.* College Station, TX: Texas A&M University.

Burati, J.; Weed, R.; Hughes, C.; and Hill, H. (2004). *Evaluation of Procedures for Quality Assurance Specifications.* McLean, VA: Federal Highway Administration Office of Research Development and Technology.

Burati, J.; Weed, R.; Hughes, C.; and Hill, H. (2003). *Optimal Procedures for Quality Assurance Specifications.* McLean, VA: Federal Highway Administration Office of Research Development and Technology.

Camargo, F.; Larsen, B.; Chadbourn, B.; Roberson, R.; and Siekmeier, J. (2006). *Intelligent Compaction: A Minnesota Case History.* 54th Annual University of Minnesota Geotechnical Conference.

Cao, Y.; Liang, N.; Qin, M.; and Lu, Z. (2010). "Research on the Correlation between Vibration Acceleration of Roller and Compaction Degree of Subgrade Soil." *ASCE 10th International Conference of Chinese Transportation Professionals*, pp. 2974-2982, Beijing, China.

Chan, C.; Huang, B.; Yan, X.; and Richards, S. (2008). *Effects of Asphalt Pavement Conditions on Traffic Accidents in Tennessee Utilizing Pavement Management System (PMS).* Seed Grand Final Report, University of Tennessee, Knoxville, TN: Southeastern Transportation Center.

Chang, G.; Turner, D.; Xu, Q.; Rasmussen, R.; Merritt, D.; Michael, L.; White, D.; and Horan, B. (2008). *Accelerated Implementation of Intelligent Compaction Technology For Embankment Subgrade Soils, Aggregate Base, and Asphalt Pavement Materials.* Annual Report FHWA-IF-07, Washington, DC: Federal Highway Administration.

Chang, G.; Xu, Q.; Rutledge, J.; Michael, L.; White, D.; and Vennapusa, P. (2011). *Accelerated Implementation of Intelligent Compaction Technology for Embankment Subgrade Soils, Aggregate Base, And Asphalt Pavement Materials.* Washington, DC: Federal Highway Administration.

Chen, J.; and Huang, L. (2000). "Developing an Aging Model to Evaluate Engineering Properties of Asphalt Paving Binders." *Journal of Materials and Structures* (Springer), vol. 33, no. 9, pp. 559-565.

Cominsky, R.; Killingsworth, B.; Anderson, M.; Anderson, D.; and Crockford, W. (1998). *Quality Control and Acceptance of Superpave-Designed Hot Mix Asphalt.* Washington, DC: National Research Council.

Commuri, S. (2010). *Final report for assistance agreement DTFH61-08-G-0002*. Highways for LIFE Technology Partnerships Program, Washington, DC: Federal Highway Administration.

Commuri, S. (2009a). *Phase 1 progress report for agreement DTFH61-08-G-0002*. Highways for Life Program Technology Partnerships Program, Washington, DC: Federal Highway Administration.

Commuri, S. (2009b). "Calibration Procedures for the Intelligent Asphalt Compaction Analyzer", Invention Disclosure # 09NOR001, University of Oklahoma, Norman, OK, July 2008. Also, filed for patent and PCT, *Method and apparatus for compaction of roadway materials*. United States of America Patent US/PCT/55619. September 1, 2009b.

Commuri, S.; and Beainy, F. (2011). "A Visco Elastic Plastic Model for Intelligent Compaction of Asphalt Pavements. " Invention Disclosure # 12NOR012, University of Oklahoma, Norman, OK, August 2011.

Commuri, S.; and Musharraf, Z. (2007). *Final Report – Intelligent Asphalt Compaction Analyzer*. Oklahoma City, OK: Oklahoma Center for the Advancement of Science and Technology (OCAST).

Commuri, S.; and Musharraf, Z. (2008). "A novel neural network-based asphalt compaction analyzer." *International Journal of Pavement Engineering* (Taylor & Francis), vol. 9, no. 3, pp. 177-188.

Commuri, S.; and Musharraf, Z. (2010). Method and Apparatus For Predicting The Density of Asphalt. United States of America Patent 7-669-458. March 02, 2010.

Commuri, S.; Mai, A.; and Musharraf, Z. (2009). "Calibration Procedures for the Intelligent Asphalt Compaction Analyzer." *ASTM Journal of Testing and Evaluation*, vol. 37, no. 5, pp. 454-462.

Commuri, S.; Mai, A.; and Musharraf, Z. (2011). "Neural Network-based Intelligent Compaction Analyzer for Estimating Compaction Quality of Hot Asphalt Mixes." *ASCE Journal of Construction Engineering and Management*, vol. 137, No. 9, 634-644.

Commuri, S.; Musharraf, Z.; Singh, D.; Mai, A.; and Beainy, F. (2010a). *Continuous Real Time Measurement of Pavement Quality during Construction.* Final report, University of Oklahoma, Midwest City, OK: Oklahoma Transportation Center.

Commuri, S.; Singh, D.; Beainy, F.; Mai, A.; and Musharraf, Z. (2010b). "A method to determine the effective modulus of an asphalt pavement during its construction," Invention Disclosure # 11NOR049, University of Oklahoma, Norman, OK, August 2010.

Connolly, C. (2008). *Asphalt Manager Intelligent Compaction.* Presentation, Bomag, Dallas, TX: Transportation Pooled Fund Intelligent Compaction Systems initial Task Working Group meeting.

CTC & Associates (CTC) (2006). *Intelligent Compaction of Soils.* Madison, WI: WisDOT Research & Communication Services Wisconsin Highway Research Program.

Dave, E.; Buttlar, W.; Paulino, G.; and Hilton, H. (2006). "Graded Viscoelastic Approach for Modeling Asphalt Concrete Pavements." *Proceedings of the International Conference FGM IX*, American Institute of Physics, pp. 736-741, Oahu Island, Hawaii

Desai, C. (2008). "Unified Constitutive Modeling for Pavement Materials with Emphasis on Creep, Rate and Interface Behavior." *Proceedings of the International Conference on Advances in Transportation Geotechnics,* CRC Press, 2008. 15-25, Nottingham, UK.

Dubravka, S.; and Davor, H. (2008). "Simulation on Vibratory Roller-Soil Interaction." *International journal Advanced Engineering* (Springer), vol. 2, no. 1, pp. 137-146.

Federal Highway Administration (FHWA) (2005). *Highway Statistics 2005 - Section V: Roadway Extent, Characteristics, and Performance.* Washington, DC: Federal Highway Administration.

Federal Highway Administration (FHWA) (2006a). *Highway Statistics 2006 - Section V: Roadway Extent, Characteristics, and Performance.* Washington, DC: Federal Highway Administration.

Federal Highway Administration (FHWA) (2006b). "Percent Within Limits: The Quality Measure of Choice." *Focus*, 2006, FHWA-HRT-06-023.

Federal Highway Administration (FHWA) (2007). *Highway Statistics 2007 - Section 12.4.1. Length by present serviceability rating (pavement condition), all systems.* Washington, DC: Federal Highway Administration, 2007.

Federal Highway Administration (FHWA) (2008). *Highway Statistics 2008 - Section 4.3.1. Public road length by type of surface and ownership/functional system.* Washington, DC: Federal Highway Administration.

Gallivan, V.; Chang, G.; and Horan, R. (2011). "Intelligent Compaction for Improving Roadway Construction." *ASCE GeoHunan International Conference,* pp. 117-124, Hunan, China.

Gee, K. (2004). *Use of Contractor Test Results in the Acceptance Decision, Recommended Quality Measures, and the Identification of Contractor/Department Risks.*

Washington, DC: Federal Highway Administration and U.S. Department of Transportation.

Goh, S.; You, Z.; Williams, C.; and Li, X. (2011). "Preliminary Dynamic Modulus Criteria of HMA for Field Rutting of Asphalt Pavements: Michigan's Experience." *ASCE Journal of Transportation Engineering*, vol. 137, no. 1, pp. 37-45.

Herbert, W.; and Jennette, R. (2011). Benefit Analysis of Nondestructive Testing For Roadway Management. Project Number: MQP-MGE-JMM-0411, Worcester, MA: Worcester Polytechnic Institute.

Hossain, M.; Mulandi, M.; Keach, L.; Hunt, M.; and Romanoschi, S. (2006). "Intelligent Compaction Control." *ASCE Airfield and Highway Pavements Specialty Conference*, pp. 304-316, Atlanta, GA.

Ismail, M.; Ikhouane, F.; and Rodellar, J. (2009). "The Hysteresis Bouc-Wen Model, a Survey." *Archives of Computational Methods in Engineering* (Springer), vol. 16, no. 2, pp. 161-188.

Lavin, P. (2003). "Asphalt Pavements: A Practical Guide to Design, Production and Maintenance for Engineers and Architects." pp. 191-261, New York, NY: Spon Press.

Ledolter, J.; and Hogg, R. (2008). *Applied Statistics for Engineers and Physical Scientists, section 4.3I*, Pearson, London, United Kingdom.

Liu, Y.; and You, Z. (2009). "Determining Burger's Model Parameters of Asphalt Materials using Creep-recovery Testing Data." *Pavements and Materials: Modeling, Testing, and Performance, Geotechnical Special Publication No. 184*, pp. 26-36.

Liu, Y.; Qingli, D.; and You, Z. (2009). "Viscoelastic Model for Discrete Element Simulation of Asphalt Mixtures." *ASCE Journal of Engineering Mechanics*, vol. 135, no. 4, pp. 324-333.

Lodewikus, H. (2004). *Compaction of asphalt road pavements: using finite elements and critical state theory.* PhD Dissertation, Enschede, the Netherlands: University of Twente.

Loulizi, A.; Flintsch, G.; and McGhee, K. (2007). "Determination of In-Place Hot-Mix Asphalt Layer Modulus for Rehabilitation Projects by a Mechanistic-Empirical Procedure." *Journal of the Transportation Research Board* (Transportation Research Board of the National Academies), no. 2037, pp. 53-62.

Masad, E.; Koneru, S.; Scarpas, T.; Kassem, E.; and Rajagopal, R. (2010). *Modeling of Hot-Mix Asphalt Compaction: A Thermodynamics-Based Compressible Viscoelastic Model.* Final Report, Washington, DC: Federal Highway Administration.

Materials Bureau (2001). *Hot Mix Asphalt Statistical Pavement Density Determination.* Albany: New York City Department of Transportation.

Mathworks (2009). *Stateflow: Design and simulate state machines and control logic.* 2009. http://www.mathworks.com/products/stateflow/ (accessed July 14, 2011).

Maupin, G. (2007). *Preliminary Field Investigation of Intelligent Compaction of Hot-Mix Asphalt.* Charlottesville: Virginia Transportation Research Council.

Micaelo, R.; Ribeiro, J.; Azevedo, M.; and Azevedo, N. (2009). "Discrete Element Modelling of Field Asphalt Compaction." *The Sixth International Conference on Maintenance and Rehabilitation of Pavements and Technological Control.* Turin, Italy.

Minchin, E.; Swanson, D.; Gruss, A.; and Randolph, T. (2008). "Computer Applications in Intelligent Compaction." *ASCE Journal of Computing in Civil Engineering,* vol. 22, no. 4.

Mooney, M.; Facas, N.; Musimbi, O.; White, D.; and Vennapusa, P. (2010). *Intelligent Soil Compaction Systems.* Washington, DC: National Cooperative Highway Research Program.

Moore, W. (2006). "Intelligent Compaction: Outsmarting soil and asphalt. *Construction Equipment,* March 31, pp. 39-48.

Minnesota Transportation Alliance (MTA) (2011). *Transportation in Minnesota A Roadmap To 2040.* Long-Range Transportation Plan, Saint Paul, MN.

National Asphalt Pavement Association (NAPA) (2007). *National Asphalt Roadmap A Commitment to the Future.* Special Report, Lanham, MD.

Nillson, R.; Hopman, P.; and Isacsson, U. (2002). "Influence of different rheological models on predicted pavement responses in flexible pavements." *Road Materials and Pavement Design: An International Journal,* no. 3, pp. 117-149.

Nino, J. (2006). *Design and Development of a Real Time Neural Network-Based Compaction Analyzer.* Master's Thesis, School of Electrical and Computer Engineering, Norman, OK: University of Oklahoma.

Pellinen, T; and Witczak, M. (2002). "Use of Stiffness of Hot-Mix Asphalt as a Simple Performance Test." *Journal of the Transportation Research Board* (Transportation Research Board of the National Academies), no. 1789, pp. 80-90.

Petersen, L. (2005). *Continuous Compaction Control MnROAD Demonstration.* Maplewood, MN: Minnesota Department of Transportation.

Peterson, L.; and Petersen, Ryan (2006). *Intelligent Compaction and In-Situ Testing at Mn/DOT TH53.* St. Paul, MN: Minnesota Department of Transportation.

Pronk, A. (2005). "The Huet–Sayegh model: a simple and excellent rheological model for master curves of asphaltic mixes." *Proceedings of the R.Lytton symposiumonmechanics of flexible pavements.* Baton Rouge, LA.

Quintus, H.; Rao, C.; Minchin, R.; Soheil, N.; Maser, K.; and Prowell, B. (2009). *NDT Technology for Quality Assurance of HMA Pavement Construction.* Washington, DC: Transportation Research Board.

Quintus, H.; Rao, C.; Titi, H.; Bhattaacharya, B; and English, R (2010). *Evaluation of Intelligent Compaction Technology for Densification of Roadway Subgrades and Structural Layers.* Final Report, Madison, WI: Wisconsin Department of Transportation.

Rakowski, S. (2008). *Intelligent Compaction CCV IC.* Presentation, Sakai, Dallas, TX: Transportation Pooled Fund Intelligent Compaction Systems initial-Task Working Group meeting.

Rawls, D.; and Potts, D. (2008). *AccuGrade® Compaction GPS Mapping & Measurement System.* Presentation, Caterpillar, Dallas, TX: Transportation Pooled Fund Intelligent Compaction Systems initial-Task Working Group meeting.

Raytek (2010). "Noncontact Temperature Measurement for Industrial Applications." Datasheet, Santa Cruz, CA.

Scherocman, J.; and Dwight, W. (2008). *Factors Affecting Asphalt Compaction.* Asphalt Institute. March 8th, 2008. http://www.asphaltmagazine.com/singlenews.asp?item_ID=1451&comm=0&list_code_int=mag01-int (last accessed April 10, 2010).

Schmitt, R.; Chetana, R.; and Quintus, H. (2006). *Non-Nuclear Density Testing Devices and Systems to Evaluate In-Place Asphalt Pavement Density.* Madison, WI: Wisconsin Highway Research Program.

Sebesta, S.; Estakhri, C.; Scullion, T.; and Liu, W. (2006). *New Technologies for Evaluating Flexible Pavement Construction: Year 1 Report.* Austin, TX: Texas Department of Transportation.

Sebesta, S.; Zeig, M.; and Scullion, T. (2003). *Evaluation Of Non-Nuclear Density Gauges For HMAC: Year 1 Report.* Austin, TX: Texas Department of Transportation.

Shen, P.; and Lin, S. (2008). "Mathematic modeling and characteristic analysis for dynamic system with asymmetrical hysteresis in vibratory compaction." *Meccanica* (Springer), vol. 43, no. 5, pp. 505-515.

Shenoy, A.; and Romero, P. (2002). "Standardized procedure for analysis of dynamic modulus (E*) data to predict asphalt pavement distresses." *Journal of the Transportation Research Board* (Transportation Research Board of the National Academies), no. 1789, pp.173-182.

Singh, D.; Beainy, F.; Mai, A.; Commuri, S.; and Musharraf, Z. (2010). "In-situ Assessment of Stiffness During the Construction of HMA Pavements." *International Journal of Pavement Research and Technology*, vol. 4, no. 3, pp. 131-139.

Spectrum Sensors & Controls (SSC) (2010). *Rugged ±10 g to ±70 g Accelerometers with Superior Zero g Bias Stability.* Technical Data, Akron, Oh: Spectrum Sensors & Controls.

Stripple, H. (2001). *Life Cycle Assessment of Road A Pilot Study for Inventory Analysis.* Gothenburg, Sweden: IVL Swedish Environmental Research Institute Ltd.

Susante, P.; and Mooney, Michael (2008). "Capturing Nonlinear Vibratory Roller Compactor Behavior through Lumped Parameter Modeling." *ASCE Journal of Engineering Mechanics*, vol. 134, no. 8, pp. 684-693.

Thompson, M. (2006). "Intelligent Soil Compaction for Assuring Subgrade Quality." *Greater Iowa Asphalt Conference.* Des Moines, IA: Iowa State University.

Thurner, H.; and Sandström, Å. (2000). "Continuous Compaction Control." *European Workshop Compaction of Soils And Granular Materials*, pp. 237-246, Paris, France.

Vermont Local Roads (VLR) (1992). *Compaction Improves Pavement Performance*. Vermont Local Roads Fact Sheet, Colchester, VT: Vermont Agency of Transportation (VTrans).

Transportation Research Board (TRB) (2005). *Transportation Research Circular E-C074: Glossary of Highway Quality Assurance Terms.* Management of Quality Assurance Committee, Transportation Research Board.

Trimble (2010). "GPS Pathfinder ProXt Receiver." Datasheet, Westminster, CO.

Texas Department of Transportation (TxDOT) (2011). *Pavement Design Guide.* Manual Notice, Austin, TX.

US Army Corps of Engineers (USACE) (2000). *Hot Mix Asphalt Paving Handbook.* Washington, DC: Airport Engineering Division, Federal Aviation Administration.

US Department of Transportation (USDOT) (2006). *2006 Status of the Nation's Highways, Bridges, and Transit: Conditions and Performance.* Report To Congress, Washington, DC.

White, D.; Thompson, Mark; Jovaag, Kari; Jaselskis, Edward; and Vernon, R. (2006). *Field Evaluation of Compaction Monitoring Technology: Phase II (TR-495).* Ames, IA: Iowa Department of Transportation.

Wisdom, B. (2009). "RoadScience Tutorial: Want Optimum Density? Get Smart." *Road Science*, November 1, 2009.

Witczak, M.; Kaloush, K.; Pellinen, T.; El-Basyouny, M.; and Quintus, H. (2002). *Simple Performance Test for Superpave Mix Design.* Washington, DC: National Academy Press.

Woo, W.; Chowdhury, A.; and Glover, C. (2008). "Field Aging of Unmodified Asphalt Binder in Three Texas Long-Term Performance Pavements." *Journal of the Transportation Research Board* (Transportation Research Board of the National Academies), no. 2051, pp. 15-22.

Xu, Q.; and Solaimanian, M. (2009). "Modelling linear viscoelastic properties of asphalt concrete by the Huet–Sayegh model." *International Journal of Pavement Engineering*, vol. 10, no. 6, pp. 401-422.

Zambrano, C.; Drnevich, V.; and Bourdeau, P. (2006). *Advanced Compaction Quality Control.* Final Report, Indianapolis, MN: Indiana Department of Transportation.

Zapata, C.; and Houston, W. (2008). *Calibration and Validation of the Enhanced Integrated Climatic Model for Pavement Design.* Washington, DC: Transportation Research Board.

DISCLAIMER

The contents of this report reflect the views of the author who is responsible for the facts and accuracy of the data presented herein. The contents do not reflect the views of the Federal Highway Administration or the Oklahoma Department of Transportation (ODOT). This dissertation does not constitute a standard, specification, or regulation. Trade names mentioned in this report are not intended as an endorsement of any machine, contractor, process or product.

APPENDIX A

NOTATIONS

The following notations are used in the derivation of the dynamic equations that represent the compaction of asphalt mix using a vibratory compactor:

F_{ec}: centrifugal force (N);

F_a: reaction force of the asphalt layer (N);

F_{a_loc}: value of F_a at loss of contact (N);

F_c: drum-asphalt contact force (N);

$m_{ec}r_{ec}$: eccentric mass moment (Kg-m);

m_d: mass of the roller drum (Kg);

m_f: mass of the roller frame (Kg);

m_a: mass of the asphalt mat under the roller drum (Kg);

g: gravitational acceleration of the earth (9.81 m/s^2);

ω_{ec}: rotational speed of the eccentric masses (rad/s);

ω_n: un-damped natural frequency of the asphalt (rad/s);

f_{ec}: frequency of rotation of the eccentrics (Hz);

t: time (s);

t_{loc}: time of loss of contact (s);

t_{roc}: time of regain of contact (s);

k_{df}: drum-frame stiffness coefficient (N/m);

η_{df}: drum-frame damping coefficient (N-s/m);

k_{av}: viscous stiffness coefficient of asphalt (N/m);

η_{av}: viscous damping coefficient of asphalt (N-s/m);

k_{ae}:: elastic stiffness coefficient of asphalt (N/m);

η_{ap}: plastic damping coefficient of asphalt (N-s/m);

$\varepsilon(t)$: total Deformation at time *t* (m);

$\sigma(t)$: total stress at time *t* (Pa);

σ_v, σ_e and σ_p: stress as translated to the three components viscous, elastic, and plastic (Pa);

ε_v: viscous deformation of asphalt (m);

ε_e: elastic deformation of asphalt (m);

ε_p: plastic deformation of asphalt (m);

$\dot{\varepsilon}_v$: rate of change of ε_v (m);

$\dot{\varepsilon}_p$: rate of change of ε_p (m/s);

$\ddot{\varepsilon}_e$: vertical acceleration of ε_e (m);

ε_{p_loc}: value of ε_p at loss of contact (m);

ε_{v_loc}: value of ε_v at loss of contact (m);

ε_{v_roc}: value of ε_v at regain of contact (m);

z_d: vertical displacement of the roller drum (m);

z_f: vertical displacement of the roller frame (m);

z_a: vertical displacement of the roller asphalt surface (m);

$\ddot{z}_d$: vertical acceleration of the roller drum (m/s^2);

$\ddot{z}_f$: vertical acceleration of the roller frame (m/s^2);

$\ddot{z}_a$: vertical acceleration of the roller asphalt surface (m/s^2);

z_{d_roc}: value of z_d at regain of contact (m);

$\dot{z}_{d\_roc}$: value of $\dot{z_d}$ at regain of contact (m/s);

C, C_1, C_2: constant of integration (unit-less).

APPENDIX B

IACA USER MANUAL

INTELLIGENT ASPHALT COMPACTION ANALYZER†

User Manual

Version 2.0

University of Oklahoma
School of Electrical and Computer Engineering
Devon Engineering Hall, Room 432
110 W. Boyd St., Norman, OK 73019

Tel. 1 - 405 - 325 - 4302
Fax. 1 - 405 - 325 – 7066

http://intelligentcompaction.ou.edu/

Email: scommuri@ou.edu

*US Patent #***7,669,458**
Issued on March 02, 2010

For further information, please contact:

The Office of Technology Development
University of Oklahoma
One Partners Place
David L. Boren Blvd., Norman, OK 73019
Tel. 1-405-325-4800

INTELLIGENT ASPHALT COMPACTION ANALYZER

User Manual

Version 2.0

B.1 Introduction

The Intelligent Asphalt Compaction Analyzer (IACA) is a roller-mounted device that can measure the density of an asphalt pavement during its construction. The IACA measures the vibrations of the drum of the vibratory compactor during the compaction process and estimates the density of the asphalt mat continuously, in real-time during the pavement's construction.

Quality control techniques currently used in the field involve the measurement of density at several locations on the completed pavement or the extraction of roadway cores. These methods are usually time consuming and do not reveal the overall quality of the construction. Furthermore, any compaction issues that are identified cannot be easily remedied after the asphalt mat has cooled down. The ability of the IACA to measure the level of compaction of the asphalt pavement during its construction will enable the roller operator to identify and remedy under-compaction of the pavement while avoiding over-compaction.

Key features of the IACA are:

- Neural network based intelligent analyzer that can estimate the density over the entire pavement.
- Display of asphalt mat density, surface temperature, roller position, speed and heading in real-time.
- Density is also displayed as a 'strip chart' to help identify the uniformity of compaction on a given stretch of the pavement.
- The displayed information is updated twice every second with a spatial resolution of better than 0.3m (1 ft.).
- Intuitive, easy to use, calibration procedures that allow for accurate estimation of density of both full-depth, as well as overlaid asphalt pavements.
- Can be used to estimate the density of thick lifts (base and intermediate lifts), as well as thin lifts of asphalt pavement (surface course).
- Built-in utilities can be used to validate the density at a given location on the pavement against Nuclear Density Gauge (NDG) readings or density measured from a roadway core.
- As-built maps to plot the overall compaction for the entire roadway construction.
- Pass-by-pass density to detect under compaction and prevent over compaction of the pavement.

B.2 Installation Procedure

The Intelligent Asphalt Compaction Analyzer (IACA) consists of a rugged Tablet PC, GPS receiver, uniaxial accelerometer, and an infrared temperature sensor. The IACA should be mounted on a Volvo DD138HF or similar roller prior to its calibration and use. The installation procedure is described in this section.

B.2.1 Components

Check and verify the following components prior to installing the IACA on a Volvo DD138HF roller.

1) Rugged Tablet PC (Figure 1).
2) Trimble Pathfinder ProXT GPS receiver (Figure 2).
3) Raytek CI non-contact infrared pyrometer (Figure 3).
4) Summit Instruments 13200C 10g accelerometer (Figure 4).
5) Tablet PC mounting platform (Figure 5).
6) Mounting bracket (Figure 6).
7) Swivel arm (Figure 7).
8) Mounting Hardware (8 – 5/8 x 6 in. bolts, 8 – 5/8 in. nuts, 16 – 5/8 in. washers, 16 – 5/8 in. lock washers. Tie wraps).

Figure B.1. T8700 Rugged Tablet PC with integrated numeric keypad (shown on mounting platform)

Figure B.2. Trimble Pathfinder ProXT GPS receiver

Figure B.3. Raytek CI non-contact infrared temperature sensor

Figure B.4. Summit Instruments 10g uniaxial accelerometer

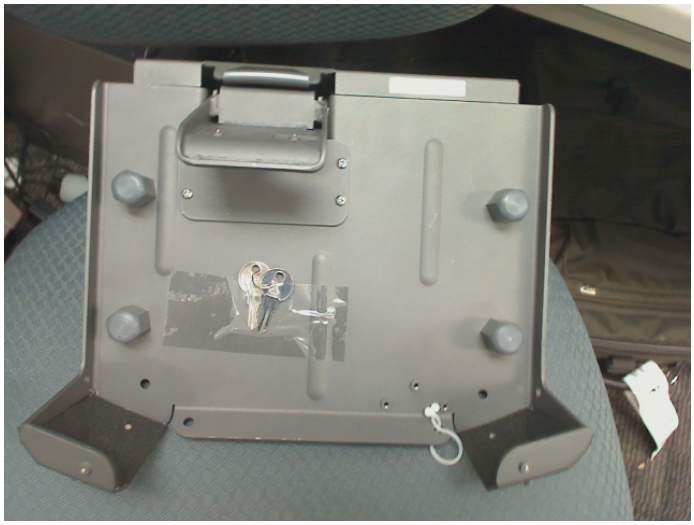

Figure B.5. TabletPC mounting platform with spring loaded latch

Figure B.6. Bracket used to attach the Tablet PC platform
to the rail on the roller

Figure B.7. Swivel arm used to attach the Tablet PC platform to the mounting bracket

B.2.2 Installation

Figure B.8. Mounting location labels on a Volvo DD118HF roller.

1 Find the best location on the drum to mount/glue the accelerometer. The closer to the drum the better and it should always be before the drum rubber mount to make sure the measured vibration is for the drum and not the roller body frame. Once the location is defined, clean it and use superglue to mount the accelerometer.

2 Mount the temperature sensor on its bracket and then glue it on a safe location on the frame pointing down towards the road surface.

3 Mount the GPS receiver on top of the roller. The GPS receiver has foam padding and a magnet that is good enough to stay in place without the need for glue or tape. Turn GPS receiver on. Write down the horizontal distance between the GPS and the accelerometer (offset distance) for later use during the post processing.

4

1. Mount the mounting bracket (Figure 6) to a convenient location on the rail. It is a good practice to use foam padding to absorb vibration. Mount the bracket by running the bar between the semicircular rods and tightening the bolts so that the bracket will not slide when the roller vibrates. Make sure the knob is facing inside the cab.
2. Attach the swivel arm (Figure 7) to the knob on the mounting bracket (Figure 6) and to the knob on the mounting platform (Figure 5) by inserting the knobs into each side

of the swivel arm and adjusting the tightening screw. Make sure the mounting platform is situated so that the ribbon cable is on top.

3. Insert the tablet PC in to the mounting platform. Do this by pulling the top bracket back and fitting the tablet PC in the space provided, and then bend the top bracket back down ensuring the tablet PC remains in place. Connect the power cord from the mounting bracket to the associated plug on the bottom of the tablet PC.
4. Connect the ribbon cable to the data acquisition on the tablet. There are three cables coming out of the back of the cradle labeled C1, C2 and C3. Connect the cable attached to the accelerometer to C1, the temperature sensor cable to C2. If needed, use straight serial cables to reach sensors.

5

1. Connect the power cable to C3 and to a 12V battery if available. Otherwise open the roller engine hood and connect to its battery. Use care when tapping to the roller's battery to avoid electric shocks and make sure polarities are correct.
2. Turn the tablet PC on by depressing the gray button on the top left hand side of the face of the tablet PC. Once this is on, connect the GPS null-modem cable to its associated port on the bottom of the tablet PC. **Wait until the tablet PC is ON before connecting the GPS using the null-modem serial cable.**

B.2.3 IACA Initialization

Boot up the Tablet PC by depressing the power button. After the Tablet PC has been powered up and the Windows XP operating system has been booted up, the IACA will be started automatically. The user interface to the application is shown in Figure 9 with different features being outlined.

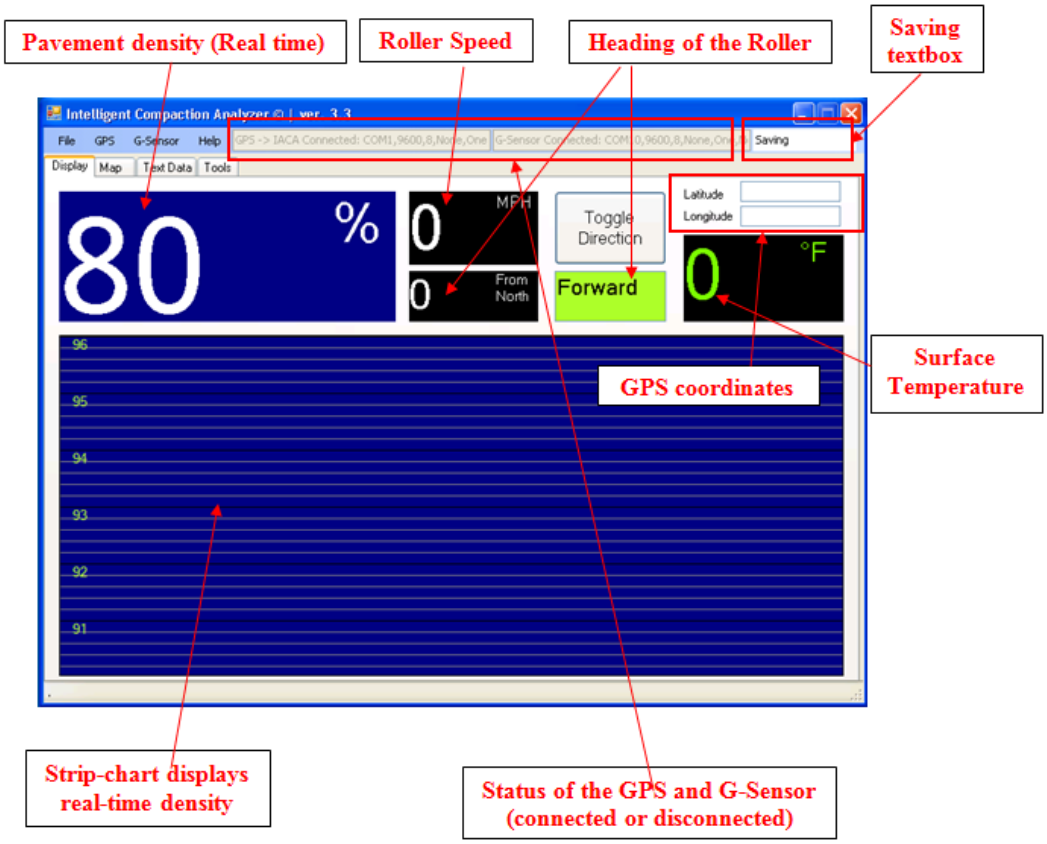

Figure B.9. IACA user interface

B.3 Calibration of the IACA

The IACA is based on the hypothesis that the hot mix asphalt layer being compacted and the vibratory compactor form a coupled system whose vibrations are affected by the stiffness of the asphalt mat. As the compaction process unfolds, the stiffness of the asphalt mat increases and as a consequence the response characteristics of the roller are altered. These changes in the response can be used to determine the level of compaction achieved. In order to determine the level of compaction, the IACA should be trained to recognize the response of the roller during the compaction process. The calibration process described below is designed to train the IACA to recognize the vibrations resulting from different levels of compaction and to generate the density information based on the characteristics of the mix.

The calibration of the IACA is a two-step process. In the first step, the vibrations of the roller are captured over successive passes on a calibration stretch. These vibrations are analyzed and features corresponding to different levels of vibrations are extracted. The extracted features correspond to the amplitude of the vibrations at salient frequencies. These features are then used to train the neural network. After the completion of the training process, the neural network can classify vibrations of the roller during compaction as those corresponding to one of the predetermined levels of

compaction. For the sake of calibration, the lowest level of vibration is assumed to correspond to the lay down density while the highest level of vibration is typically encountered when the target density is achieved.

In the second step of the calibration procedure, the calibration performed in step one is refined to improve the accuracy of the density measurements. After the calibration stretch is compacted, three cores are extracted from the completed pavement and the estimated densities at these locations are compared to the densities measured from the cores according to the AASHTO T-166 standard. The calibration parameters are then modified to minimize the error between the estimated and measured densities at these locations.

B.3.1 Selection of a pavement section for calibration of IACA

i) First a control strip of approximately 33m (100 ft.) long needs to be selected. Mark off a 30 foot calibration section in the middle of this control strip (Figure 11). The start and end of the calibration section need to be marked by GPS coordinates at the center line of the pavement. The GPS receiver is used to trigger the collection of the vibration data when the roller starts compacting this section of the pavement.

ii) Mark test locations at the center of the lane at distances of, 1.5m (5 ft.), 4.6m (15 ft.) and 7.6m (25 ft.) from the beginning of the test section.

iii) Stop the compaction process when no appreciable increase in the density is seen after the roller pass. After the final pass of the roller, three core locations are marked as shown in Figure 11. The GPS location of the cores is collected in the Tablet PC as explained in the section 4.0. Also, the density at the core and in the immediate vicinity of the core is recorded for each of the three cores using a non-nuclear density gauge.

iv) The cores marked in the previous step need to be extracted and their density is measured in accordance with the AASHTO T-166 method.

v) The densities of the extracted cores are used to train and calibrate the IACA as detailed in the following sections of this manual.

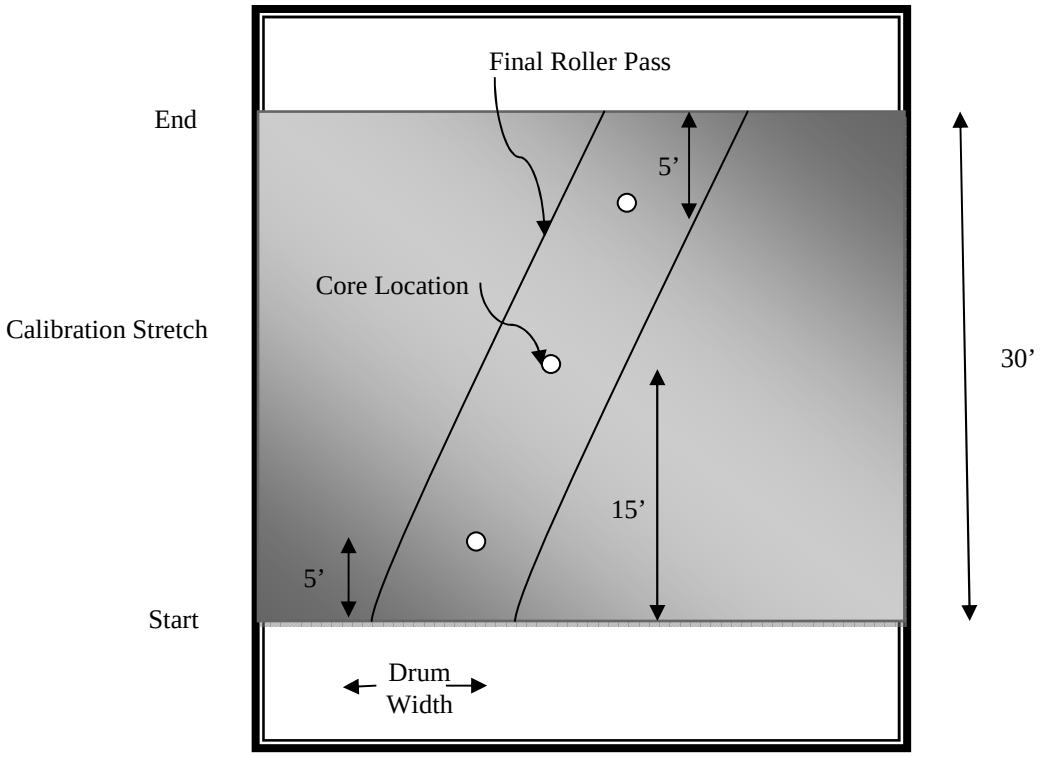

Figure B.11. Selection of core locations after the final pass of the roller

B.3.2 Calibration procedure

1. Make sure that the GPS is updating by looking at the coordinates textbox on the display (see figure below).

2. Let the roller compact a couple of stretches (not passes) and make sure that the data is being saved by looking at the status textbox (see figure above).

3. Mark a calibration region of 9m (30 ft.) as shown in the figure below:

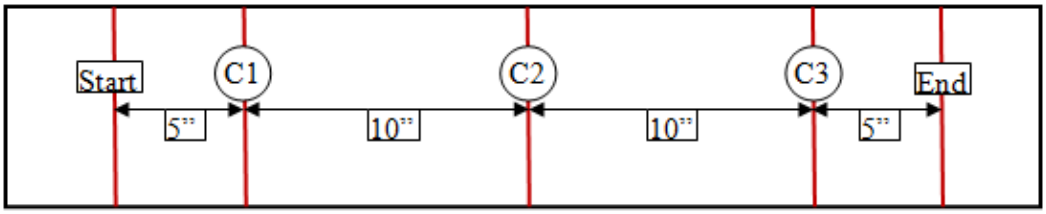

4. Make sure that the roller compacts all the passes without stopping and within 13 minutes. Also make sure that the roller stops for at least 1 minute before and after the calibration stretch for the roller to save data.
5. The last pass of the calibration region should be in the middle of the road.
6. In the tools tab of IACA, push "Start Point" button while the roller is aligned with the start line and the "End Point" button at the end of the calibration stretch.

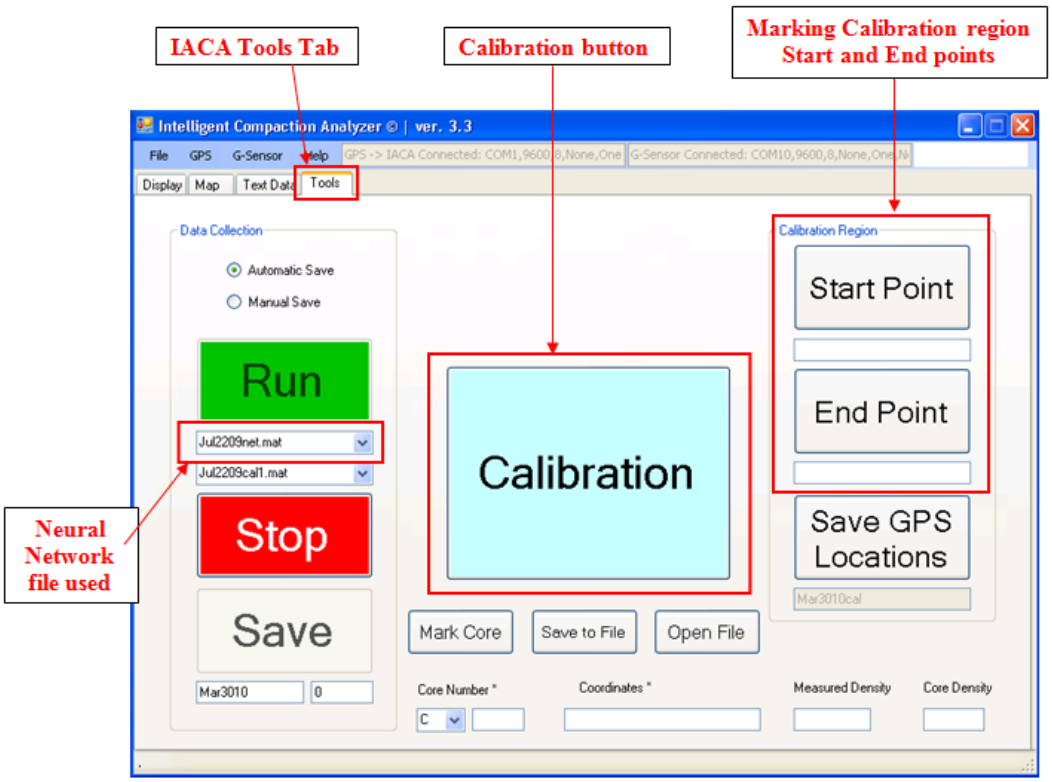

Figure B.12. IACA Tools window

7. After the calibration region is compacted and the roller is stopped for the data to be saved (remember the file number), go to the tools tab and push the "Calibration" button (Figure 12). The following three windows appear on the screen.

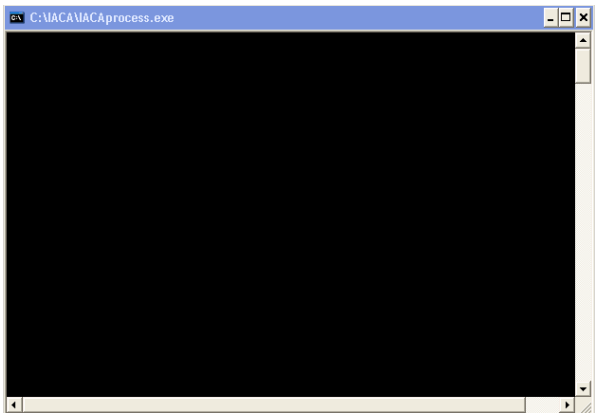

Figure B.13. IACA command editor window

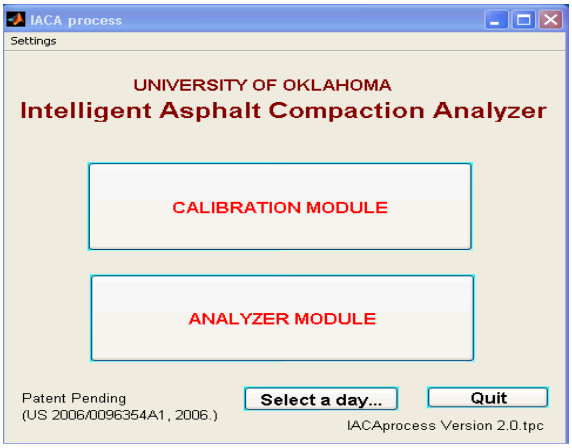

Figure B.14. IACA process window

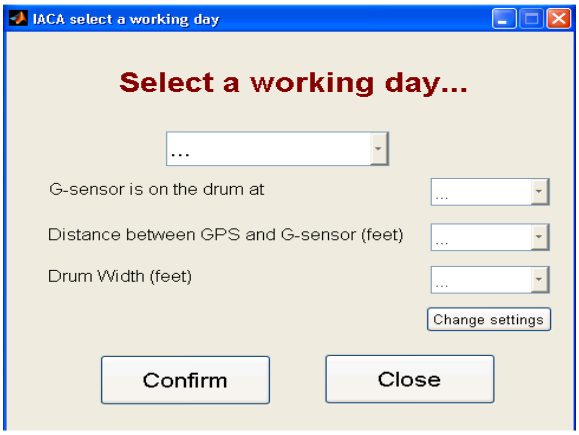

Figure B.15. IACA Select a working day window

8. Select a working day as shown in the figure below.

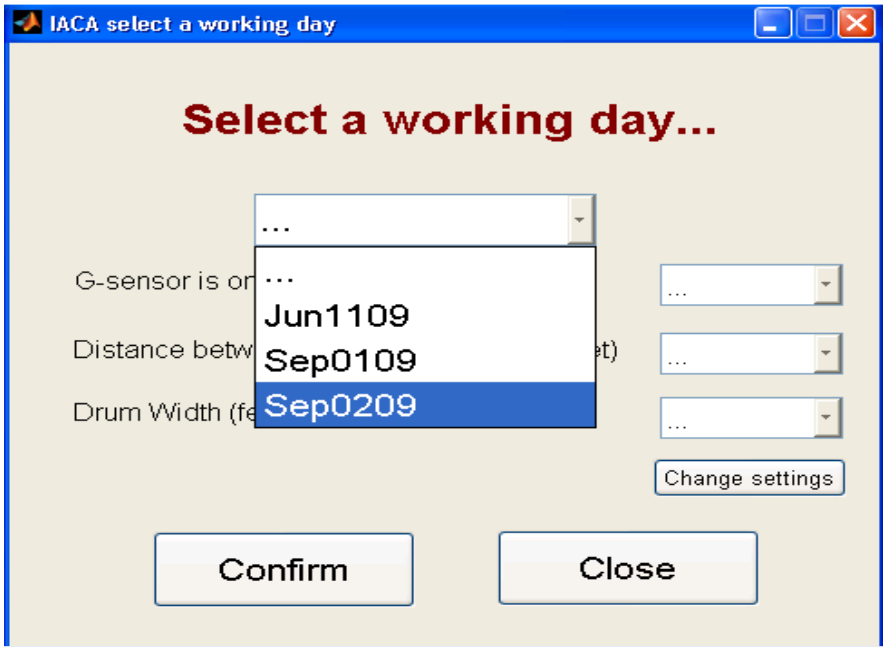

After selecting the working day, enter the following parameters: G-sensor position on the drum (front or rear), distance between GPS and G-sensor (offset distance) in feet and drum width in feet (as shown in the figure below) and push the "Confirm" button.

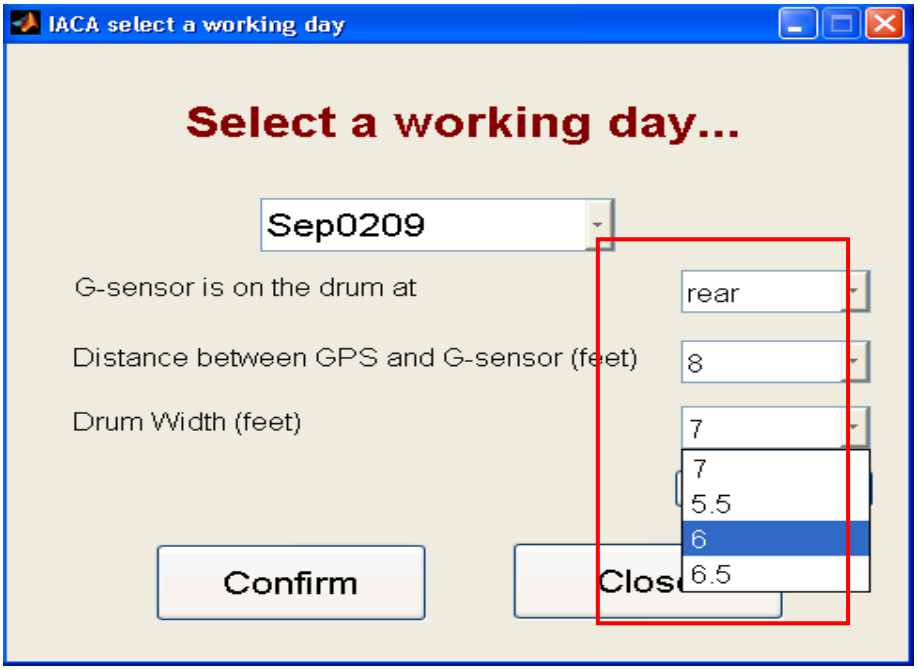

9. Push on the "CALIBRATION MODULE" button in the IACA process window of Figure 14.

The following window appears after the successful initaialization of the calibration module. Click “OK”.

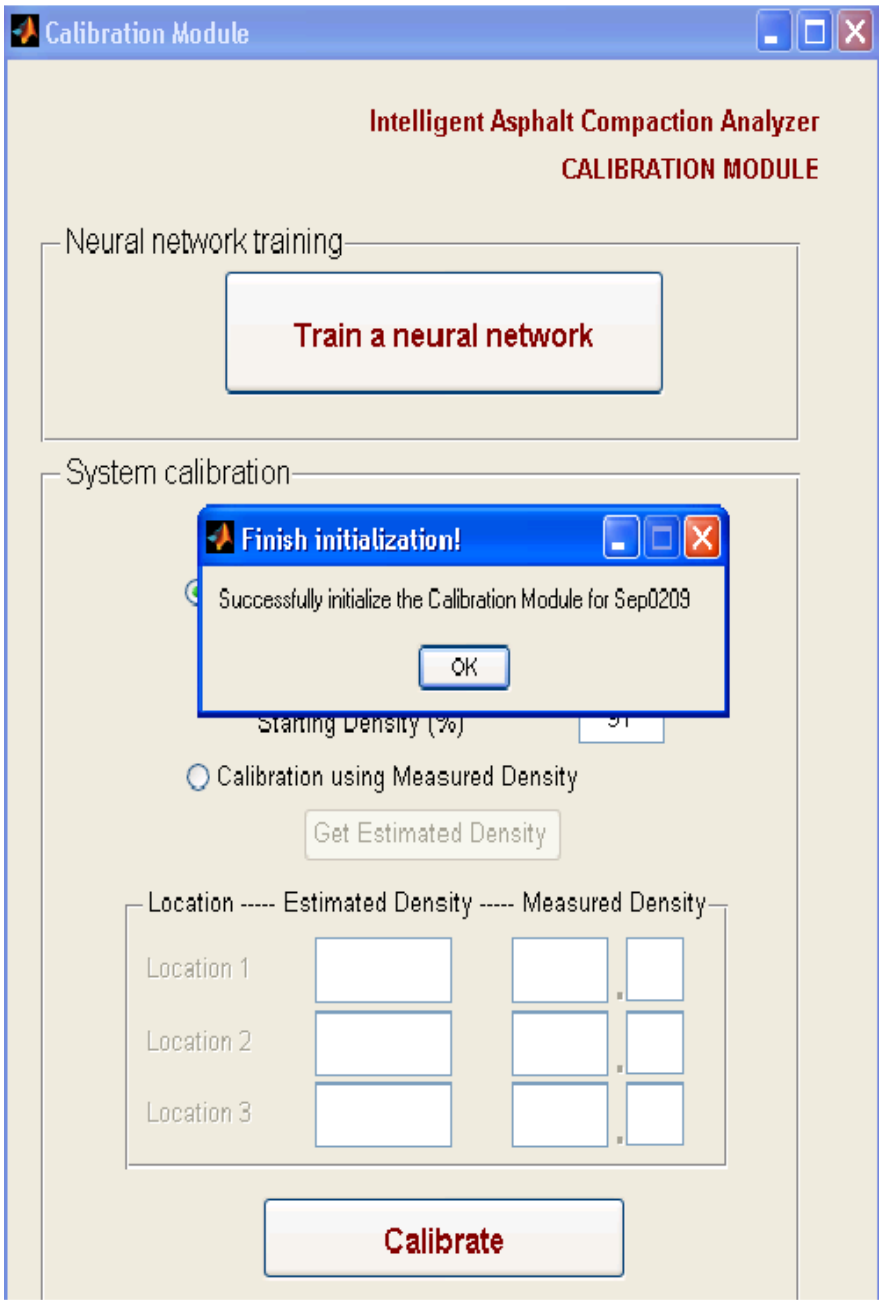

Figure B.16. IACA Calibration Module window

10. Push “Train a neural network” button in the figure above.
11. After training is finished, select the theoretical maximum density as 96% and minimum density as 91% then push the “Calibrate” button. A new file named datecalRaw.mat is created and the new Calibration parameters are saved to it.

12. Close everything including the IACA application then open it again and make sure the right Neural Network is selected in the IACA Tools tab (see figure 12).
13. After you get the core densities of the calibration region from the lab, go back to the Calibration Module (figure 16) and change the selection from "Raw Calibration using Maximum Density" to "Calibration using Measured Density".
14. Push the "Get Estimated Density" button to get the estimated densities at the three core locations. Enter the corresponding Lab densities on the right side and push the "Calibrate" button (see figure below).

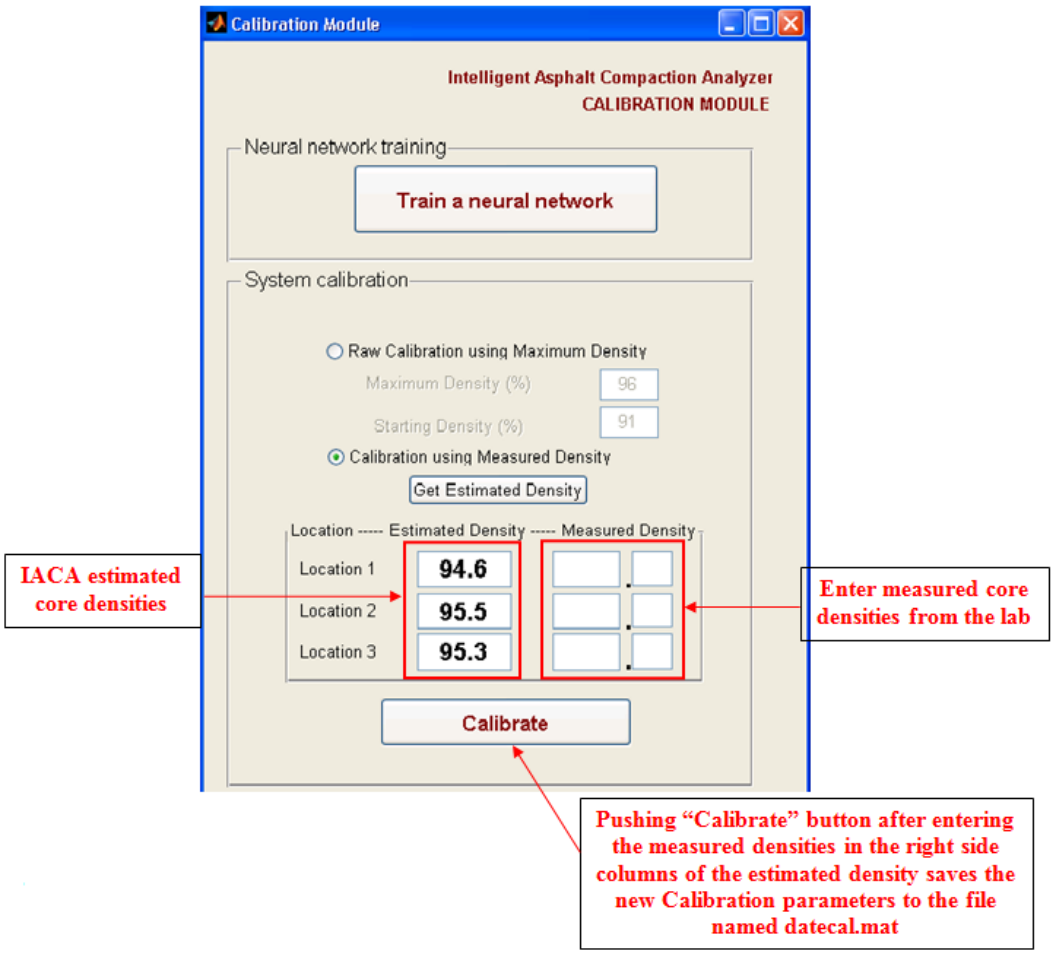

15. Close everything and then reopen IACA.

This completes the calibration procedure.

B.4 Marking Cores

At the end of each day or whenever needed, GPS location of the cores should be collected to be able to correlate estimated density with the measured ones. The following steps describe core marking operation:

1. Remove the GPS receiver from the roller and reconnect it to the tablet PC if the cable was disconnected during the operation.
2. Disconnect the ribbon cable coming from the cradle to the data acquisition on the tablet PC.
3. Remove the tablet from the cradle and put the GPS receiver on top of the core to be marked.
4. On the Tools tab of the IACA GUI (Figure 12), select a letter from the drop down menu as a core name for the day and type in the core number in the box next to it (see figure below).

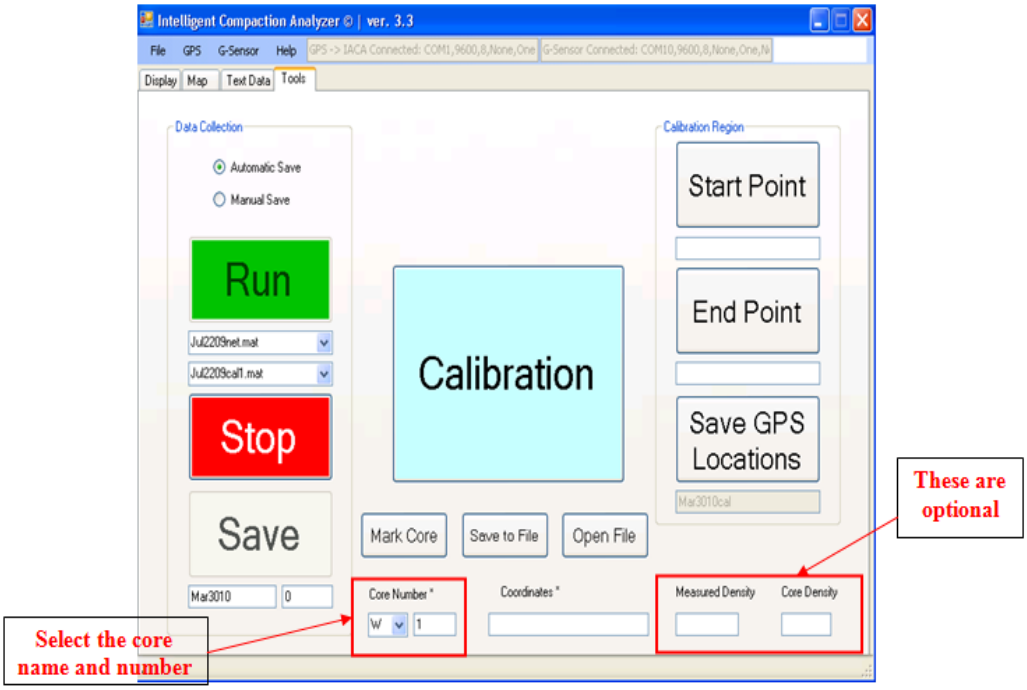

5. Push the “Mark Core” button to register the GPS coordinates in the box. The “Mark Core” button can be pushed as many times as the operator wants, without the data (GPS coordinates) being saved. Once the GPS coordinates are ready to be saved, the “Save to File” button should be pressed to automatically save or append the information to a text file named datecore.txt.
6. The “Measured Density” and “Core Density” boxes are optional information that can be filled in case it is a PQI or Nuclear Gauge measurement.
7. Repeat steps 4 to 7 for each core location.

B.5 Run Time Monitoring of Compaction

The calibrated IACA can be used to monitor the progress of compaction as well as to evaluate the quality of the construction. The capability of the IACA to influence the quality of compaction of asphalt pavements during their construction is described in this section.

B.5.1 Monitoring of compaction

To monitor the progress during compaction, select the 'Display' option in the IACA user interface (Figure 17). The interface shown in Figure 17, displays the roller position (latitude and longitude), the roller speed and heading, the surface temperature of the asphalt mat and the density of the pavement at the current location. The display is updated two times every second.

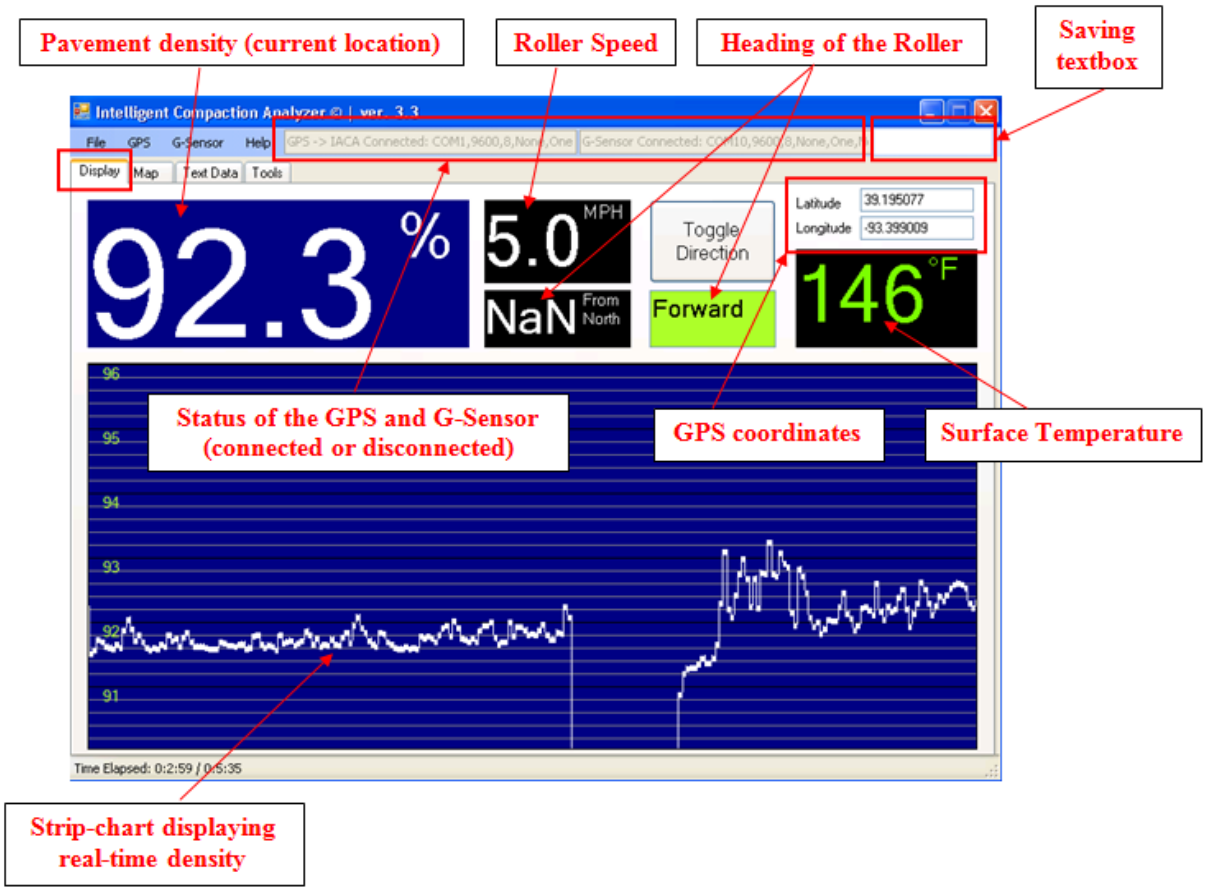

Figure B.17. Real-time display of compaction density

The above figure also displays the density of the asphalt mat during the compaction as a 'strip chart.' This chart provides visual feedback on the uniformity of compaction to the roller operator.

B.5.2 Compaction maps and tools for analysis

In addition to providing real-time information on the density achieved during compaction, the IACA can also be used to evaluate the overall quality of compaction over the entire project.

1. On the tools tab of the IACA GUI push the “Calibration” button and select a working day.

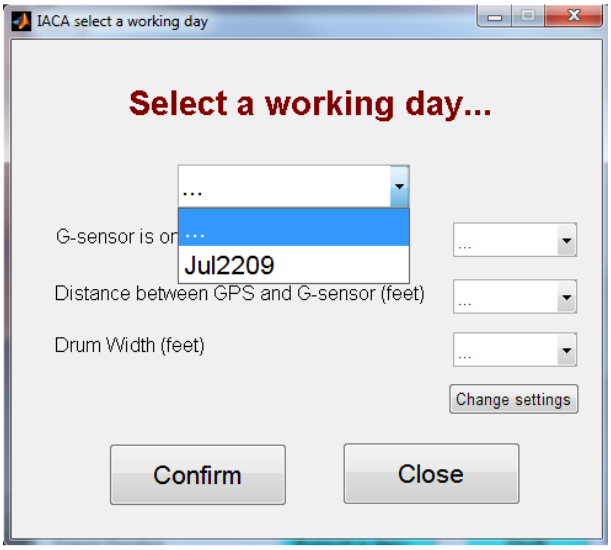

2. On the main window push “ANALYZER MODULE”.

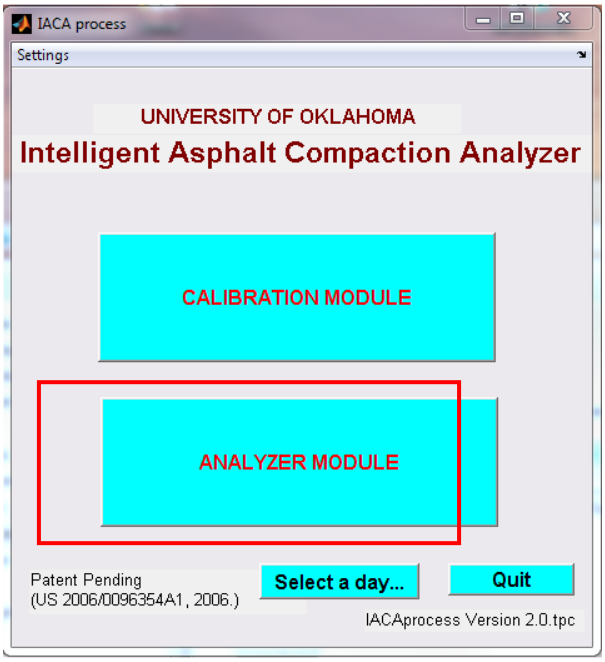

3. On the Analyzer Module window select a task to be performed.

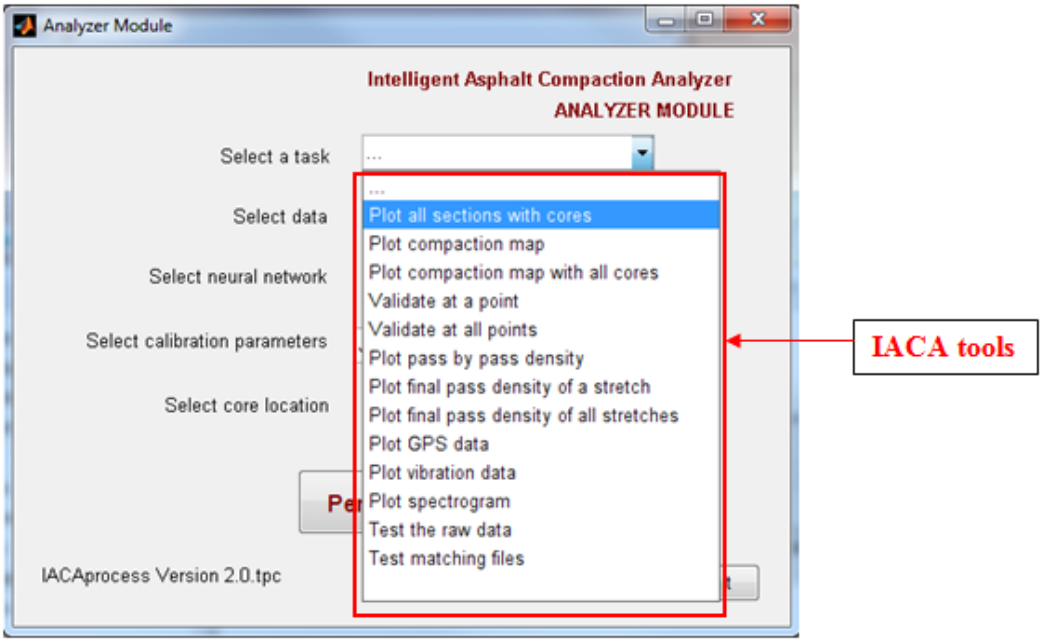

Figure B.18. IACA Analyzer Module

There are a number of useful tools in IACA (as depicted in the figure above) which are helpful to understand the compaction process as well as to estimate the overall quality of the construction. A few of these tools are described below.

B.5.2.1 Generation of as-built maps

We can generate compaction map of a particular stretch using “Plot compaction map” tool in the IACA Analyzer module of Figure 18. Once the tool is selected, we need to choose the stretch for which the map is required, neural network, calibration parameters and then push “Perform the selected task” button (see Figure 19 below).

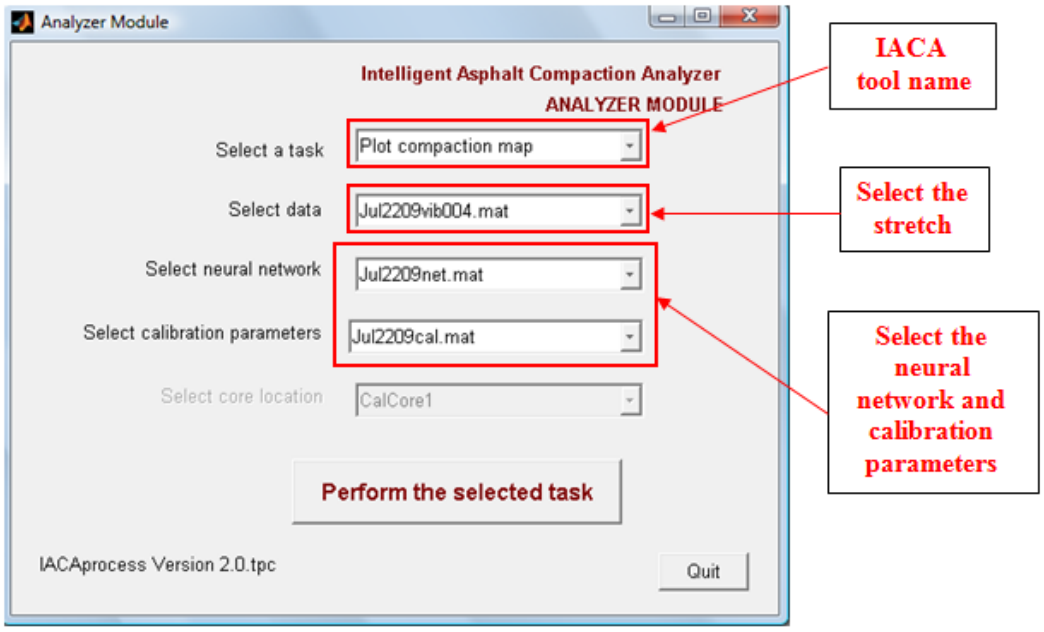

Figure B.19. IACA "Plot Compaction tool"

An example plot is shown below.

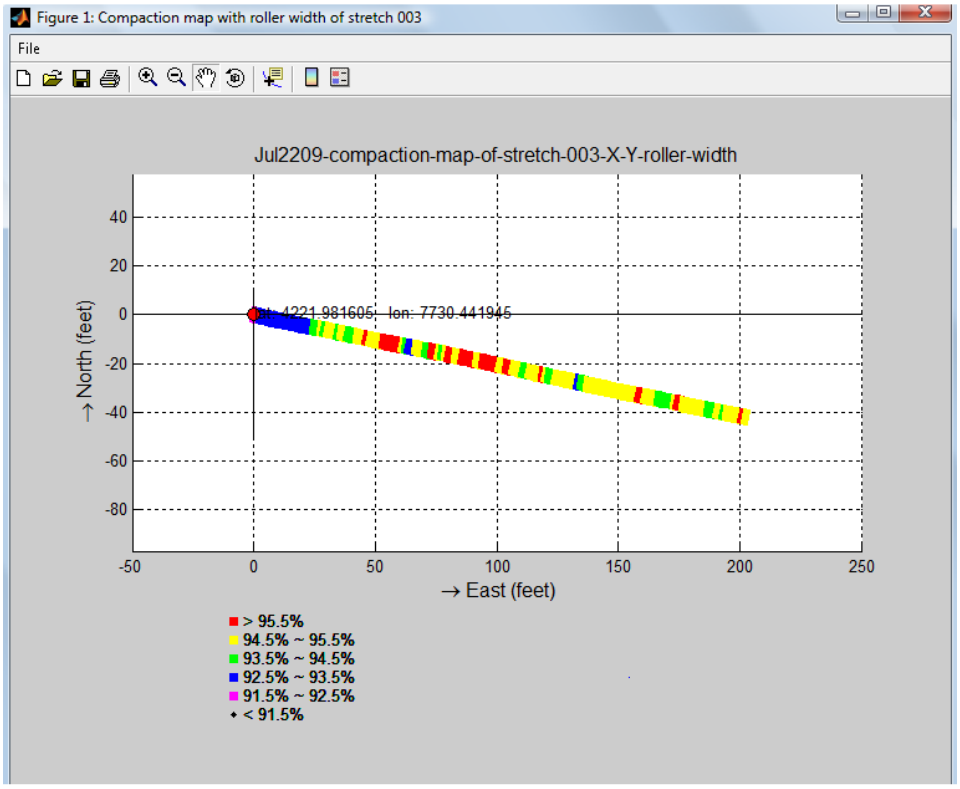

In the above plot, each color corresponds to a different density level. So this map basically shows an outline of the approximate density achieved during the compaction of the stretch.

B.5.2.2 Plotting of GPS data

We can obtain a plot showing the compactor rolling pattern of a particular stretch by using the tool "Plot GPS data" in the IACA Analyzer module (figure 18). Once the tool is selected from the scroll down list, we need to choose the stretch for which the data is to be plotted and then push "Perform the Selected task" button (see Figure 20 below).

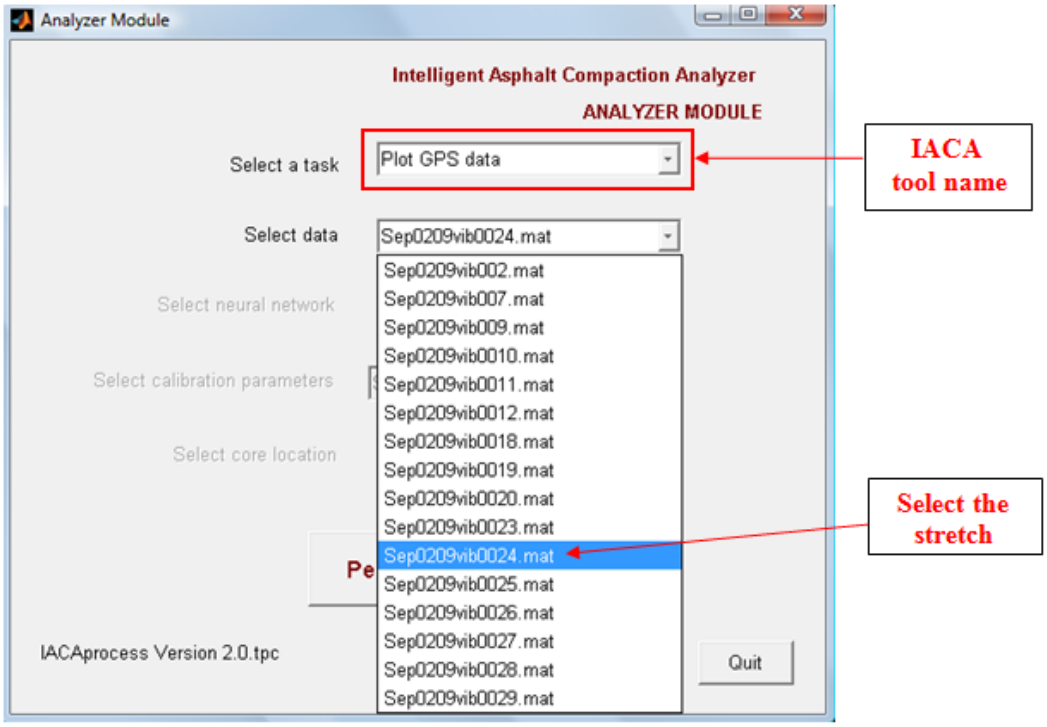

Figure B.20. IACA "Plot GPS data" tool

An example plot is shown below.

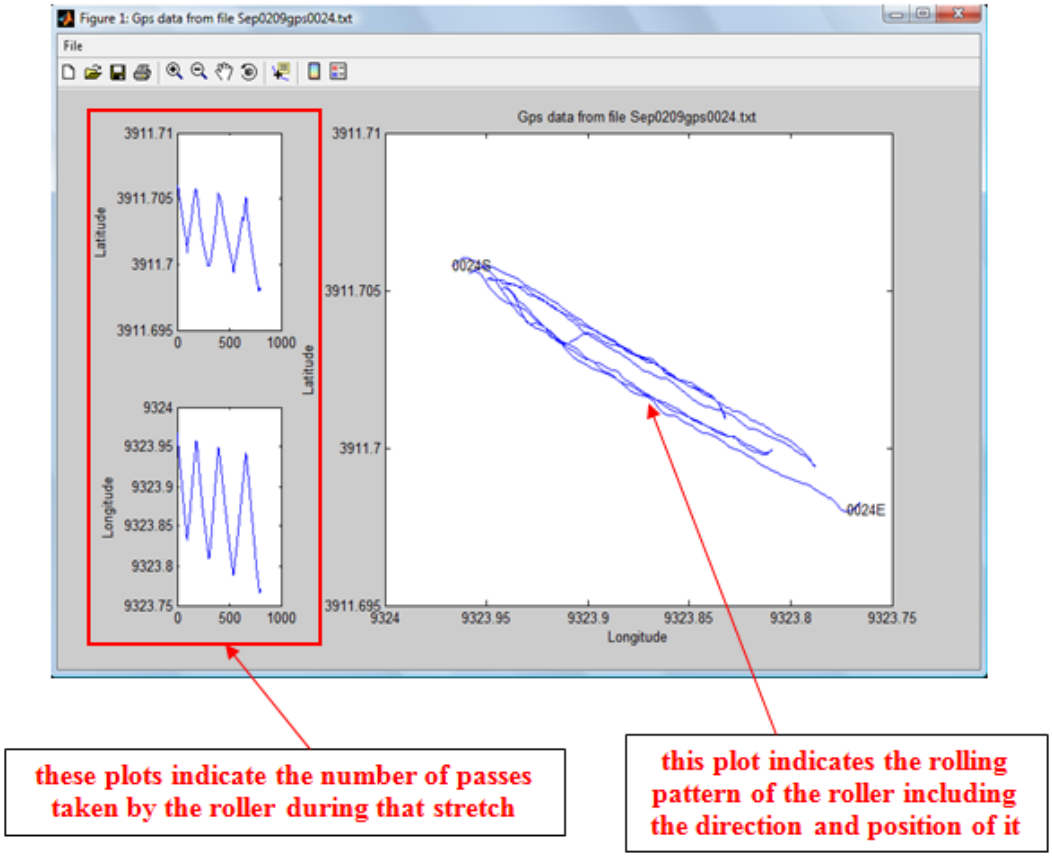

these plots indicate the number of passes taken by the roller during that stretch

this plot indicates the rolling pattern of the roller including the direction and position of it

B.5.2.3 Validate the compaction values at a point

Using the "Validate at a point " tool in IACA, we can estimate the density of a particular point or location on the pavement. Use the scroll down menu (as shown in the figure below) to select the core location and then push "Perform the selected task" button. This will generate a figure displaying the density during each pass for the selected core.

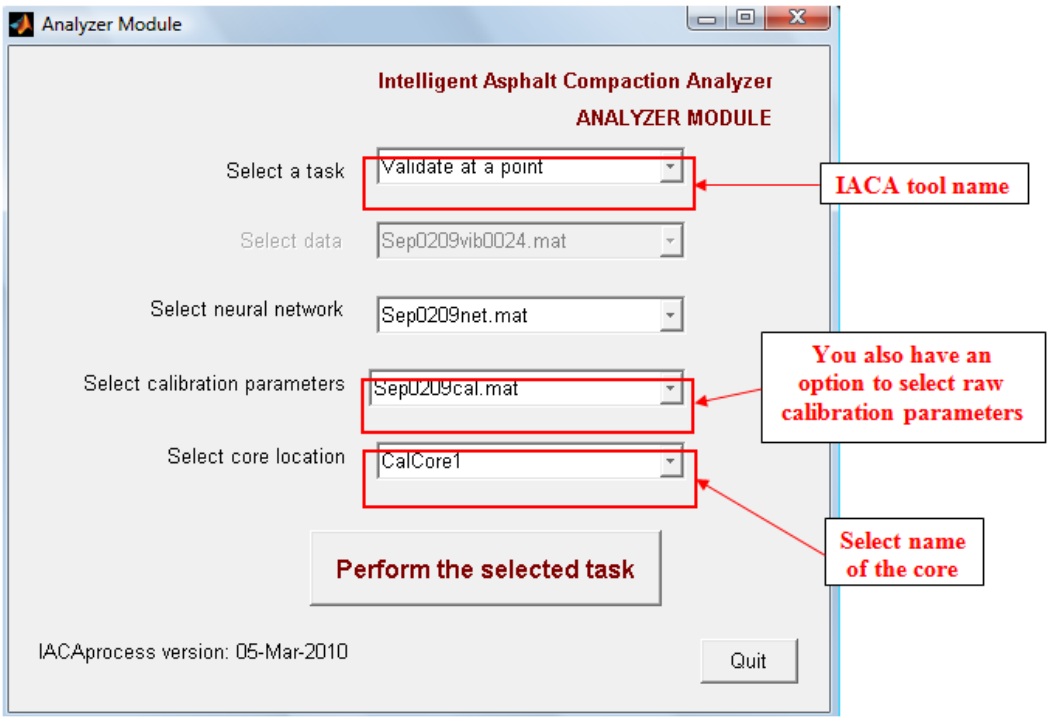

An example figure is shown below and the details are outlined.

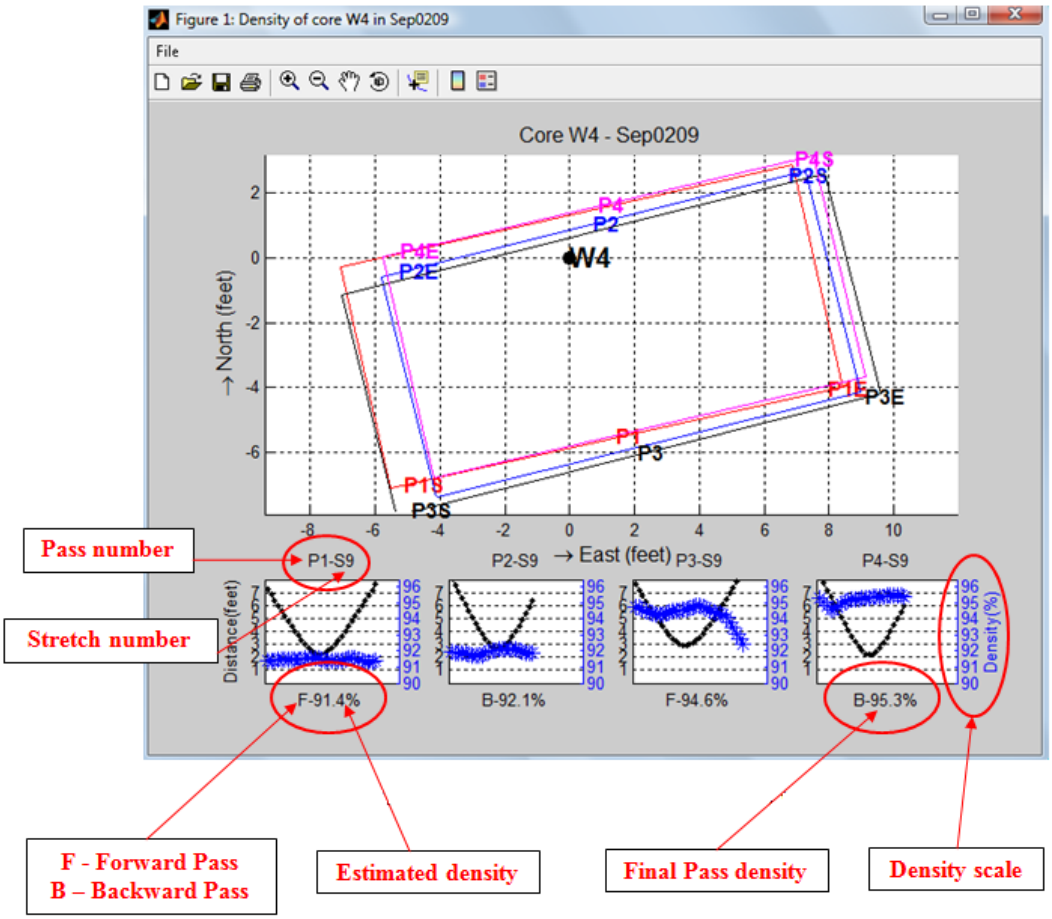

Figure B.21. Estimated Density of a core using IACA tool

B.6 Usage and Precautions

The IACA is capable of displaying the density of the asphalt mat continuously during its compaction. This information is also stored along with the GPS data and other relevant information for analysis of the quality achieved. While the accuracy of the measured densities have been found to be comparable to hand held devices used for in-situ testing of the density, a proper understanding of the technology and the calibration process is essential to obtaining accurate measurements. The following points must be kept in mind during the calibration and use of the IACA.

- Proper calibration is key to getting accurate measurements of density.

- The density obtained on compaction of an asphalt pavement depends on the mix, lift thickness, compacting equipment, and more importantly on the underlying layers of asphalt as well as the subgrade. Inability to obtain desired compaction can usually be traced to a poor asphalt mix or to insufficient preparation of the site.

- For accurate results, the IACA must be calibrated for each layer of the pavement under construction. Furthermore, recalibration is warranted whenever there is an appreciable change in either the mix or the site characteristics.

- GPS sensors require a clear line of sight to the satellites for their proper functioning. Roadway construction under bridges and overpasses, as well as in cities with tall structures, poses a problem in determining the spatial location of the roller.

B.7 Removal and Care of IACA Components

The IACA and associated components have been designed for easy installation and removal. While it may be necessary to retain the equipment for a period of several weeks during the evaluation process, it is necessary to remove the computational platform (Tablet PC) and the GPS receiver at the end of each day's activities. The following steps must be followed to safely remove the Tablet PC and the sensor.

Step 1. Save all relevant files and terminate the IACA application on the Tablet PC.

Step 2. Power off the Tablet PC and disconnect connectors C1-C3. Also, carefully disconnect the ribbon cable connector and the GPS connector.

Step 3. Ensure that the compactor is turned off and securely parked. Remove the GPS receiver from the room of the compactor by gently prying the magnet off from the frame.

Step 4. Use the power adapter to charge the internal battery of the GPS sensor for future use.

Step 5. Carefully pack the Tablet PC taking care to not scratch or damage the PC display.

At the completion of the evaluation, the user is required to remove all the IACA components, place them in their original packages, and ship the IACA back to the University of Oklahoma.

The address for shipping is:

Attn. Dr. Sesh Commuri
University of Oklahoma
School of Electrical and Computer Engineering,
Devon Engineering Hall, Room 432
110 Boyd St., Norman, OK 73019

B.8 Troubleshooting

- Make sure the tablet PC is **ON** before connecting the GPS receiver.
- When charging the battery of GPS receiver, please disconnect the battery from the receiver before attaching the cable.
- There is a fuse connector on the power cable. If power is not being received by the tablet PC, the fuse may be the reason.